NASA CONTRACTOR REPORT

NASA CR-2907

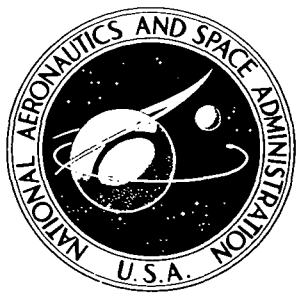

NASA CR-2907

AUTOMATED LANDING, ROLLOUT, AND TURNOFF USING MLS AND MAGNETIC CABLE SENSORS

S. Pines, S. F. Schmidt, and F. Mann

Prepared by
ANALYTICAL MECHANICS ASSOCIATES, INC.
Jericho, N. Y. 11753
for Langley Research Center

NATIONAL AERONAUTICS AND SPACE ADMINISTRATION • WASHINGTON, D. C. • OCTOBER 1977

1. Report No.	2. Government Accession No.	3. Recipient's Catalog No.
NASA CR-2907		

4. Title and Subtitle	5. Report Date
Automated Landing, Rollout, and Turnoff Using MLS and Magnetic Cable Sensors	October 1977
	6. Performing Organization Code

7. Author(s)	8. Performing Organization Report No.
S. Pines, S.F. Schmidt, F. Mann	AMA No. 77-3
	10. Work Unit No.

9. Performing Organization Name and Address	11. Contract or Grant No.
Analytical Mechanics Associates, Inc. 50 Jericho Turnpike Jericho, New York 11753	NAS1-14311
	13. Type of Report and Period Covered
12. Sponsoring Agency Name and Address	Final
Langley Research Center NASA Hampton, VA 23665	14. Sponsoring Agency Code

15. Supplementary Notes

Langley Technical Monitor: Richard M. Hueschen
Topical Report

16. Abstract

This report contains a description of the simulation program used to study the landing approach, rollout and turn-off of the B737-100 aircraft utilizing MLS and a buried magnetic leader cable as navigation aids. The results of the simulation are contained in the report and show the concept to be both feasible and practical for commercial type aircraft terminal area control.

17. Key Words (Suggested by Author(s))	18. Distribution Statement
Automatic landing; Rolloff and Turnoff; Navigation and Guidance; Magnetic Leader Cable; MLS; Kalman Filter;Complementary Filter	Unlimited - Unclassified Subject Category 17

19. Security Classif. (of this report)	20. Security Classif. (of this page)	21. No. of Pages	22. Price*
Uncl.	Uncl.	151	$6.75

*For sale by the National Technical Information Service, Springfield, Virginia 22161

TABLE OF CONTENTS

LIST OF FIGURES

LIST OF FIGURES (Cont.)

LIST OF FIGURES (Cont.)

LIST OF TABLES

Page
Intentionally
Left Blank

AUTOMATED LANDING, ROLLOUT, AND TURNOFF USING MLS AND MAGNETIC CABLE SENSORS

S. Pines
S. F. Schmidt
F. Mann

Analytical Mechanics Associates, Inc.

SUMMARY

This report contains a description of the simulation program used to study the landing approach, rollout and turn-off of the B737-100 aircraft utilizing MLS and a buried magnetic leader cable as navigation aids. The results of the simulation are contained in the report and show the concept to be both feasible and practical for commercial type aircraft terminal area control.

INTRODUCTION

The use of inertial navigations in conjunction with navigation aids such as ILS, MLS, TACAN, etc., in commercial aircraft is rapidly becoming a common state-of-the-art technology. As part of the Terminal Configured Vehicle program (TCV), sponsored jointly by NASA and FAA, this study was undertaken to: (1) investigate the compatability of existing Autoland guidance laws utilizing a Microwave Landing System (MLS) in place of the conventional ILS navigation aids during landing approach; and (2) to extend the concept of automated flight to rollout and turnoff for reduced runway occupancy during normal and adverse (CAT III) landing conditions. In order to achieve acceptable tracking performance in dry and adverse weather conditions, a buried magnetic runway cable and an aircraft mounted three coil magnetic pickup were investigated.

For the purpose of the study, a dynamical model of the B737 was generated in a computer program (ALERT) to simulate the aircraft forces and moments during landing approach, rollout and turnoff. A simulation of the existing Autoland guidance

equations for the B737 was supplied by the Langley Research Center. Optimal Kalman filtering, utilizing a square root formulation for onboard implementation, and a non-optimal fixed gain complementary filter were studied. A rollout and turnoff guidance law was generated. Both Kalman type filtering and fixed gain complementary filtering are shown to be useable with little change to conventional guidance equations presently in use in commercial aircraft.

This report includes a study of the requirements for the Kalman filter and the rollout and turnoff guidance laws.

I. AIRCRAFT DYNAMICS

This section contains the derivation of the equations used in the simulation of the dynamic model of the B-737 during landing approach, capture, decrab, flare, touchdown, rollout and turnoff.

A. Choice of the Coordinate Systems

It is customary to utilize linearized equations of motion describing the deviation of the aircraft from a constant-speed, fixed-flight path angle, wings-level equilibrium condition in the body-stability axis system. While this is sufficient for the landing approach phase, it is inadequate for rollout and turnoff due to large deviations in air speed, flight path angle, and sizable changes in yaw during turnoff. In order to accommodate the broad spectrum of conditions, it was decided to use nonlinear equations of motion in a runway Cartesian coordinate system to describe the linear acceleration of the aircraft and to use the body axes and the Euler angles of roll, pitch, and yaw to describe the angular acceleration equations.

Since the nonlinear variation of the aerodynamic coefficients is small over the range of Mach numbers and aircraft altitudes in landing, and since the aerodynamic forces during rollout and turnoff become relatively unimportant when compared to the landing gear and thrust forces and moments, it was decided to use a simplified form of constant lift, drag, and moment coefficients fitted to the B-737 for the landing simulation. Numerical values of these aerodynamic coefficients were obtained from NASA Langley Research Center and are given in Appendix A.

The orientation and sign convention for the runway inertial Cartesian coordinate system is given in Figure 1. The aircraft position vector, $R(x, y, z)$, is measured relative to the origin fixed on the center line of the runway with the positive x axis pointing forward along the runway center line. The z axis is

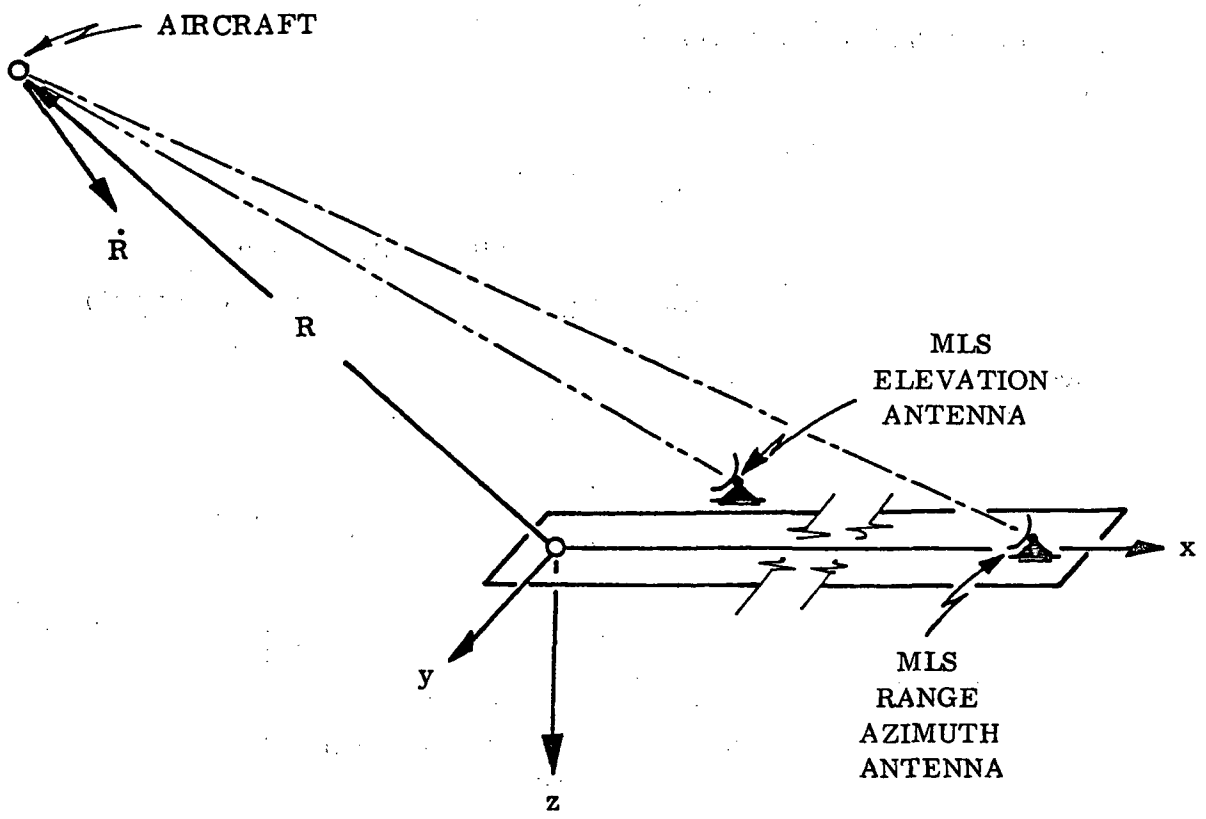

Figure 1. Runway (Inertial) Coordinates and Aircraft Position, Velocity Vectors (R, $\dot{R}$).

positive down, and the y axis is positive to the right in a right-handed orthogonal coordinate system.

The transformation from the body system to the inertial runway system is given in terms of the Euler angles.

Let

ϕ = roll

θ = pitch

Ψ = yaw (measured from magnetic north)

Ψ_R = runway yaw (measured from magnetic north)

Then,

$$T_1(\phi) = \begin{bmatrix} 1 & 0 & 0 \\ 0 & \cos\phi & \sin\phi \\ 0 & -\sin\phi & \cos\phi \end{bmatrix} \tag{1a}$$

$$T_2(\theta) = \begin{bmatrix} \cos\theta & 0 & -\sin\theta \\ 0 & 1 & 0 \\ \sin\theta & 0 & \cos\theta \end{bmatrix} \tag{1b}$$

$$T_3(\sigma) = \begin{bmatrix} \cos\sigma & \sin\sigma & 0 \\ -\sin\sigma & \cos\sigma & 0 \\ 0 & 0 & 1 \end{bmatrix} \tag{1c}$$

where

$$\sigma = \Psi - \Psi_R \tag{1d}$$

A vector in body system V_B is transformed into a vector in runway inertial system by the matrix L_{IB},

$$V_I = L_{IB} V_B \tag{2}$$

where

$$L_{IB} = T_3(-\sigma)\ T_2(-\theta)\ T_1(-\phi) \tag{2a}$$

It follows that the three unit-body-axes vectors $\hat{a}_1$, $\hat{a}_2$, and $\hat{a}_3$ may be expressed in the inertial system in terms of the Euler angles (ϕ, θ, σ). See Figs. 2a and 2b. The $\hat{a}_1$ axis is along the aircraft center line, positive forward.

$$\hat{a}_1 = \begin{Bmatrix} \cos\theta\ \cos\sigma \\ \cos\theta\ \sin\sigma \\ -\sin\theta \end{Bmatrix} \tag{3a}$$

The $\hat{a}_2$ axis is the lateral aircraft axis, pointing positive along the right wing.

$$\hat{a}_2 = \begin{Bmatrix} -\sin\sigma\ \cos\phi\ +\cos\sigma\ \sin\phi\ \sin\theta \\ \cos\sigma\ \cos\phi\ +\sin\sigma\ \sin\phi\ \sin\theta \\ \sin\phi\ \cos\theta \end{Bmatrix} \tag{3b}$$

The $\hat{a}_3$ axis is the vertical body axis pointing positive downward.

$$\hat{a}_3 = \begin{Bmatrix} \sin\sigma\ \sin\phi\ +\cos\sigma\ \cos\phi\ \sin\theta \\ -\cos\sigma\ \sin\phi\ +\sin\sigma\ \cos\phi\ \sin\theta \\ \cos\phi\ \cos\theta \end{Bmatrix} \tag{3c}$$

B. The Aircraft Equations of Motion

The aircraft inertial velocity vector, $\dot{R}(\dot{x}, \dot{y}, \dot{z})$ is given by the time rate of change of the position vector

$$\frac{d}{dt} R = \dot{R} \tag{4}$$

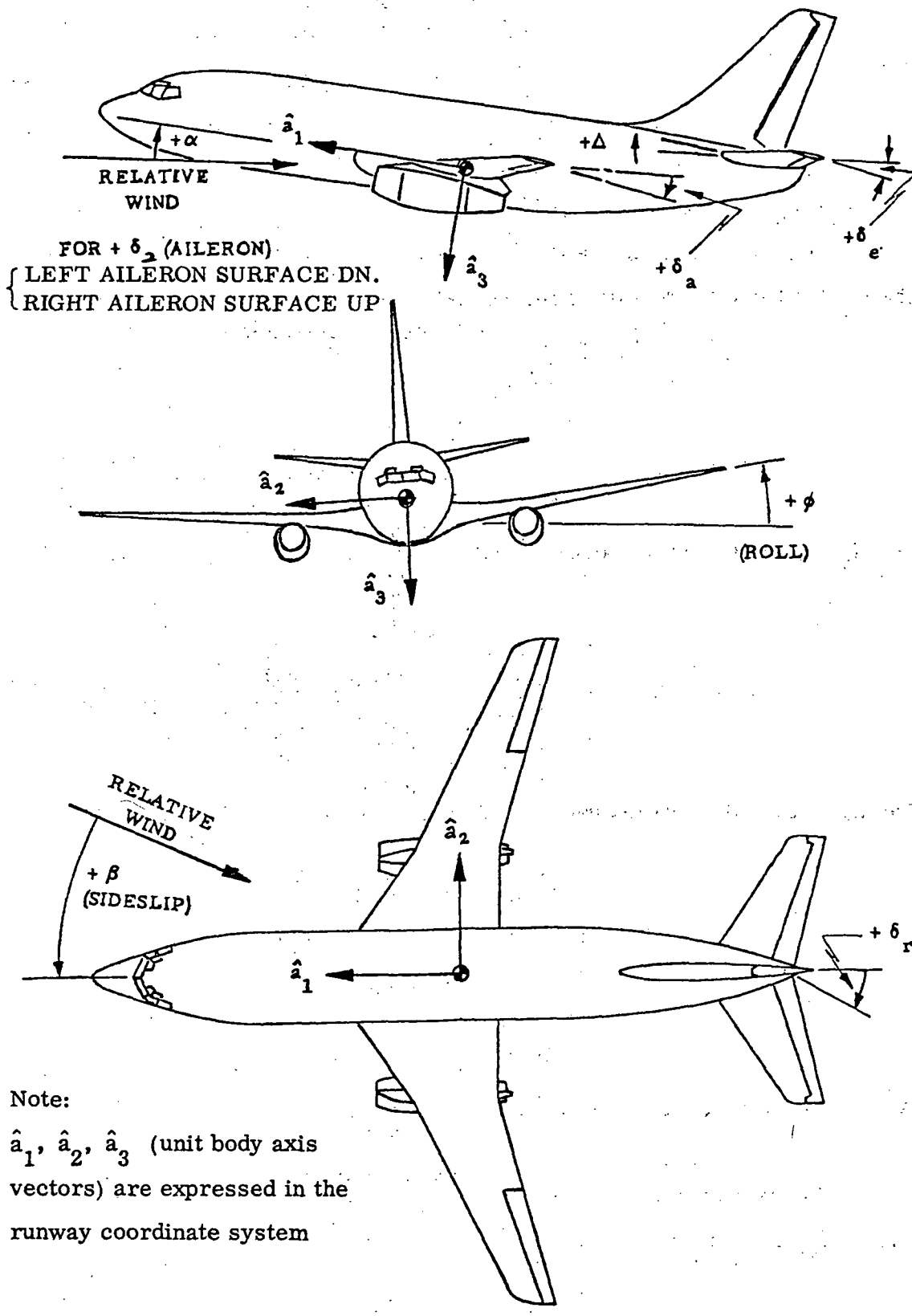

Note:

$\hat{a}_1$, $\hat{a}_2$, $\hat{a}_3$ (unit body axis vectors) are expressed in the runway coordinate system

Figure 2(a). Aircraft Body Coordinate System, Control Surface Deflections, and Aerodynamic Angles.

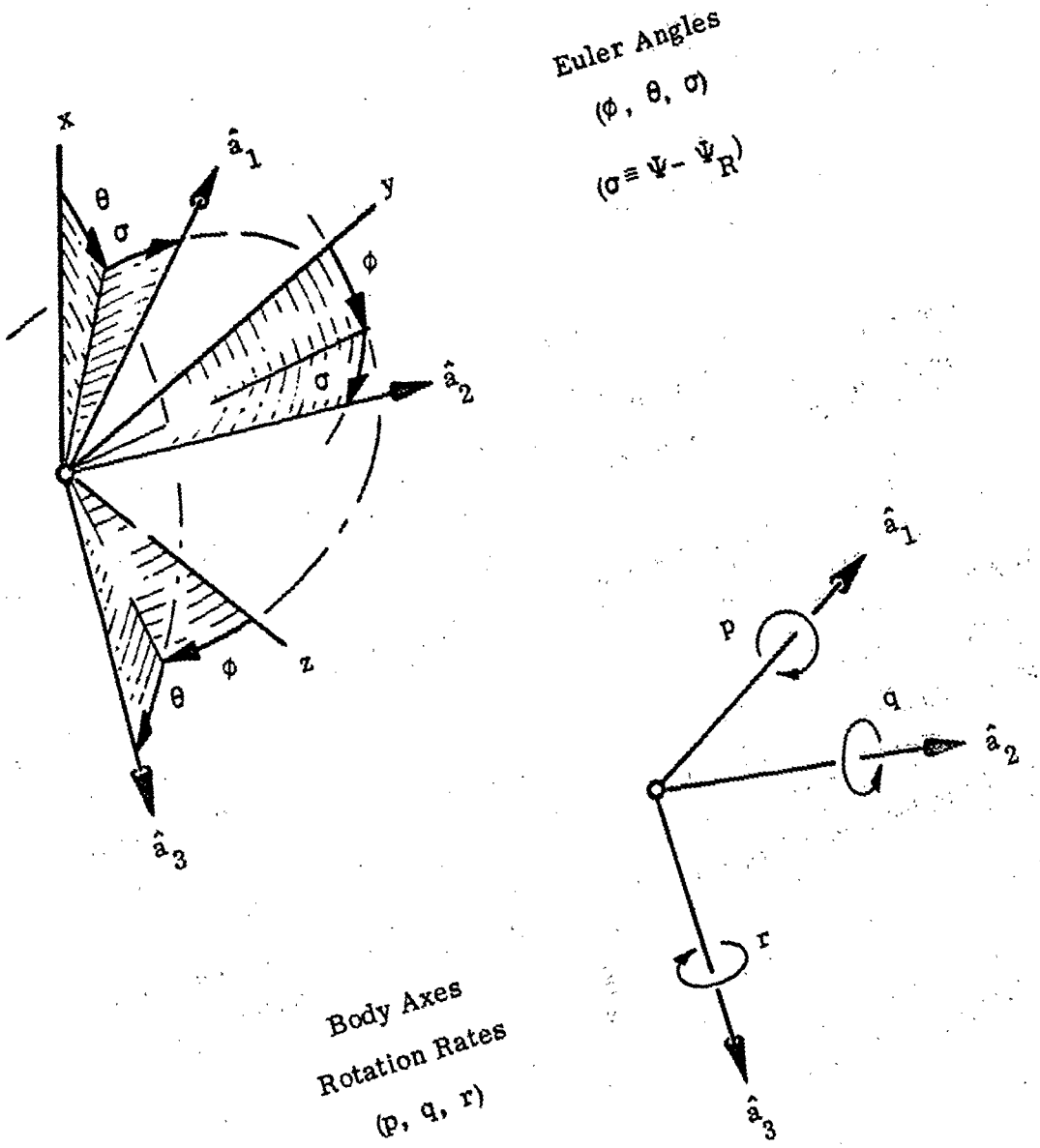

Figure 2(b). Euler Angles and Rotation Rates Defined.

The vector velocity of the aircraft relative to the atmosphere $V(v_1, v_2, v_3)$ is given by the aircraft inertial velocity vector and the winds.

$$V = R - \{W + G + S\} \tag{5}$$

where

W = constant wind vector

G = gust vector

S = wind shear vector

The simulation of wind, shear, and gust is not derived in this report and was supplied by the NASA Langley Research Center.

The aerodynamic coefficients for lift, drag, and side force are obtained from wind tunnel data and relate to forces in the so-called aircraft stability axis system. In this system, the lift acts normal to the aircraft relative velocity vector, V, and in the $\hat{a}_1, \hat{a}_3$ plane. The drag acts in the $\hat{a}_1, \hat{a}_3$ plane and is perpendicular to the lift in the direction negative to the relative velocity vector, V. The side force acts along the $\hat{a}_2$ axis. To express the stability axes $(\hat{s}_1, \hat{s}_2, \hat{s}_3)$ in the inertial runway system, we have the transformation

$$L_{IS} = L_{IB}\, T_2(\alpha) \tag{6}$$

where α is the angle of attack of the aircraft

$$\alpha = \sin^{-1} \frac{\hat{a}_3 \cdot V}{\sqrt{(\hat{a}_1 \cdot V)^2 + (\hat{a}_3 \cdot V)^2}} \tag{7}$$

or

$$\tan^{-1} \frac{\hat{a}_3 \cdot V}{\hat{a}_1 \cdot V}$$

Thus the lift acts along the negative $\hat{s}_3$ axis

$$\hat{s}_3 = -\sin\alpha\,\hat{a}_1 + \cos\alpha\,\hat{a}_3 \tag{8a}$$

The drag acts along the negative $\hat{s}_1$ axis

$$\hat{s}_1 = \cos\alpha\,\hat{a}_1 + \sin\alpha\,\hat{a}_3 \tag{8b}$$

The aerodynamic side force acts along the positive $\hat{s}_2$ axis

$$\hat{s}_2 = \hat{a}_2 \tag{8c}$$

The total forces acting on the aircraft, expressed in the runway-referenced frame, are given by

$$\bar{F} = \bar{q}\,S\,L_{IS}\begin{Bmatrix} -C_D \\ C_Y \\ -C_L \end{Bmatrix} + \begin{Bmatrix} F_{XG} \\ F_{YG} \\ F_{ZG} \end{Bmatrix} + \begin{Bmatrix} F_{XT} \\ F_{YT} \\ F_{ZT} \end{Bmatrix} \tag{9}$$

where

$\bar{q} = \frac{1}{2}\rho V^2$ (dynamic pressure)

S = wing reference area

C_D, C_Y, C_L = effective drag, side force, and lift coefficients (see Appendix A)

F_{XG}, F_{YG}, F_{ZG} = landing gear forces expressed in the runway system

F_{XT}, F_{YT}, F_{ZT} = thrust forces expressed in the runway system (9a)

The time rate of change of the inertial velocity vector in the runway frame is given by

$$\frac{d}{dt}\dot{R} = A_G + \frac{\bar{q}S}{m}\{-C_D\,\hat{s}_1 + C_Y\,\hat{s}_2 - C_L\,\hat{s}_3\} + \frac{1}{m}\begin{Bmatrix} F_{XG} \\ F_{YG} \\ F_{ZG} \end{Bmatrix} \tag{10}$$

$$+ \frac{k}{m}\{\cos\alpha_o\,\hat{a}_1 - \sin\alpha_o\,\hat{a}_3\}$$

where

$$A_G = \begin{Bmatrix} 0 \\ 0 \\ G \end{Bmatrix} \quad \text{(gravity vector)} \tag{10a}$$

k = magnitude of the thrust

α_o = thrust offset angle in the $\hat{a}_1, \hat{a}_3$ plane. Positive α_o is a rotation about the $\hat{a}_2$ axis.

It is convenient to integrate the angular accelerations of the aircraft in the body system since the mass moments of inertia do not change in that frame. The kinematic equations relating the Euler angles and the body angular rates (p, q, r) are given by

$$\begin{aligned} \dot{\theta} &= \cos\phi\; q - \sin\phi\; r \\ \dot{\Psi} &= (r\cos\phi + q\sin\phi)/\cos\theta \\ \dot{\phi} &= p + \sin\theta\;\dot{\Psi} \end{aligned} \tag{11}$$

The differential equations for the angular accelerations in the body system are given by

$$\frac{d}{dt}\{\omega\} = -(I_B)^{-1}\{\omega \times (I_B)\omega + T_B\} \tag{12}$$

where

$$I_B = \begin{Bmatrix} I_{XX} & 0 & -I_{XZ} \\ 0 & I_{YY} & 0 \\ -I_{XZ} & 0 & I_{ZZ} \end{Bmatrix} \tag{12a}$$

$$\omega = \begin{Bmatrix} p \\ q \\ r \end{Bmatrix} \tag{12b}$$

$$T_B = T_2(-\alpha) \begin{Bmatrix} L_S \\ M_S \\ N_S \end{Bmatrix} + \begin{Bmatrix} L_G \\ M_G \\ N_G \end{Bmatrix} + \begin{Bmatrix} L_T \\ M_T \\ N_T \end{Bmatrix} \tag{12c}$$

The aerodynamic moments, L_S, M_S, N_S, in the stability frame are given in Appendix A. The landing gear moments, L_G, M_G, N_G, are in the body frame and are derived in Section C. The moment due to thrust is given by

$$\begin{Bmatrix} L_T \\ M_T \\ N_T \end{Bmatrix} = \begin{Bmatrix} 0 \\ a_T k \\ 0 \end{Bmatrix} \tag{12d}$$

a_T is the moment arm of the engine thrust and is listed in Appendix A.

C. Landing Gear Dynamics

The landing gear is modeled as an airspring and damper. Strut compression is initiated whenever the strut load exceeds a preset preload, P_{L_i}.

For loads less than the preload, tire compression provides a linear spring (initial tire compression). Elastic deflection of the strut and inertial acceleration of the unsprung mass of the strut and tire are considered high frequency phenomena and are neglected in the analysis.

In order to determine the forces and moments acting on the aircraft due to ground reactions in landing and braking, the locations of the main gear and nose strut with respect to the center of gravity are required. The locations of the three extended, uncompressed gears of the B-737 are given in Ref. 1 and illustrated in Fig. 3. The positions of the three gears are measured from an origin at the leading edge of the MAC.

Let the coordinates of the i^{th} gear with respect to the leading edge of the MAC be given by

$$\bar{x}_i, \bar{y}_i, \bar{z}_i \qquad \text{(see Table 1)}$$

During landing, rollout, and turnoff, it is assumed that the aircraft experiences small values of pitch and roll. Large values of yaw are permitted. Thus, small angle theory is used to model roll and pitch motions but the full nonlinear theory holds in yaw.

The height of the i^{th} gear above the runway is given by

$$h_{iG} = -z_{iG} = -z - \phi \bar{y}_i + \theta(\bar{x}_i + \bar{c}\, g^*) \tag{13}$$

where

g^* = center of gravity expressed as the percentage of mean aerodynamic chord

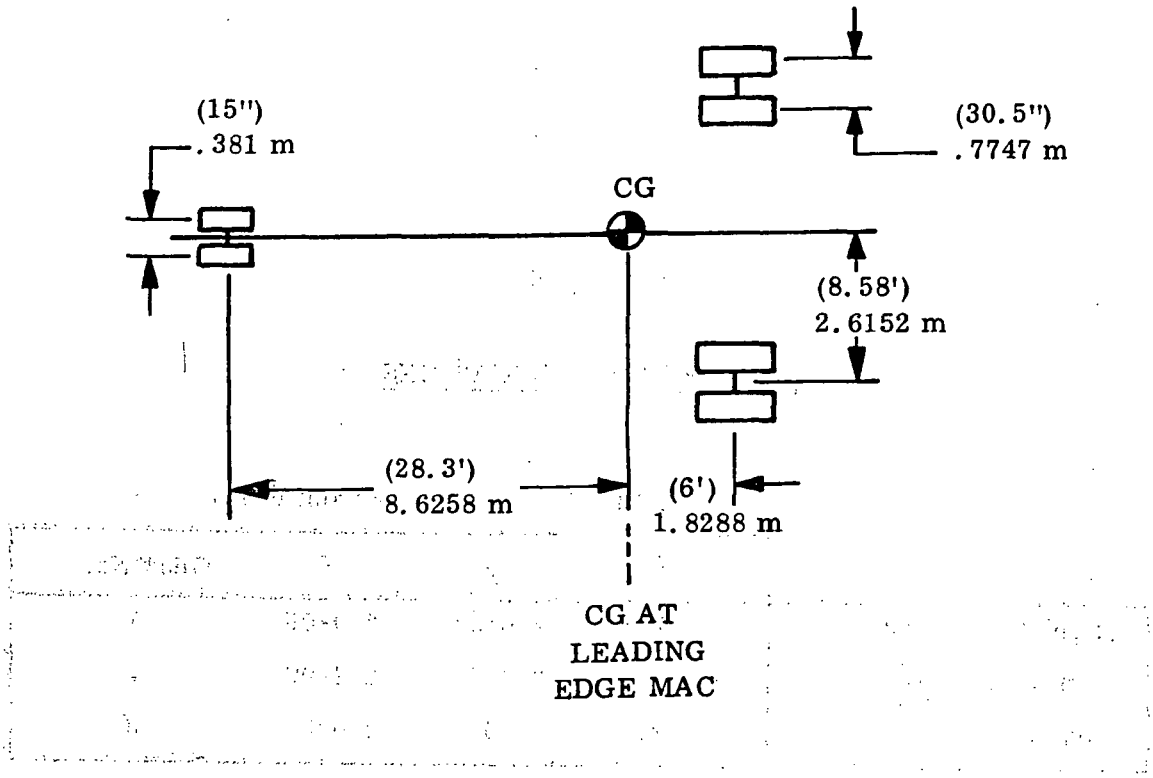

LANDING GEAR LOCATION

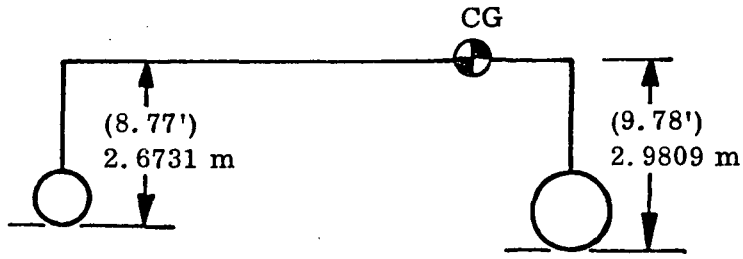

EXTENDED GEAR HEIGHTS

Figure 3. Landing Gear Geometry

TABLE 1

EXTENDED GEAR LOCATIONS

(Distances in meters from c.g.)

	$\bar{x}$	$\bar{y}$	$\bar{z}$	Gear No.
Right Main Gear	-1.8288	2.6152	2.9809	1
Left Main Gear	-1.8288	-2.6152	2.9809	2
Nose Gear	8.6258	0	2.6731	3

Ground contact occurs whenever

$$h_{iG} < 0 \quad \text{or} \quad z_{iG} > 0 \tag{13a}$$

Since the strut is preloaded, no strut deflection occurs until z_{iG} exceeds the preload tire deflection, z_{ipL}. Thus, for

$$0 \leq z_{iG} \leq z_{ipL} \tag{13b}$$

the strut load is a linear function of z_{iG}

$$F_i = -F_{pi} \frac{z_{iG}}{z_{ipL}} \tag{14}$$

Once the preload has been exceeded, the strut begins to compress and the force is given by the isothermal compression law

$$F_i = -F_{pi} \left(\frac{1}{1 - \dfrac{z_{iG} - z_{ipL}}{\ell_i}} \right) \tag{15}$$

where ℓ_i is the bottom-out maximum deflection permitted by the strut design. Equation (15) holds for all z_{iG} such that

$$z_{ipL} \leq z_{iG} \leq \ell_i \tag{15a}$$

The strut deflection is given by

$$z_{iD} = z_{iG} - z_{ipL} \tag{15b}$$

The damping force is generated by the strut deflection rate, $\dot{z}_{iD}$, given by

$$\dot{z}_{iD} = \dot{z} + p\,\bar{y}_i - q(\bar{x}_i + \bar{c}\,g^*) \tag{16}$$

The damping force of the i^{th} strut is given by

$$F_{iD} = -\dot{z}_{iD}\left|\dot{z}_{iD}\right| c_{iv} \tag{17}$$

where c_{iv} is the damping coefficient, which is modeled as a function of the strut deflection

$$c_{iv} = a_{1i}\,z_{iD} + a_{2i}\,z_{iD}^2 \tag{17a}$$

where a_{1i}; a_{2i} are strut damping design constants. Figures 4 and 5 illustrate the strut compression curves for the main and nose gears.

The net vertical strut force in the body frame is given by

$$F_{Ni} = F_i + F_{Di} \tag{18}$$

The tire drag force may now be computed as a function of the normal strut force and the friction coefficient. The drag force acts in the plane of the tire and in a direction opposite to the axle velocity. We have

$$F_{Hi} = -\mu\left|F_{Ni}\right| \tag{19}$$

The tire friction coefficient, μ, is the sum of the rolling friction coefficient, μ_R, and the friction coefficient developed by brake application, μ_B. We have, for dry runway conditions,

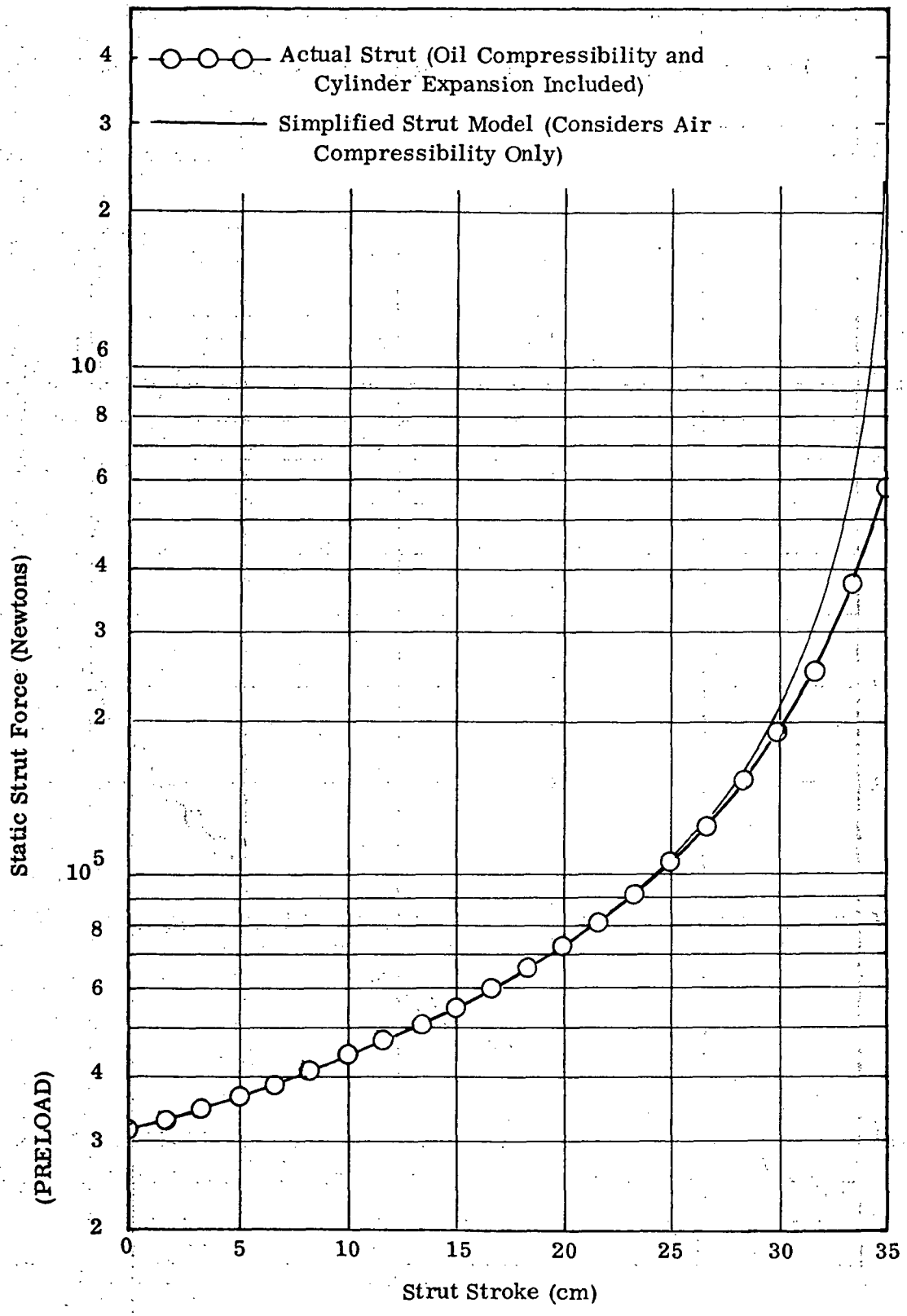

Figure 4. Main Gear Strut Compression Force

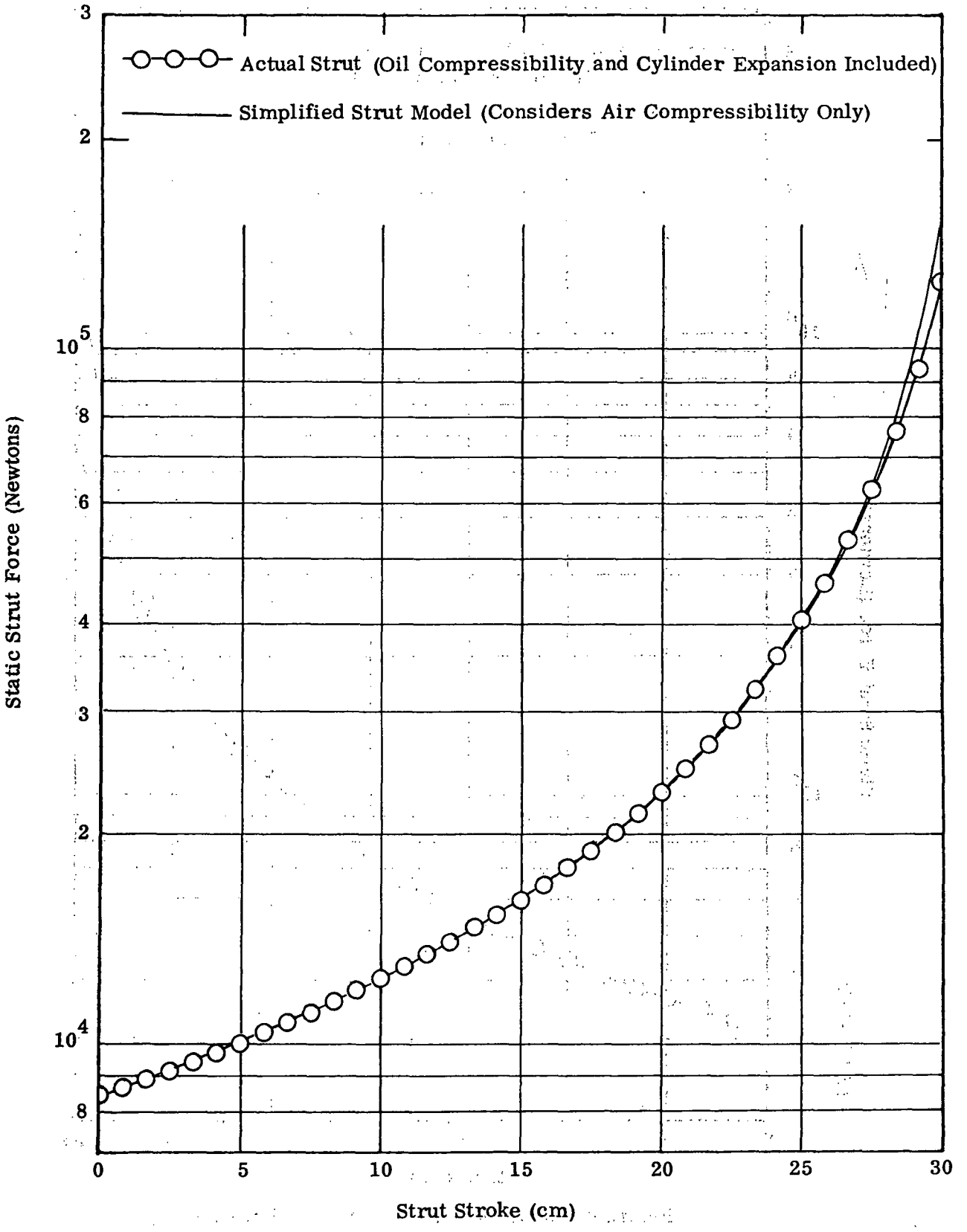

Figure 5. Nose Gear Strut Compression Force.

$$\mu_B = .5 \frac{b_p}{b_{pmax}} \tag{20}$$

where b_p is the brake pressure and b_{pmax} is the maximum pressure available. For wet runways, we have (from Ref. 1)

$$\mu_B \cong \frac{V_G + 100}{10\,V_G + 200} \frac{b_p}{b_{pmax}} \tag{20a}$$

where V_G is the ground speed in knots. The tire friction curves are given in Fig. 6.

The guidance law for brake pressure application is given in the Guidance and Control Section of this report.

Finally, we have

$$\mu = \mu_R + \mu_B \tag{21}$$

where μ_R is the coefficient of rolling friction. Braking is not available on the nose wheel so that only rolling friction prevails.

The landing gear lateral forces and steering is taken from the theory developed by W. B. Horne in Ref. 2. We first compute the tire compression coefficient η_i:

$$\eta_i = \frac{.5\,|F_{Ni}|}{(p_i + .08\,p_{ri})\,w_i\,(w_i\,d_i)^{\frac{1}{2}}} \tag{22}$$

If

$$\eta_i > .09$$

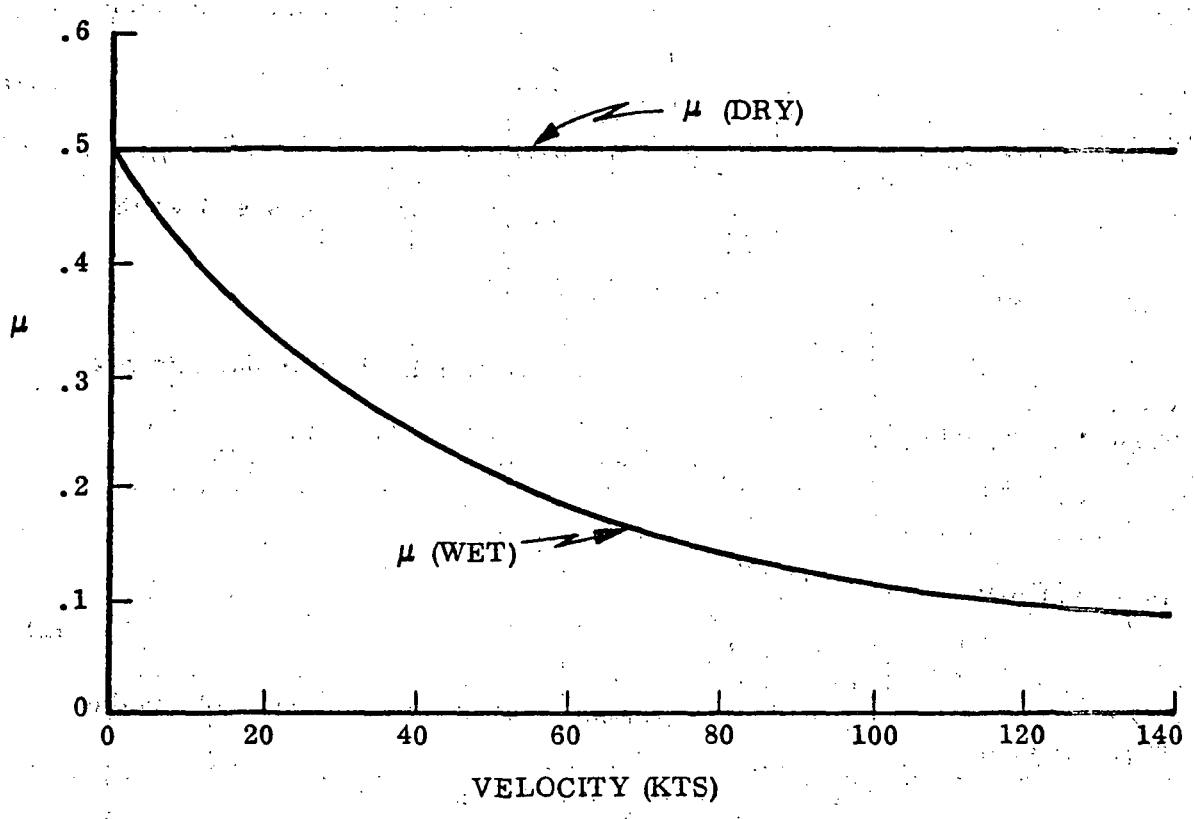

Figure 6. Friction Coefficients.

the tire compression is given by

$$\delta_{ti} = w_i (.03 + .42\ \eta_i) \tag{22a}$$

If

$$\eta_i < .09$$

tire compression is

$$\delta_{ti} = \frac{3}{4}\ w_i\ \eta_i \tag{22b}$$

The tire cornering force coefficient is given by

$$C_{Ni} = \frac{2\pi}{180} (p_i + .44 p_{ri}) w_i^2 \tag{23}$$

(The factor, 2, multiplying $\pi/180$ represents the number of tires per strut. Thus, for a single tire strut, the factor would be 1.)

For

$$\delta_{ti} \geq .0875 d_i$$

$$N_i = C_{Ni} \left(.067 + .34 \frac{\delta_{ti}}{d_i} \right) \tag{24a}$$

and for

$$\delta_{ti} < .0875\ d_i$$

$$N_i = C_{Ni} \left[1.2 \frac{\delta_{ti}}{d_i} - 8.8 \left(\frac{\delta_{ti}}{d_i} \right)^2 \right] \tag{24b}$$

The lateral tire cornering force acts normal to the plane of the tire and is given by

$$F_{Li} = N_i(\gamma_i + \sigma - \varepsilon_i) \tag{25}$$

where ε_i is the ground track angle

$$\varepsilon_i = \tan^{-1} \frac{\dot{y} + r[(\bar{x}_i + \bar{c}\, g^*)\cos\sigma - \bar{y}_i \sin\sigma]}{\dot{x}} \tag{25a}$$

$$(\sigma = \Psi - \Psi_R)$$

and γ_i is the steering angle of the wheel. For the main gear, $\gamma_i = 0$, and for the nose wheel, γ_i is supplied by the control logic.

The plane of the main tire is parallel to the $\hat{a}_1, \hat{a}_3$ body frame. However, the nose wheel develops a drag and cornering force which must be resolved into the body axes. Let γ_3, F_{H3}, and F_{L3} be the nose wheel steering angle and horizontal forces developed in the plane of the nose wheel and perpendicular to it. Then we have, for the forces in the body system,

$$\begin{aligned} F_{Xi} &= F_{Hi} - \theta F_{Ni} - \delta_{i3}\gamma_3 F_{L3} \\ F_{Yi} &= F_{Li} + \phi F_{Ni} + \delta_{i3}\gamma_3 F_{H3} \\ F_{Zi} &= \theta F_{Hi} - \phi F_{Li} + F_{Ni} - \delta_{i3}\gamma_3(\theta F_{L3} + \phi F_{H3}) \end{aligned} \tag{26}$$

To obtain the moments in the body frame, we have

The lateral tire cornering force acts normal to the plane of the tire and is given by

$$F_{Li} = N_i(\gamma_i + \sigma - \varepsilon_i) \tag{25}$$

where ε_i is the ground track angle

$$\varepsilon_i = \tan^{-1} \frac{\dot{y} + r[(\bar{x}_i + \bar{c}\, g^*)\cos\sigma - \bar{y}_i \sin\sigma]}{\dot{x}} \tag{25a}$$

$$(\sigma = \Psi - \Psi_R)$$

and γ_i is the steering angle of the wheel. For the main gear, $\gamma_i = 0$, and for the nose wheel, γ_i is supplied by the control logic.

The plane of the main tire is parallel to the $\hat{a}_1, \hat{a}_3$ body frame. However, the nose wheel develops a drag and cornering force which must be resolved into the body axes. Let γ_3, F_{H3}, and F_{L3} be the nose wheel steering angle and horizontal forces developed in the plane of the nose wheel and perpendicular to it. Then we have, for the forces in the body system,

$$\begin{aligned} F_{Xi} &= F_{Hi} - \theta F_{Ni} - \delta_{i3}\gamma_3 F_{L3} \\ F_{Yi} &= F_{Li} + \phi F_{Ni} + \delta_{i3}\gamma_3 F_{H3} \\ F_{Zi} &= \theta F_{Hi} - \phi F_{Li} + F_{Ni} - \delta_{i3}\gamma_3(\theta F_{L3} + \phi F_{H3}) \end{aligned} \tag{26}$$

To obtain the moments in the body frame, we have

$$L_G = \sum_{i=1}^{3} (F_{Zi}\,\bar{y}_i - F_{Yi}\,z_{iG})$$

$$M_G = \sum_{i=1}^{3} [F_{Xi}\,z_{iG} - F_{Zi}(\bar{x}_i + \bar{c}\,g^*)] \qquad (27)$$

$$N_G = \sum_{i=1}^{3} [F_{Yi}(\bar{x}_i + \bar{c}\,g^*) - F_{Xi}\,\bar{y}_i]$$

To obtain the forces in the runway frame, we have

$$F_{XG} = \left(-\gamma_3 F_{L3} + \sum_{i=1}^{3} F_{Hi}\right)\cos\sigma - \left(\gamma_3 F_{H3} + \sum_{i=1}^{3} F_{Li}\right)\sin\sigma$$

$$F_{YG} = \left(\gamma_3 F_{H3} + \sum_{i=1}^{3} F_{Li}\right)\sin\sigma + \left(-\gamma_3 F_{L3} + \sum_{i=1}^{3} F_{Hi}\right)\cos\sigma \qquad (28)$$

$$F_{ZG} = \sum_{i=1}^{3} F_{Ni}$$

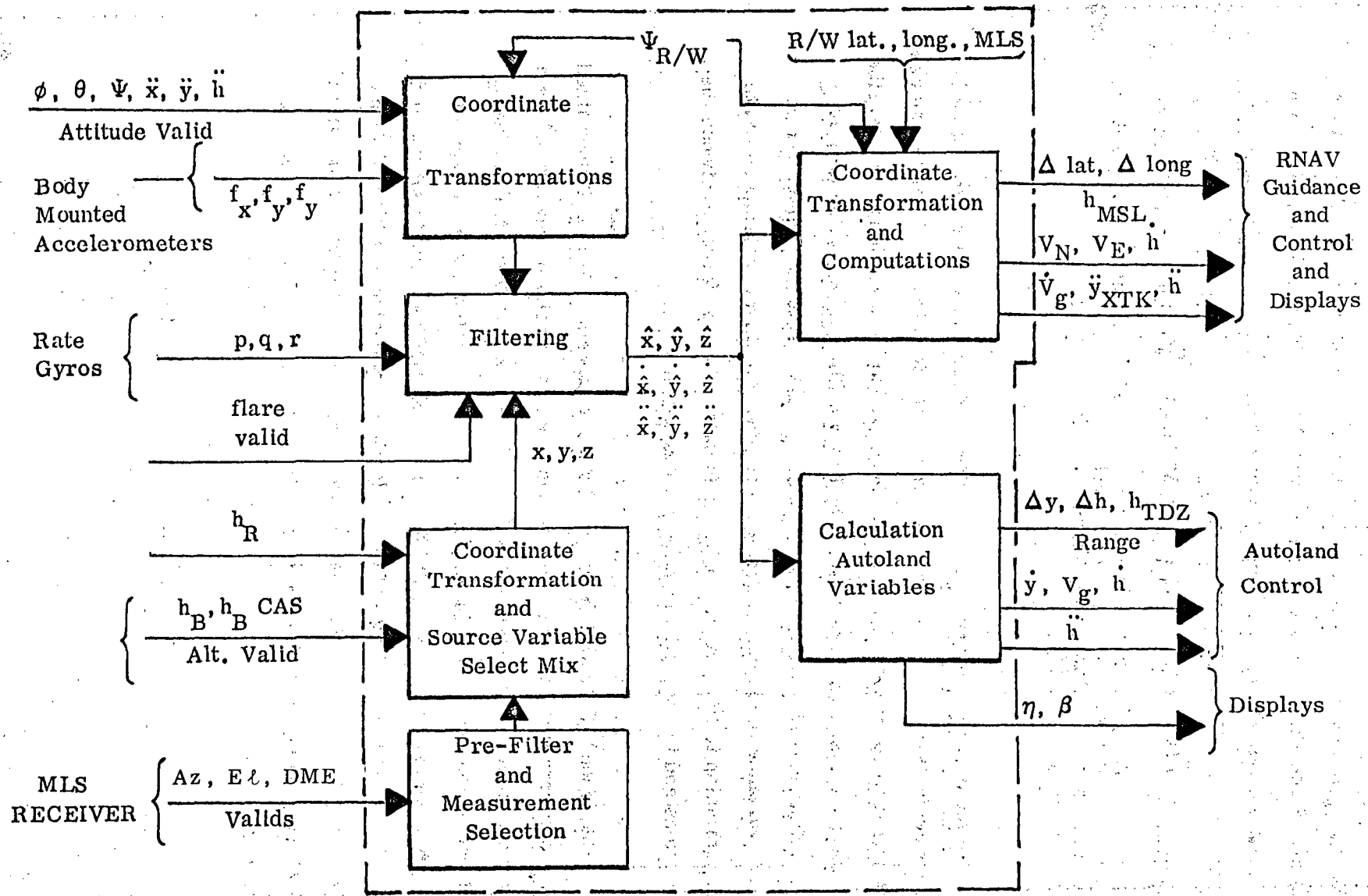

Figure 7. Navigation System Block Diagram

where f_{SFB} is the specific force measured in the body frame by the accelerometers. Since the accelerometer and gyro data are sampled at 20 Hz, we may integrate Eq. (30) with a simple Taylor series

$$\bar{R}(t + \Delta t) = \bar{R}(t) + \dot{\bar{R}}(t)\,\Delta t + \ddot{\bar{R}}(t)\,\frac{\Delta t^2}{2}$$

$$\dot{\bar{R}}(t + \Delta t) = \dot{\bar{R}}(t) + \ddot{\bar{R}}(t)\,\Delta t \qquad (31)$$

$$\Delta t = .05 \text{ sec.}$$

In the presence of error sources cited earlier, the dead reckoning estimates become useless after some time, and navigation aids and filter techniques are required to correct for the errors. In the subsequent sections, we describe two such filter systems. The first is the Kalman filter. This filter utilizes a priori estimates of the uncertainty in the error states to be corrected and the expected variance in the observations, to obtain a minimum variance estimate of the correction to the states as a linear function of the difference between the observations and the expected value of the observation.

The second filter system is called a complementary filter. It uses fixed gains to estimate the corrections to the position and velocity of the aircraft as a linear function of the observation residual. Since it knows nothing about the a priori uncertainty of the aircraft errors or the observation noise, it depends solely upon the concept of exponentially correlated random noise to smooth out noise. As shown in the results of the study, the complementary filter does as well as the Kalman filter in landing approach, but does not do as well in turnoff because of the effect of gyro misalignment biases.

B. Kalman Filter Implementation

The optimal filter algorithm involves a very large number of machine operations. The basic algorithm separates into the following:

1. Calculations associated with a change in the time reference of the filter, and
2. Calculations of the incremental state estimate from the measurement information.

In order to keep the number of operations within the capabilities of current airborne computers, the accelerometers and gyros are sampled at a rate of 20 Hz, the observations are sampled at a rate of 10 Hz, and the filter is updated at a rate of 1 Hz.

Past experience has shown that the square root implementation of the optimal filter algorithm (Ref. 3) can reduce the effects of numerical errors to insignificant levels. The square root implementation is therefore incorporated in the proposed design. Modeling errors are compensated for by the appropriate use of random forcing functions. This technique causes the more recent measurements to be weighted higher than past measurements; therefore, the estimate tends to follow the more recent measurements.

The proposed filter will operate in a manner illustrated in the sketch below:

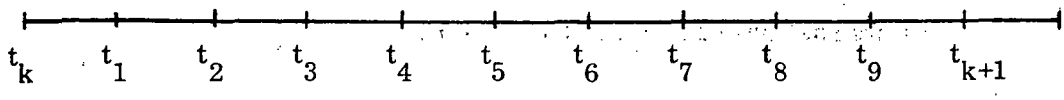

At the start of the sequence, we assume that the filter has its covariance matrix referenced to time t_k. At the times t_k, t_1, ..., t_9, measurements

are accepted and residual sums and partials are computed and saved in pre-processing routines. After accepting the measurement at time t_9, the residual sums and partials are transferred to arrays for processing by the filter; and the locations used for the pre-processing are cleared for use in pre-processing the t_{k+1} and subsequent measurements. The residual sums are processed by the filter and the incremental state change computed in lower priority logic. When these lower priority calculations have been completed, the logic sets markers which cause the higher priority logic to pick up the state change and add it to the system. Meanwhile, the lower priority logic updates the covariance matrix to the time t_{k+1} and readies the filter for processing the residual sums in the next interval. The onboard program operations for executing such logic will be described in a later report.

The error state is assumed to obey a linear differential equation

$$\dot{dx} = F_x\, dx + F_n\, n \tag{32}$$

where

dx = the n-component error state vector $(n=15)$

F_x = an $n \times n$ matrix

F_n = an $n \times m$ matrix

n = an m-vector of random forcing functions for compensation of error growth caused by unmodeled error sources.

An approximate solution of Eq. (32) is

$$dx(t_{k+1}) = \Phi(t_{k+1}\,;\, t_k)\, dx(t_k) + \Phi_u(t_{k+1}\,;\, t_k)\, u(t_k) \tag{33}$$

where

Φ = the transition matrix

Φ_u = the forcing function sensitivity matrix

$u(t_k)$ = a constant (in the interval t_k to t_{k+1}) vector for approximating the effects of the noise vector, n, of Eq. (32)

The covariance matrix for the error state at time t_k is given by

$$P(t_k) = W(t_k)\, W(t_k)^T = \mathcal{E}\left[dx(t_k)\, dx(t_k)^T\right] \tag{34}$$

where

$W(t_k)$ = the square root covariance. (W^T is calculated in the proposed square root implementation of the optimal filter)

$\mathcal{E}[\ ]$ = the expected value operator.

We assume that $u(t_k)$ is a random independent vector such that

$$\begin{aligned} \mathcal{E}\left[u(t_{k+i})\, u(t_{k+\ell})^T\right] &= 0 && i \neq \ell \\ &= U(t_{k+i})\, U(t_{k+i})^T && i = \ell \end{aligned} \tag{35}$$

where $U(t_k)$ is the square root of the process noise variance.

The appropriate use of the expected value operator with Eq. (33) gives the time update of the covariance matrix

$$P(t_{k+1}) = W(t_{k+1})\, W(t_{k+1})^T = \left[\Phi W(t_k),\ \Phi_u U\right] \begin{bmatrix} W(t_k)^T \Phi^T \\ U^T \Phi_u^T \end{bmatrix} \tag{36}$$

We see from Eq. (36) that we can form $W(t_{k+1})^T$ in two steps as follows:

$$W(t_{k+1})^T = \begin{bmatrix} W(t_k)^T \Phi(t_{k+1}; t_k)^T \\ U(t_k)^T \Phi_u(t_{k+1}; t_k)^T \end{bmatrix} \tag{37}$$

The matrix, $W(t_{k+1})^T$ of Eq. (37), has dimension $(n+m) \times n$. The Householder algorithm described in Ref. 4 can be used to reduce this matrix to an upper triangular form; that is, all the terms below the diagonal are zero in the reduced matrix. The matrix reduction algorithm leaves the product $W W^T$ invariant.

The measurement residual, Δy, is defined by

$$\Delta y(t) = y(t) - y(\hat{x}, t) \tag{38}$$

where $y(t)$ = measured value

$y(\hat{x}, t)$ = the computed value of the measurement based on the current estimate of state indicated by the output of the navigation equations.

It is assumed that the residual is related to the error state by

$$y(t) = H\, dx(t) + q \tag{39}$$

where

q = the random error in the measurement

Since we may have an estimate of dx given by $d\hat{x}$ from other measurements, we write Eq. (39) as

$$\Delta y = y(t) - H\, d\hat{x}(t) = H\, d\tilde{x}(t) + q \tag{40}$$

= our best estimate of the residual including any past measurements whose effect is not yet included in the estimate of state carried by the navigation equations

As was mentioned in the beginning of this section, the filter operates with the reference time t_k for measurements in the interval t_k to t_{k+1}. This means that we estimate $d\hat{x}(t_k)$ rather than $d\hat{x}(t)$. Hence we make the assumption for $t_k < t < t_{k+1}$ that

$$d\tilde{x}(t) = \Phi(t;t_k)\, d\tilde{x}(t_k) \tag{41}$$

Equation (40) can then be written as

$$\Delta y = y(t) - H\, \Phi(t;t_k)\, d\hat{x}(t_k) \tag{42}$$

One may note that Eqs. (41) and (33) are in disagreement since the influence of the random forcing function, $u(t_k)$, is ignored in Eq. (41). The effect of this simplification is that measurements are not quite optimally weighted. Experience has shown that this simplification is justified if the batch interval $\Delta_k = t_{k+1} - t_k$ is short compared to natural periods of INS error growth (e.g., the Schuler period).

We let

$$\begin{aligned} H_m &= H\, \Phi(t;t_k) \\ K_m &= W(t_k)\, W(t_k)^T\, H_m^T \,/\, (H_m\, W(t_k)\, W(t_k)^T\, H_m^T + Q) \\ Q &= \mathcal{E}[q^2] \end{aligned} \tag{43}$$

Then the estimate of the error state following inclusion of the measurement is

$$d\hat{x}(t_k)_a = d\hat{x}(t_k)_b + K_m \Delta y \tag{44}$$

In Eq. (44), the subscript notation $(\,)_b$ and $(\,)_a$ means before and after inclusion of the measurement, respectively.

The square root covariance matrix, $W(t_k)^T$, after inclusion of the measurement is given by

$$W(t_k)_a^T = W(t_k)_b^T - \zeta \eta^T / \varkappa \tag{45}$$

where

$$\zeta = W(t_k)_b^T H_m^T$$

$$\eta = W(t_k)_b \zeta$$

$$\varkappa = (\zeta^T \zeta + Q)\left(1 + \sqrt{Q/(\zeta^T \zeta + Q)}\right)$$

Equation (45) is referred to as Potter's algorithm (see Ref. 3).

In order to minimize the number of measurement operations, we will use accumulated residuals over about a one-second period. This means that the residual, $\Delta y(t)$ of Eq. (38), is the accumulated residual for all the measurements of the same type in a half-second interval. The partials of the observations with respect to the error state, H of Eq. (43), are calculated and accumulated simultaneously with the residual accumulation. The Q of Eq. (43) is the assumed variance of the random noise in the accumulated residual sum.

C. Error Model of the Estimated Variables

We choose for our aircraft error state a vector of 15 variables. These are:

$\tilde{R}$ error in position (3)

$\dot{\tilde{R}}$ error in velocity (3)

$\tilde{\omega}$ gyro drift rate (3)

$\tilde{y}$ bias error in observables (3)

$\ddot{\tilde{z}}$ vertical accelerometer scale factor error (1)

$\tilde{w}$ error in the horizontal wind (2)

These prove sufficient to maintain a stable continuous estimate of the aircraft state, and to provide the Autoland guidance equations and pilot displays with usable information over long time periods (several hours).

The time history of the 15-dimensioned error vector is described by differential equations. The derivative of the position error vector $\tilde{R}(t)$ is given by

$$\frac{d}{dt}\,\tilde{R}(t) = \dot{\tilde{R}} \tag{46}$$

Let the specific force in the runway frame be $\{f\}_I$ which is given by

$$\{f\}_I = L_{IB}(\hat{\sigma}, \hat{\theta}, \hat{\phi})\,\{f_{SFB}\} \tag{47}$$

The error in the inertial specific force is given by

$$\{\tilde{f}\}_I = \{\tilde{\omega}\} \times \{f\}_I + L_{IB} \begin{Bmatrix} 0 \\ 0 \\ \ddot{\tilde{z}} \end{Bmatrix} \tag{48}$$

The differential equation for the error velocity vector is given by

$$\frac{d}{dt}\dot{\tilde{R}} = \{\tilde{f}\}_I + \{\varepsilon\}_{\dot{\tilde{R}}} \tag{49}$$

where $\{\varepsilon\}_{\dot{\tilde{R}}}$ is white noise.

The three gyro drifts, the three sensor biases, the horizontal wind components, and the vertical accelerometer scale factor are described as exponentially correlated random variables, and their differential equations are

$$\frac{d}{dt}\tilde{x}_i = -\frac{1}{\tau_i}\tilde{x}_i + \sigma_i\sqrt{\frac{2}{\tau_i}}\,\varepsilon_i \qquad i = 7, 15 \tag{50}$$

where τ_i is the correlation time constant, σ_i is the variance, and ε_i is white noise.

The solution of the above equations, for the short time span of the filter update, is given by

$$\begin{aligned}
\tilde{R}(t+\Delta t) &= \tilde{R}(t) + \dot{\tilde{R}}(t)\,\Delta t + \{\tilde{f}\}_I\frac{\Delta t^2}{2} \\
\dot{\tilde{R}}(t+\Delta t) &= \dot{\tilde{R}}(t) + \{\tilde{f}\}_I\Delta t + \{\varepsilon\}_{\dot{\tilde{R}}}\,\Delta t \\
\{\tilde{x}_i(t+\Delta t)\} &= \left\{e^{-(\Delta t/\tau_i)}\tilde{x}_i(t)\right\} + \left\{\sigma_i\,\varepsilon_i\sqrt{\frac{2\,\Delta t}{\tau_i}}\right\} \qquad i = 7, 15
\end{aligned} \tag{51}$$

Equation (51) provides the elements for the state transition matrices $\Phi(t_{k+1}, t_k)$ and $\Phi_u(t_{k+1}, t_k)$. These are listed in Tables 2 and 3.

TABLE 2

STATE TRANSITION MATRIX

Nonzero Elements

$$\Phi_{1,1} = 1 \qquad \Phi_{1,4} = \Delta t \qquad \Phi_{1,8} = f_z \frac{\Delta t^2}{2} \qquad \Phi_{1,9} = -f_y \frac{\Delta t^2}{2}$$

$$\Phi_{2,2} = 1 \qquad \Phi_{2,5} = \Delta t \qquad \Phi_{2,7} = -f_z \frac{\Delta t^2}{2} \qquad \Phi_{2,9} = f_x \frac{\Delta t^2}{2}$$

$$\Phi_{3,3} = 1 \qquad \Phi_{3,6} = \Delta t \qquad \Phi_{3,7} = f_y \frac{\Delta t^2}{2} \qquad \Phi_{3,8} = -f_x \frac{\Delta t^2}{2} \qquad \Phi_{3,15} = \frac{\Delta t^2}{2}$$

$$\Phi_{4,4} = 1 \qquad \Phi_{4,8} = f_z \Delta t \qquad \Phi_{4,9} = -f_y \Delta t$$

$$\Phi_{5,5} = 1 \qquad \Phi_{5,7} = -f_z \Delta t \qquad \Phi_{5,9} = f_x \Delta t$$

$$\Phi_{6,6} = 1 \qquad \Phi_{6,7} = f_y \Delta t \qquad \Phi_{6,8} = -f_x \Delta t \qquad \Phi_{6,15} = \Delta t$$

$$\Phi_{7,7} = e^{-(\Delta t/\tau_\omega)} \qquad \Phi_{8,8} = e^{-(\Delta t/\tau_\omega)} \qquad \Phi_{9,9} = e^{-(\Delta t/\tau_\omega)}$$

$$\Phi_{10,10} = e^{-(\Delta t/\tau_{Az})} \qquad \Phi_{11,11} = e^{-(\Delta t/\tau_{E\ell})} \qquad \Phi_{12,12} = e^{-(\Delta t/\tau_{RG})}$$

$$\Phi_{13,13} = e^{-(\Delta t/\tau_x)} \qquad \Phi_{14,14} = e^{-(\Delta t/\tau_y)} \qquad \Phi_{15,15} = e^{-(\Delta t/\tau_z)}$$

TABLE 3

SQUARE ROOT PROCESS NOISE MATRIX

Nonzero Elements

$$\Phi_{u_{4,1}} = \sigma_v \Delta t \qquad \Phi_{u_{5,2}} = \sigma_v \Delta t \qquad \Phi_{u_{6,3}} = \sigma_v \Delta t$$

$$\Phi_{u_{7,4}} = \sigma_\omega \sqrt{\frac{2\,\Delta t}{\tau_\omega}} \qquad \Phi_{u_{8,5}} = \sigma_\omega \sqrt{\frac{2\,\Delta t}{\tau_\omega}} \qquad \Phi_{u_{9,6}} = \sigma_\omega \sqrt{\frac{2\,\Delta t}{\tau_\omega}}$$

$$\Phi_{u_{10,7}} = \sigma_{Az} \sqrt{\frac{2\,\Delta t}{\tau_{Az}}} \qquad \Phi_{u_{11,8}} = \sigma_{E\ell} \sqrt{\frac{2\,\Delta t}{\tau_{E\ell}}} \qquad \Phi_{u_{12,9}} = \sigma_{RG} \sqrt{\frac{2\,\Delta t}{\tau_{RG}}}$$

$$\Phi_{u_{13,10}} = \sigma_{\omega x} \sqrt{\frac{2\,\Delta t}{\tau_x}} \qquad \Phi_{u_{14,11}} = \sigma_{\omega y} \sqrt{\frac{2\,\Delta t}{\tau_y}} \qquad \Phi_{u_{15,12}} = \sigma_{\omega z} \sqrt{\frac{2\,\Delta t}{\tau_z}}$$

D. Kalman Filter Data Updates

The guidance and control functions require smooth and current data corrected for the errors listed above. Since the Kalman filter updates the aircraft corrections every second, ΔT_s, and the dead reckoning estimates of Eq. (31) are updated every .05 seconds, ΔT, the corrections to the dead reckoning estimates are smoothed and updated as follows:

Let the Kalman correction vector of $\bar{R}(t)$ and $\dot{\bar{R}}(t)$ be $\hat{\Delta x}(t)$. We define an exponential smoother, a six-element vector function, $CS(t)$, to be given by

$$CS(t+\Delta T) = e^{-(\Delta T/\Delta T_s)} [CS(t) - \hat{\Delta x}(T_s)] + \hat{\Delta x}(T_s) \qquad (52)$$

$$\text{with } CS(0) = 0$$

The corrected, smoothed values of the $\bar{R}(t)$ and $\dot{\bar{R}}(t)$ vectors are given by

$$\begin{aligned} \hat{R}(t) &= \bar{R}(t) + CS_R(t) \\ \dot{\hat{R}}(t) &= \dot{\bar{R}}(t) + CS_{\dot{R}}(t) \end{aligned} \qquad (53)$$

To correct for the gyro drifts, we have the following:

Let $\hat{\Delta p}$, $\hat{\Delta q}$, and $\hat{\Delta r}$ be the current best estimates of the gyro drift rates and let $\bar{\Psi}$, $\bar{\theta}$, and $\bar{\phi}$ be current readout of the uncorrected Euler angles. Then, to obtain the best estimates of the Euler angles, we have

$$
\begin{aligned}
\hat{\phi}(t) &= \bar{\phi}(t) + [\cos \bar{\Psi}(t)\, \hat{\Delta p}(t) + \sin \bar{\Psi}(t)\, \hat{\Delta q}(t)]/\cos \bar{\theta}(t) \\
\hat{\theta}(t) &= \bar{\theta}(t) + \cos \bar{\Psi}(t)\, \hat{\Delta q}(t) - \sin \bar{\Psi}(t)\, \hat{\Delta p}(t) \\
\hat{\Psi}(t) &= \bar{\Psi}(t) + \hat{\Delta r} + [\hat{\phi}(t) - \bar{\phi}(t)] \sin \bar{\theta}(t) \\
\hat{\sigma}(t) &= \hat{\Psi}(t) - \Psi_R
\end{aligned}
\tag{54}
$$

Finally, to obtain the best estimate of acceleration vector in the runway frame, we have

$$
\ddot{\hat{R}}(t) = \begin{Bmatrix} 0 \\ 0 \\ G \end{Bmatrix} + L_{IB}(\hat{\sigma}, \hat{\theta}, \hat{\phi})\, \{f_{SFB}\} + \begin{Bmatrix} 0 \\ 0 \\ \ddot{\hat{\Delta z}} \end{Bmatrix} \tag{55}
$$

where $\ddot{\hat{\Delta z}}$ is the best estimate of the bias in the vertical accelerometer.

E. Complementary Filter

A complementary filter can be designed to provide a set of nonvarying gains, without any relationship to the uncertainty in the aircraft state or the biases in the INS and MLS measurements. By adjusting the complementary filter gains to pass the relative low frequency of the true aircraft acceleration, it is possible to filter out the high frequency noise in the MLS measurements. The main criterion for such a filter is to provide a stable estimator, one that decays disturbances exponentially and lets the low frequency motions persist. A block diagram of the complementary filter is shown in Fig. 8.

Let one of the coordinates of the $\hat{R}(t)$ vector be $\hat{x}_i(t)$. The differential equations of the complementary filter for the $\hat{x}_i$ coordinate are given by

COMPLEMENTARY FILTER FOR NAVIGATION WITH
BODY MOUNTED ACCELEROMETERS
USING MLS MEASUREMENTS

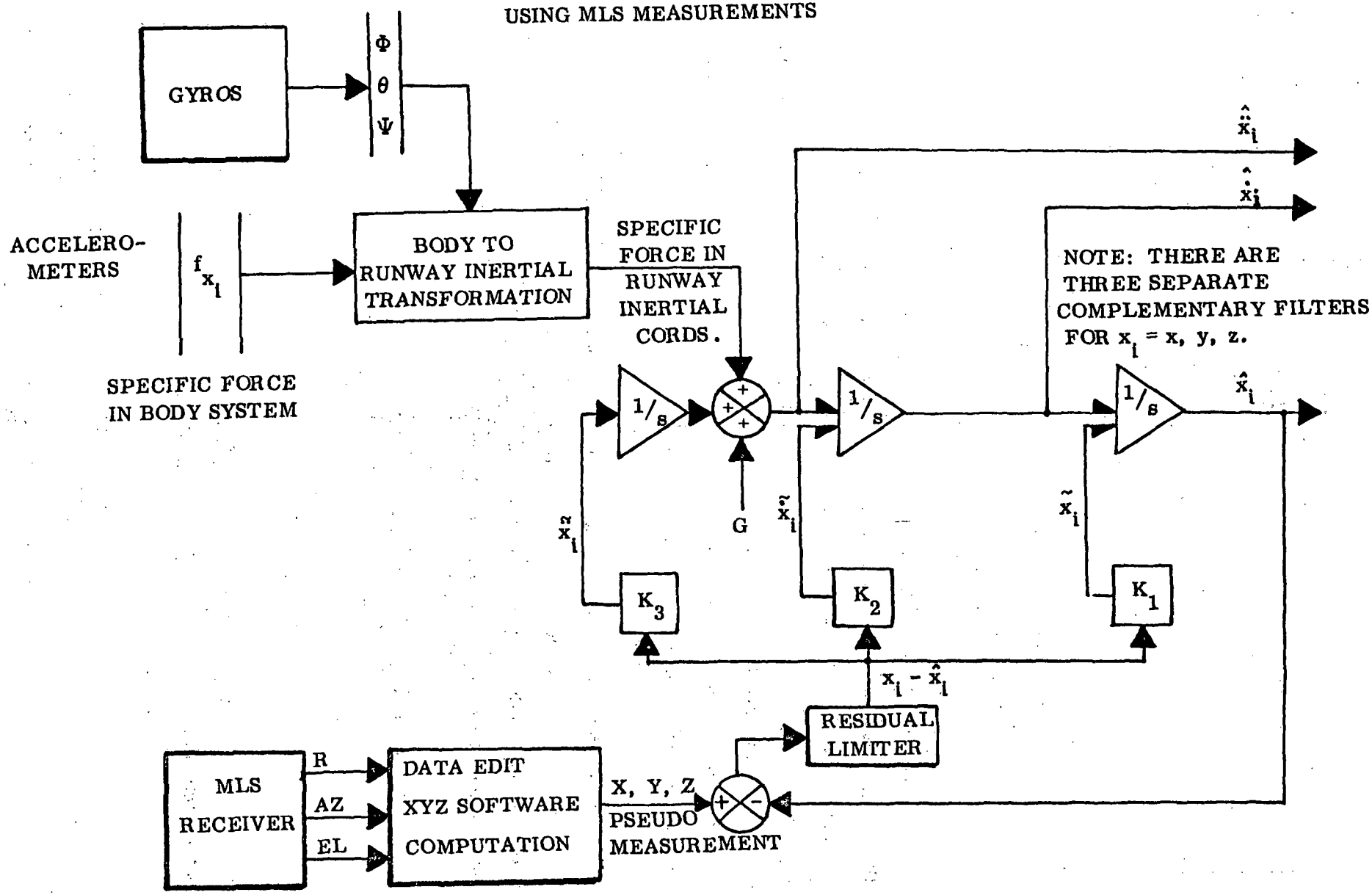

Figure 8. Complementary Filter for Navigation With Body-Mounted Accelerometers Using MLS Measurements

$$\frac{d}{dt}\hat{x}_{i1}(t) = K_1[x_{MLS_i} - \hat{x}_{i1}(t)] + \hat{x}_{i2}(t)$$

$$\frac{d}{dt}\hat{x}_{i2}(t) = K_2[x_{MLS_i} - \hat{x}_{i1}(t)] + \hat{x}_{i3}(t) + \ddot{\bar{x}}_i(t) \qquad (56)$$

$$\frac{d}{dt}\hat{x}_{i3}(t) = K_3[x_{MLS_i} - \hat{x}_{i1}(t)]$$

where

$$\ddot{\bar{x}}_i(t) = i^{th} \text{ component of } \ddot{\bar{R}}(t) \quad [\text{Eq. (30)}]$$

It is plain that if the residual $x_{MLSi} - \hat{x}_{i1}(t)$ is zero, the complementary filter will provide the dead reckoning solution of the aircraft motion in the runway system. Moreover, the system is linear with constant coefficients K_1, K_2, and K_3 (the filter gains), with nonhomogeneous forcing functions due to the noisy MLS measurements, and the aircraft measurement of acceleration obtained from the gyros and accelerometers. By choosing the values of K_1, K_2, and K_3, the solution can be designed to be stable and to filter out the high frequency noise.

Since the MLS measurements are available only in a discrete form at fixed intervals and the output of the accelerometers are available at fixed intervals, we may produce a pseudo MLS measurement which is continuous and is equal to the actual MLS measurement at the discrete sampling time.

We model $\bar{x}_{MLS_i}(t)$, the pseudo MLS, to be:

$$\bar{x}_{MLS_i}(t) = \bar{x}_{MLS_i}(t_o) + \hat{x}_{i2}(t_o)(t-t_o) + [\ddot{\bar{x}}_i(T) + \hat{x}_{i3}(t_o)]\frac{(t-t_o)^2}{2} \qquad (57)$$

We choose $\bar{x}_{MLS_i}(t_o)$ so that at $t = T$, the observation time, the pseudo MLS is the same as the observed MLS.

$$\bar{x}_{MLS_i}(t_o) = x_{obs_i}(T) - \hat{x}_{i2}(t_o)\Delta T - [\ddot{\bar{x}}_i(T) + \hat{x}_{i3}(t_o)]\frac{\Delta T^2}{2} \tag{57a}$$

With this definition of the MLS measurement, we can effect an explicit solution of the system of differential equations [Eqs. (56)] which has the required condition of giving the dead reckoning solution if the residual is zero, and which corrects the state to match the MLS observations without the high frequency component. The solution is given by

$$\begin{aligned}
\hat{x}_{i1}(T) &= \hat{x}_{i1}(t_o) + \hat{x}_{i2}(t_o)\Delta T + [\ddot{\bar{x}}_i(T) + \hat{x}_{i3}(t_o)]\frac{\Delta T^2}{2} + b_1[\bar{x}_{MLS_i}(t_o) - x_{i1}(t_o)] \\
\hat{x}_{i2}(T) &= \hat{x}_{i2}(t_o) + [\ddot{\bar{x}}_i(T) + \hat{x}_{i3}(t_o)]\Delta T + b_2[\bar{x}_{MLS_i}(t_o) - x_{i1}(t_o)] \\
\hat{x}_{i3}(T) &= \hat{x}_{i3}(t_o) + b_3[\bar{x}_{MLS_i}(t_o) - x_{i1}(t_o)]
\end{aligned} \tag{58}$$

where the constants b_1, b_2, and b_3 are functions of K_1, K_2, K_3, and ΔT.

$$\begin{aligned}
b_1 &= \left(\begin{array}{l} \alpha^2 e^{-\alpha\Delta T} + [\omega^2 + \beta^2 - 2\alpha\beta] e^{-\beta\Delta T} \cos(\omega\Delta T) \\ + [\alpha(\beta^2 - \omega^2) - \beta(\beta^2 + \omega^2)] e^{-\beta\Delta T} \sin(\omega\Delta T)/\omega \end{array} \right) \frac{1}{\alpha^2 + \omega^2 + \beta^2 - 2\alpha\beta} \\
b_2 &= \left(\begin{array}{l} 2\alpha^2\beta[e^{-\alpha\Delta T} - e^{-\beta\Delta T}\cos(\omega\Delta T)] \\ + [\alpha^2(\beta^2 - \omega^2) - (\omega^2 + \beta^2)^2] e^{-\beta\Delta T} \sin(\omega\Delta T)/\omega \end{array} \right) \frac{1}{\alpha^2 + \omega^2 + \beta^2 - 2\alpha\beta} \\
b_3 &= K_3 \left(\begin{array}{l} \alpha[e^{-\alpha\Delta T} - e^{-\beta\Delta T}\cos(\omega\Delta T)] \\ - [\omega^2 + \beta^2 - \alpha\beta] e^{-\beta\Delta T} \sin(\omega\Delta T)/\omega \end{array} \right) \frac{1}{\alpha^2 + \omega^2 + \beta^2 - 2\alpha\beta}
\end{aligned} \tag{59}$$

The constants, α, β, ω are the roots of the characteristic equation of the system defined by Eqs. (56)

$$(S+\alpha)(S+\beta-i\omega)(S+\beta+i\omega) = S^3 + K_1 S^2 + K_2 S + K_3 = 0$$

$$\begin{aligned} K_1 &= \alpha + 2\beta \\ K_2 &= 2\alpha\beta + \beta^2 + \omega^2 \\ K_3 &= \alpha(\beta^2 + \omega^2) \end{aligned} \tag{60}$$

By choosing small positive values of α, β, and ω we can obtain a stable low pass filter. We recommend values of

$$\begin{aligned} \alpha &= .08 \\ \beta = \omega &= \frac{\alpha}{\sqrt{2}} \end{aligned} \tag{61}$$

To provide the best estimates of the aircraft position, velocity, and acceleration in the runway frame using the complementary filter output, we have

$$\begin{aligned} \hat{R}(t) &= \begin{Bmatrix} \hat{x}_{11}(T) \\ \hat{x}_{21}(T) \\ \hat{x}_{31}(T) \end{Bmatrix} \\ \dot{\hat{R}}(t) &= \begin{Bmatrix} \hat{x}_{12}(T) \\ \hat{x}_{22}(T) \\ \hat{x}_{32}(T) \end{Bmatrix} \\ \ddot{\hat{R}}(t) &= \begin{Bmatrix} \hat{x}_{13}(T) \\ \hat{x}_{23}(T) \\ \hat{x}_{33}(T) \end{Bmatrix} + \ddot{\bar{R}}(t) \end{aligned} \tag{62}$$

It is to be noted that the complementary filter provides no correction to the errors in the estimates of aircraft attitude due to gyro drift or to the position error due to MLS biases.

III. THE MLS OBSERVABLES

The characteristics of the MLS observables are described in documents supplied by NASA Langley Research Center. The system used is for conical coordinates of azimuth, β, elevation, α, and range. The range and azimuth origin is at the center of azimuth antenna facing outward toward the approaching aircraft along the runway centerline. The elevation origin is offset from the runway and is at the center of the elevation antenna. Thus, the Cartesian coordinate system for the MLS observable is the negative of the runway inertial system in the x and z directions and in the same direction as the y of the runway. We have, in the runway coordinate system

$$\begin{bmatrix} x \\ y \\ z \end{bmatrix}_{\text{MLS}} = - \begin{bmatrix} x \\ -y \\ z \end{bmatrix}_{\text{Runway}} + \begin{bmatrix} x \\ -y \\ z \end{bmatrix}_{\text{Antenna}} \tag{63}$$

where the antenna vector specifies the azimuth antenna position in the runway system. The origin of the MLS system is at the azimuth antenna and the position of the elevation antenna is measured relative to it. (See Fig. 9a)

Let the MLS coordinates of the aircraft be X_M, Y_M, Z_M. Then the observables in the MLS coordinate system are

$$\begin{aligned} \text{RANGE} &= \sqrt{X_M^2 + Y_M^2 + Z_M^2} \\ \beta &= \sin^{-1}(-Y_M / \text{RANGE}) \\ \alpha &= \sin^{-1} \frac{Z_M - Z_{OE}}{\sqrt{(X_M - X_{OE})^2 + (Y_M - Y_{OE})^2 + (Z_M - Z_{OE})^2}} \end{aligned} \tag{64}$$

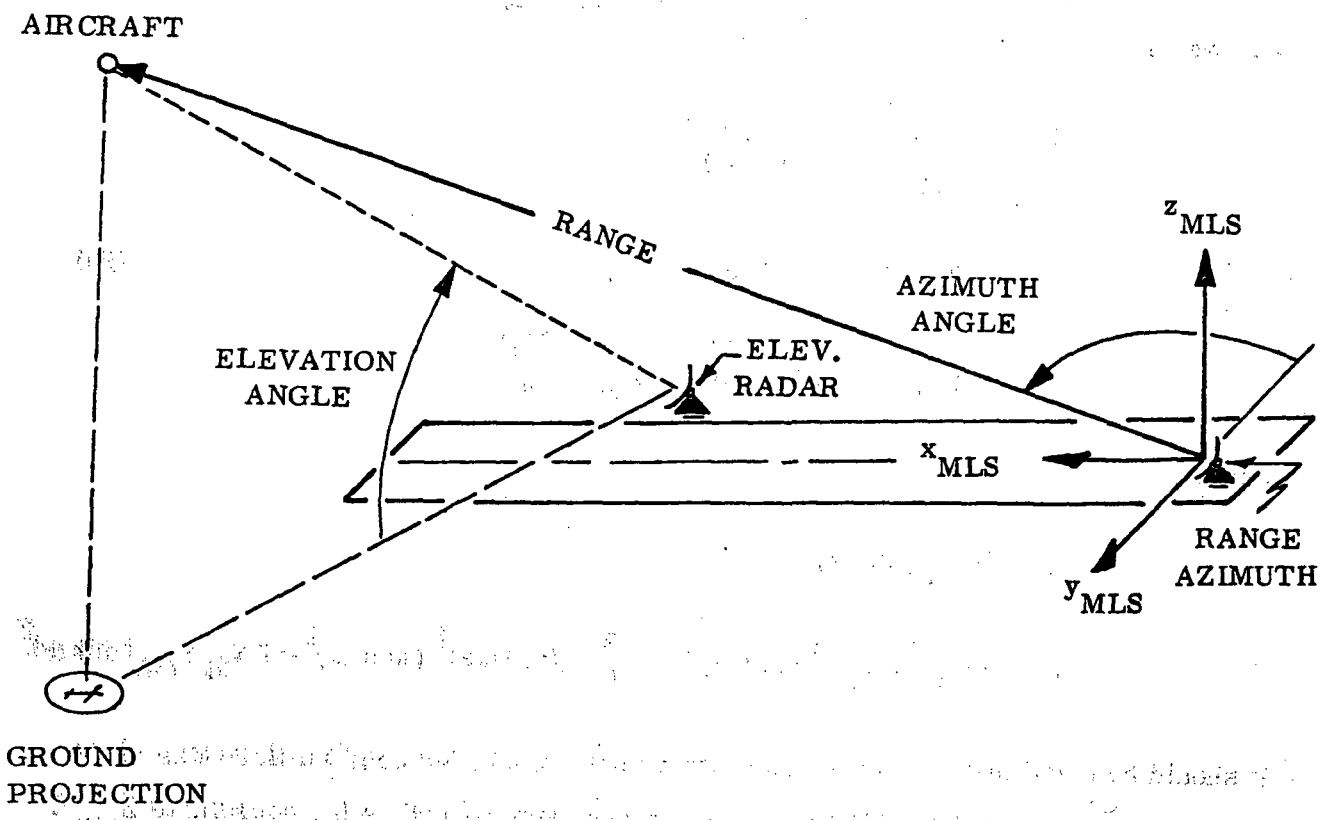

Figure 9(a). The MLS Coordinate System.

In the above, X_{OE} and Y_{OE} are the coordinates of the elevation antenna from the azimuth origin, and Z_{OE} is the coordinate of the elevation antenna in the MLS system.

To invert the solution and obtain X_M, Y_M, Z_M from RANGE, β, and α, we have

$$X_M = g + \sqrt{g^2 - h}$$

$$Y_M = - \text{RANGE} (\sin \beta) \tag{65}$$

$$Z_M = \sqrt{(\text{RANGE})^2 - X_M^2 - Y_M^2}$$

where

$$g = X_{OE} (\sin \alpha)^2$$

$$h = (X_{OE}^2 + Y_{OE}^2)(\sin \alpha)^2 + Y_M^2 - (\text{RANGE})^2 (\cos \alpha)^2 - 2 Y_M Y_{OE} (\sin \alpha)^2$$

It should be noted that the above equations do not account for height differences of the elevation antenna from the MLS origin which has been defined as the coordinate Z_{OE}".

Finally, to obtain the aircraft coordinates in the runway inertial system, we have

$$\begin{bmatrix} x \\ y \\ z \end{bmatrix}_{\text{Runway}} = \begin{bmatrix} x \\ y \\ z \end{bmatrix}_{\text{Azimuth Ant.}} - \begin{bmatrix} x_M \\ -y_M \\ z_M \end{bmatrix} \tag{66}$$

A. MLS Noise Model

The noise characteristics are obtained from Ref. 5. For the exponential correlated noise of RANGE, β, and α, we have

$$\eta_{EL}(t) = \sigma_{EL}\sqrt{1-A_{EL}^2}\ u(t)+A_{EL}\ \eta_{EL}(t-1)$$

$$\eta_{AZ}(t) = \sigma_{AZ}\sqrt{1-A_{AZ}^2}\ u(t)+A_{AZ}\ \eta_{AZ}(t-1) \qquad (67)$$

$$\eta_{R}(t) = \sigma_{R}\sqrt{1-A_{R}^2}\ u(t)+A_{R}\ \eta_{AZ}(t-1)$$

where $u(t)$ is a random number of zero mean, σ_i is the standard deviation of the i^{th} measurement and

$$A_i = e^{-(\Delta T/T_i)} \qquad (68a)$$

For initialization

$$\eta_i(0) = u(0) \qquad (68b)$$

Table 4 contains the values of the noise characteristics used in the MLS error model.

To simulate data dropout, we use a random number with uniform distribution from -1 to 1 and set the observation equal to zero whenever the random number exceeds .98. Thus, 2% of each observation string is lost. Since there are three observation types, 6% of the pseudo state observations are lost. This percentage can be varied.

TABLE 4

MLS ERROR MODELS

Function	Model	A	$\alpha(\frac{1}{sec})$	Γ	u(n)
Elevation	$y(n) = \Gamma\sqrt{1 - A^2}\ u(n) + Ay(n-1)$	$e^{-\alpha T}$	19.100	7.01×10^{-2} Deg.	IGRS
Azimuth	$y(n) = \Gamma\sqrt{1 - A^2}\ u(n) + Ay(n-1)$	$e^{-\alpha T}$	0.971	5.10×10^{-3} Deg.	IGRS
Range	$y(n) = \Gamma\sqrt{1 - A^2}\ u(n) + Ay(n-1)$	$e^{-\alpha T}$	1.013	(21.1 Ft.) 6.431 Meters	IGRS

Note: IGRS = Independent Gaussian Random Sample

Initialization is achieved by setting $y(0) = u(0)$.

See Figures 9(c) and 9(d) for illustrations of MLS jitter in azimuth and elevation.

To simulate bad data, a similar random number with a uniform distribution is used, and an average percentage of the observations is set equal to a large number (1000 times the bias) even though the data valid flag is set true. Thus bad data enters the system marked good a small percentage of the time.

Biases are included in the simulation. Values of the biases are initially chosen from a random number generator and retained for the simulation run. The bias values are also given in Table 4.

MLS "jitter" or "stagger" is simulated to produce the data train sequence as shown on Figs. 9b, 9c, and 9d.

To accommodate data dropout, MLS invalids, and bad data generally, the recommended course of action is to replace the bad data type by the aircraft estimate of the data missing (or considered rejectable) by the best estimate of the data type based on the current values of the vehicle state. Thus, if data is missing, we replace the bad data by range, azimuth, or elevation from Eq. (64), using $\hat{X}_M$, $\hat{Y}_M$, and $\hat{Z}_M$ computed from Eq. (63). This mode is still under study.

B. Radar Altimeter

The radar altimeter readout is activated when the aircraft estimate of altitude is below 150 ft. The MLS elevation readout is simultaneously deactivated. For the purposes of this study, the error model of the radar altimeter is described by an exponentially correlated bias variable driven by white noise. Thus, the radar signal readout is given by

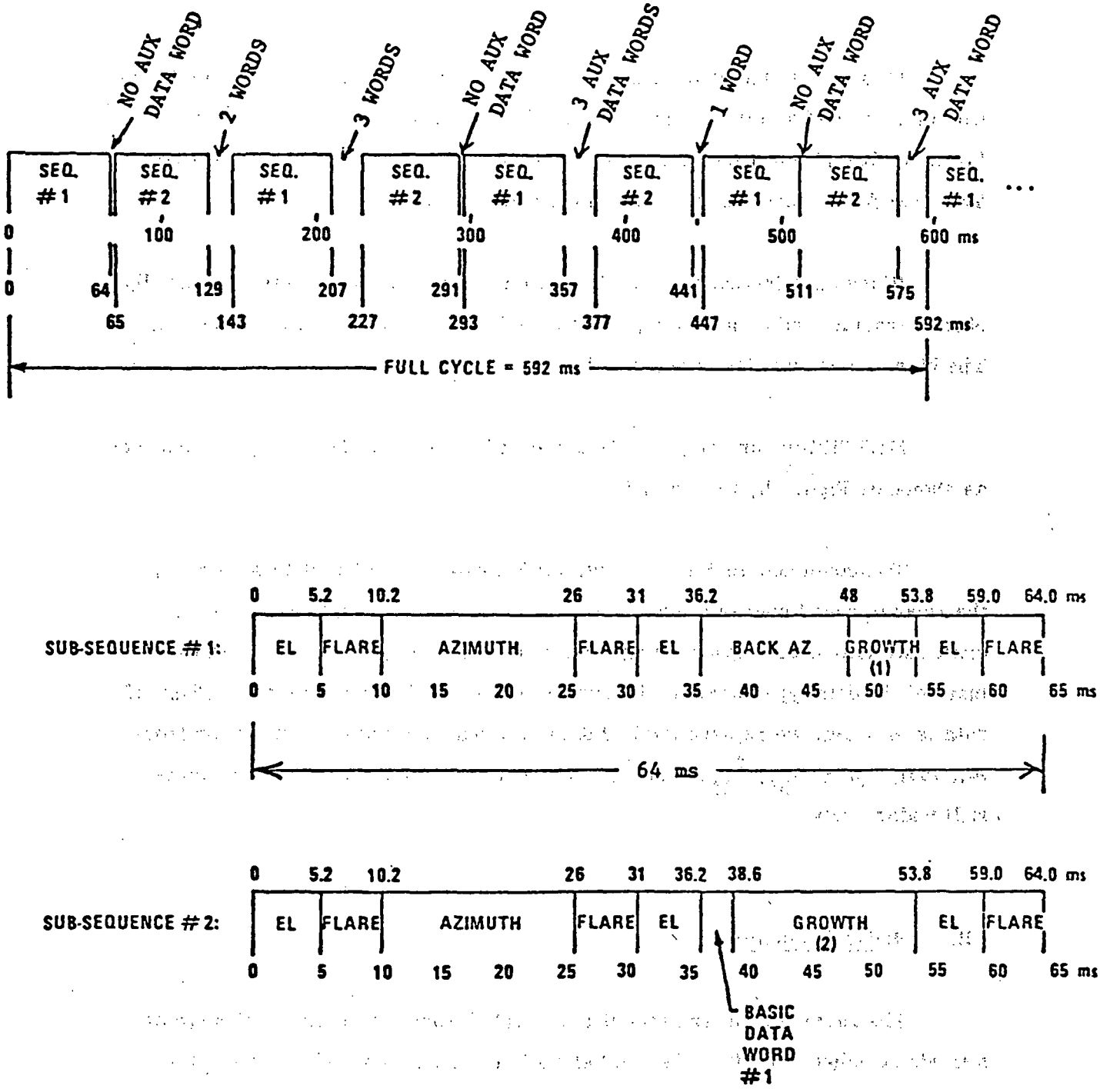

NOTES: (1) AUXILIARY DATA (1 WORD) OR BACK ELEVATION
(2) 360° AZIMUTH

Figure 9(b). MLS Conical Scan Time Sequence.

Figure 9(c). MLS Jitter, Azimuth

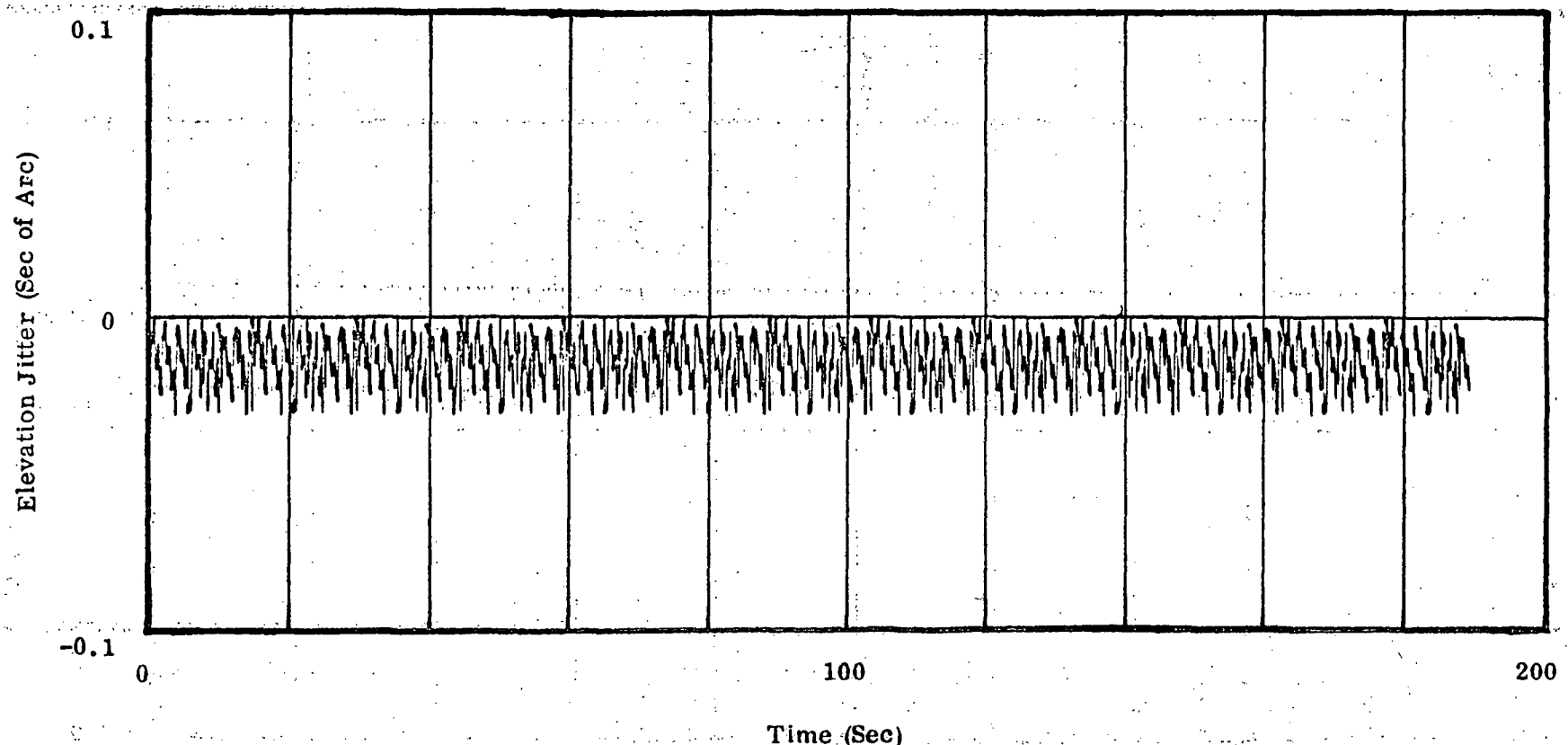

Figure 9(d). MLS Jitter, Elevation

$$h(t) = -z(t) + \tilde{b}_h(t) \tag{69}$$

where

$$\frac{d}{dt}\,\tilde{b}_h(t) = -\frac{\tilde{b}_h(t)}{\tau_h} + \sigma_h \sqrt{\frac{2}{\tau_h}}\;\varepsilon_h \tag{69a}$$

C. MLS Partials

The Kalman filter requires the partial derivatives of the MLS observables with respect to the 15 estimated variables.

We have, for the azimuth observable,

$$\frac{\partial \beta}{\partial x} = -\frac{X_M\, Y_M}{\text{RANGE}^2 \sqrt{X_M^2 + Z_M^2}}$$

$$\frac{\partial \beta}{\partial y} = -\frac{1}{\sqrt{X_M^2 + Z_M^2}} + \frac{Y_M^2}{\text{RANGE}^2 \sqrt{X_M^2 + Z_M^2}} \tag{70}$$

$$\frac{\partial \beta}{\partial z} = -\frac{Z_M\, Y_M}{\text{RANGE}^2 \sqrt{X_M^2 + Z_M^2}}$$

For the bias in azimuth, we have

$$\frac{\partial \beta}{\partial \tilde{b}_R} = 1 \tag{70a}$$

For the remaining 11 variables, we have

$$\frac{\partial \beta}{\partial x_i} = 0 \tag{70b}$$

The elevation observable is

$$\frac{\partial \alpha}{\partial x} = \frac{(Z_M - Z_{OE})(X_M - X_{OE})}{R_{OE}^2 \sqrt{(X_M - X_{OE})^2 + (Y_M - Y_{OE})^2}}$$

$$\frac{\partial \alpha}{\partial y} = -\frac{(Y_M - Y_{OE})(Z_M - Z_{OE})}{R_{OE}^2 \sqrt{(X_M - X_{OE})^2 + (Y_M - Y_{OE})^2}} \tag{71}$$

$$\frac{\partial \alpha}{\partial z} = \frac{1}{\sqrt{(X_M - X_{OE})^2 + (Y_M - Y_{OE})^2}} \left[-1 + \frac{(Z_M - Z_{OE})^2}{R_{OE}^2} \right]$$

where

$$R_{OE}^2 = (X_M - X_{OE})^2 + (Y_M - Y_{OE})^2 + (Z_M - Z_{OE})^2 \tag{71a}$$

For the bias in elevations, we have

$$\frac{\partial \alpha}{\partial b_\alpha} = 1 \tag{71b}$$

For the remaining 11 variables, we have

$$\frac{\partial \alpha}{\partial x_i} = 0 \tag{71c}$$

The range observable is

$$\frac{\partial \text{RANGE}}{\partial x} = \frac{X_M}{\text{RANGE}}$$

$$\frac{\partial \text{RANGE}}{\partial y} = \frac{Y_M}{\text{RANGE}} \tag{72}$$

$$\frac{\partial \text{RANGE}}{\partial z} = \frac{Z_M}{\text{RANGE}}$$

For the bias in range, we have

$$\frac{\partial \text{RANGE}}{\partial b_r} = 1 \tag{72a}$$

For the remaining 11 variables, we have

$$\frac{\partial \text{RANGE}}{\partial x_i} = 0 \tag{72b}$$

For the radar altimeter, we have

$$\frac{\partial h(t)}{\partial z} = 1 \tag{73}$$

For the altimeter bias, we have

$$\frac{\partial h(t)}{\partial \tilde{b}_h} = 1 \tag{73a}$$

For the remaining 13 variables, we have

$$\frac{\partial h(t)}{\partial x_i} = 0 \tag{73b}$$

IV. MAGNETIC LEADER CABLE SENSOR

While the MLS sensor described in the previous section proves adequate for landing approach through touchdown, problems in multipath distortion and other biases create serious problems against relying solely on the use of MLS in rollout and turnoff. In order to provide a navigation sensor aid with smaller errors, the concept of a single magnetic leader cable embedded along the centerline of the runway and along the turnoff lane is recommended.

Initial studies of such devices began in the 1960's. Reference 6 contains a description of a magnetic cable system and a three-coil sensor developed in England. A series of studies for use in automotive steering along reinforced concrete highway systems is presently sponsored by DOT. Reference 7 contains a description of such an automotive steering aid for lateral control.

For our purposes, the British system and experience seems to be more applicable and is incorporated into this report.

A. Three-Coil Sensor

The magnetic field is generated by a single conductor set beneath the nonconducting concrete and along the runway centerline. A detector, consisting of three coils having an equal number of windings of conducting wire with identical characteristics, is used to generate three voltages. The coils are mounted about a spherical, nonconductive shell in three perpendicular planes. Figure 10 illustrates the leader cable and the three coils.

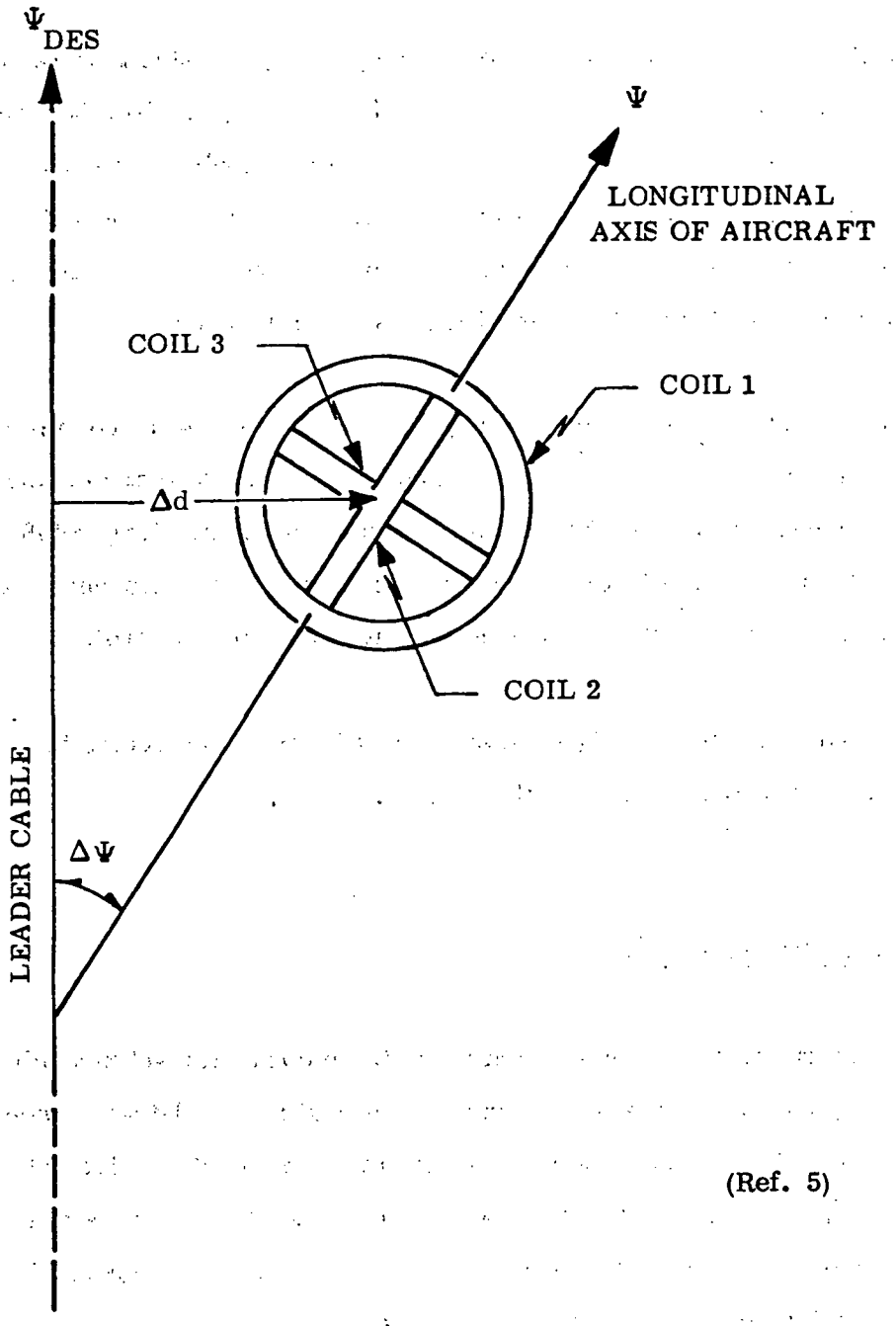

Figure 10. Magnetic Leader Voltage Signals.

Let the Cartesian components of the magnetic field be

$$H = (H_x, H_y, H_z) \tag{74}$$

as illustrated in Fig. 11. We have, for the three induced voltages,

$$\begin{aligned} v_1 &\cong H_z \\ v_2 &\cong H_y \cos(\Delta\Psi) \\ v_3 &\cong H_y \sin(\Delta\Psi) \end{aligned} \tag{75}$$

For the yaw deviation, we have

$$\tan(\Delta\Psi) \cong \frac{v_3}{v_2} \tag{76a}$$

and for the lateral displacement

$$\Delta d = \Delta z \frac{H_z}{H_y} \cong \Delta z \frac{v_1}{\sqrt{v_2^2 + v_3^2}} \tag{76b}$$

The error in yaw and the error in lateral displacement are directly obtainable from the voltages. To obtain the time rates of these quantities, which are required for damping stability in the Autoland guidance equations, we have chosen not to rely on differentiation of the magnetic coil signals, but to generate the required information analytically. The equations for these functions are given in the Guidance Section of this report.

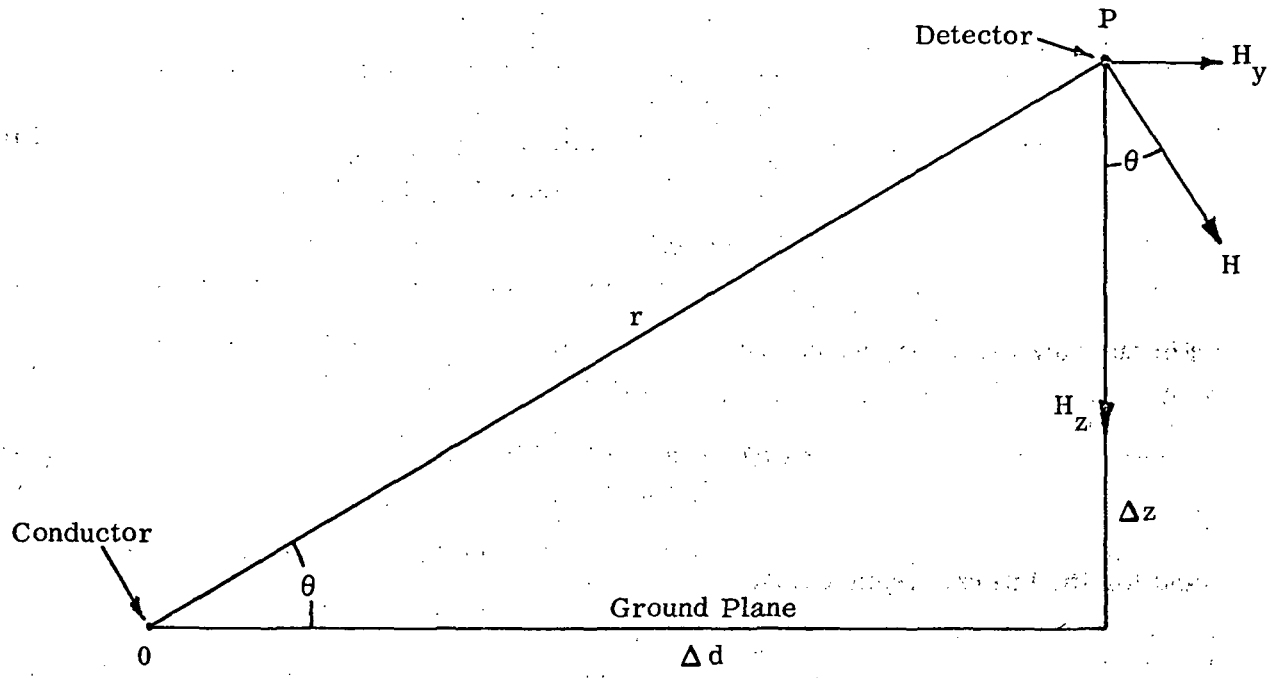

(Ref. 5)

Figure 11. Magnetic Field Equations.

B. Error Model of the Magnetic Coil Sensor

The distortion in signal strength is due to several sources, as shown in Refs. 6 and 7.

1. ground conduction
2. nonlinearity
3. phase modulation

The effect of ground conduction is described in Ref. 6. The effect is especially serious for concrete runways containing steel reinforcing rods. Reference 6 recommends using a low carrier frequency (165 Hz) to minimize the distortion effect due to ground conductivity.

Nonlinear effects are most troublesome in the lateral deviation equation where the linear relationship between Δd and Δz is relied upon in Eq. (76b). By restricting the use of the detector to rollout and turnoff, we are assured of operating within a narrow range of vertical displacement ($\pm$ 2 ft.) due to strut compression and pitch oscillations. Thus, we can expect to operate in a linear range during those phases of the flight where the magnetic cable is required.

Finally, phase modulation can be eliminated as a serious error source by restricting the use of the detector to small range in Δz. In general, none of the references indicated any difficulty in obtaining a good $\Delta\Psi$ signal.

For the purposes of simulating the error sources, the following equations were used to generate realistic magnetic measurements of $\Delta\Psi_M$ and

$$\Delta\Psi_M = \Delta\Psi_{true} + \varepsilon_{\Delta\Psi}$$

$$\Delta d_M = \Delta d_{true}(1 - .1 \cos \bar{\omega} t)\frac{z}{z_{nom}} + \varepsilon_{\Delta d} \tag{77}$$

where

$\varepsilon_{\Delta d}$, $\varepsilon_{\Delta\Psi}$ are white noise

$\bar{\omega}$ is the carrier frequency (165 Hz)

z_{nom} is the nominal height of the detector above ground and a fixed constant for the aircraft, for all landings

V. NONCRITICAL FLIGHT PHASE NAVIGATIONAL AIDS

In addition to the MLS Radar altimeter and the magnetic leader cable, which are required for the flight critical phases of landing approach, rollout, and turnoff, we include VORTAC range and bearing devices and a baro-altimeter as additional navigational aids for the noncritical phases of the aircraft flight regime. These instruments have relatively large bias errors. However, since they are used only for navigation between way points away from the terminal area, they can provide adequate control for the gyro drift and accelerometer scale factor error sources in conjunction with a Kalman filter.

A. VORTAC Range and Bearing

Let the VORTAC station coordinates be x_V, y_V, z_V in a level frame at the VORTAC station. The axes are: $\hat{x}_V$ due north; $\hat{y}_V$ due west; and $\hat{z}_V$ vertical, positive upward. Let the aircraft position in the VORTAC coordinate system be x_a, y_a, z_a. In the measured VORTAC range, we have

$$r_V = \sqrt{(x_a - x_V)^2 + (y_a - y_V)^2 + (z_a - z_V)^2} + b_r + \varepsilon_r \tag{78}$$

and for the measured VORTAC relative bearing

$$\Delta\Psi = \bar{\Psi} - \Psi_V = \tan^{-1} \frac{y_V - y_a}{x_a - x_V} + b_\Psi + \varepsilon_\Psi \tag{79}$$

To complete the triad, we obtain the barometer measurement of altitude

$$\bar{h}_V = -z_a + b_h + \varepsilon_h \tag{80}$$

In the above, b_r, b_Ψ, and b_h are biases modeled as exponentially correlated random errors and ε_r, ε_Ψ, and ε_h are white noise. The biases are modeled as follows:

$$\frac{d}{dt} b_r = -\frac{b_r}{\tau_r} + \sigma_r \sqrt{\frac{2}{\tau_r}} \eta_r$$

$$\frac{d}{dt} b_\Psi = -\frac{b_\Psi}{\tau_\Psi} + \sigma_\Psi \sqrt{\frac{2}{\tau_\Psi}} \eta_\Psi \qquad (81)$$

$$\frac{d}{dt} b_h = -\frac{b_h}{\tau_h} + \sigma_h \sqrt{\frac{2}{\tau_h}} \eta_h$$

where τ_r, τ_Ψ, and τ_h are the correlation times; σ_r, σ_Ψ, and σ_h are the variances; and η_r, η_Ψ, and η_h are white noise samples. (See Table 5)

To complete the necessary equations for the Kalman filter, we derive the partials of the three observables with respect to the 15-element state. For the range partials, we have

$$\frac{\partial r_V}{\partial x_a} = \frac{x_a - x_V}{r_V}$$

$$\frac{\partial r_V}{\partial y_a} = \frac{y_a - y_V}{r_V} \qquad (82a)$$

$$\frac{\partial r_V}{\partial z_a} = \frac{z_a - z_V}{r_V}$$

$$\frac{\partial r_V}{\partial b_r} = 1$$

TABLE 5

VORTAC ERROR MODEL

Variable	Time Constant	Variances	
		bias	observ.
Range	900 sec.	300 meters	40 meters
Bearing	900 sec.	0.7^{o}	0.7^{o}
Baro-altimeter	100 sec.	40 meters	40 meters

The other 11 partials are zero. For the bearing partials, we have

$$\frac{\partial \Delta\Psi}{\partial x_a} = \frac{y_a - y_V}{(x_a - x_V)^2 + (y_a - y_V)^2}$$

$$\frac{\partial \Delta\Psi}{\partial y_a} = \frac{x_a - x_V}{(x_a - x_V)^2 + (y_a - y_V)^2} \tag{82b}$$

$$\frac{\partial \Delta\Psi}{\partial b_\Psi} = 1$$

The other 12 partials are zero. For the barometer partials, we have

$$\frac{\partial h}{\partial z_a} = -1. \tag{82c}$$

$$\frac{\partial h}{\partial b_h} = 1.$$

The remaining 13 partials are zero.

VI. GUIDANCE AND CONTROL

The Langley TCV program utilizes a modified Boeing 737 aircraft for its research. It contains an automated guidance and control system for landing approach and rollout. The simulation of the guidance laws were supplied by the Langley Research Center. These laws utilize ILS navigation aids. In adapting the B-737 aircraft for the Kalman filter and the complementary filter utilizing MLS navigation aids and a magnetic cable for rollout and turnoff, certain changes had to be made to the Boeing Autoland guidance laws. The changes are outlined below:

1. The Boeing complementary filters were removed from the flight critical glideslope and localizer control laws.
2. Since no requirement for turnoff guidance existed in the original B-737 TCV aircraft, the Boeing rollout laws were modified to permit a uniform guidance law to hold for both rollout and turnoff.

In general, except for the above changes, the control laws, gains, etc. used in the Boeing Autoland equations were maintained.

This section contains guidance and control laws for the following phases:

1. Flight critical lateral control for oncourse landing approach.
2. Flight critical vertical control in landing approach for capture and flare.
3. Rudder control for landing and decrab.
4. Lateral control for noncritical level flight and coordinated banked turns.

5. Vertical control for noncritical level flight and descent.

6. Steering laws for rollout and turnoff.

A. Flight Critical Lateral Control Guidance

The flight critical lateral guidance contains two control functions, localizer engage and oncourse. These are triggered by deviation criteria computed from data supplied by the navigation filter and the desired glide slope path.

The computations required for these control modes are

$$
\begin{aligned}
\text{RANGE} &= \left[(x_L - \hat{x})^2 + \hat{y}^2 + \hat{z}^2\right]^{\frac{1}{2}} \\
\eta &= -\frac{\hat{y}}{\text{RANGE}}\frac{180}{\pi} \\
\dot{\eta} &= -\left\{\frac{\dot{\hat{y}}}{\text{RANGE}} - \frac{\hat{y}}{\text{RANGE}^3}\left[-\dot{\hat{x}}(x_L - \hat{x}) + \dot{\hat{y}}\hat{y} + \dot{\hat{z}}\hat{z}\right]\right\}\frac{180}{\pi} \\
h_r &= -\hat{z} - h_G \\
V &= (\dot{\hat{x}}^2 + \dot{\hat{y}}^2 + \dot{\hat{z}}^2)^{\frac{1}{2}} \\
\hat{\phi}_{deg} &= \hat{\phi}\frac{180}{\pi} \\
P_{deg} &= \hat{p}\frac{180}{\pi}
\end{aligned}
\tag{83}
$$

where h_G is the extended landing gear height (see Fig. 3).

The triggers for localizer engage and capture are

$$\text{L.E. is TRUE} \quad \text{if} \quad |\eta| < 2.5^{\circ}$$

$$\text{O/C is TRUE} \quad \text{if} \quad |\eta| < \eta_{LIM}, \; |\dot{\eta}| < .027^{\circ}/\text{sec.},$$

$$\text{and} \; |\hat{\phi}_{deg}| < 3.^{\circ}$$

Two block diagrams describe the flight critical lateral control mode. The first, Fig. 12, generates the aileron roll command signal as a function of the lateral deviation from the glide slope descent path. The second, Fig. 13, is the flight control lateral inner loop which generates the aileron command to the aileron servo.

It should be noted that the inner loop logic contains an input from the rudder decrab command, δ_{RDC}. The guidance logic for this input is given in Fig. 15 covering the rudder command signals.

B. Flight Critical Vertical Control Guidance

The flight critical vertical control guidance covers three modes: capture, capture plus 10 seconds, and flare. As in the case of the flight critical lateral control guidance, the inputs for these modes are generated by the navigation filter equations to control the vertical deviation from the glide slope trajectory.

The equations for the required inputs are given below:

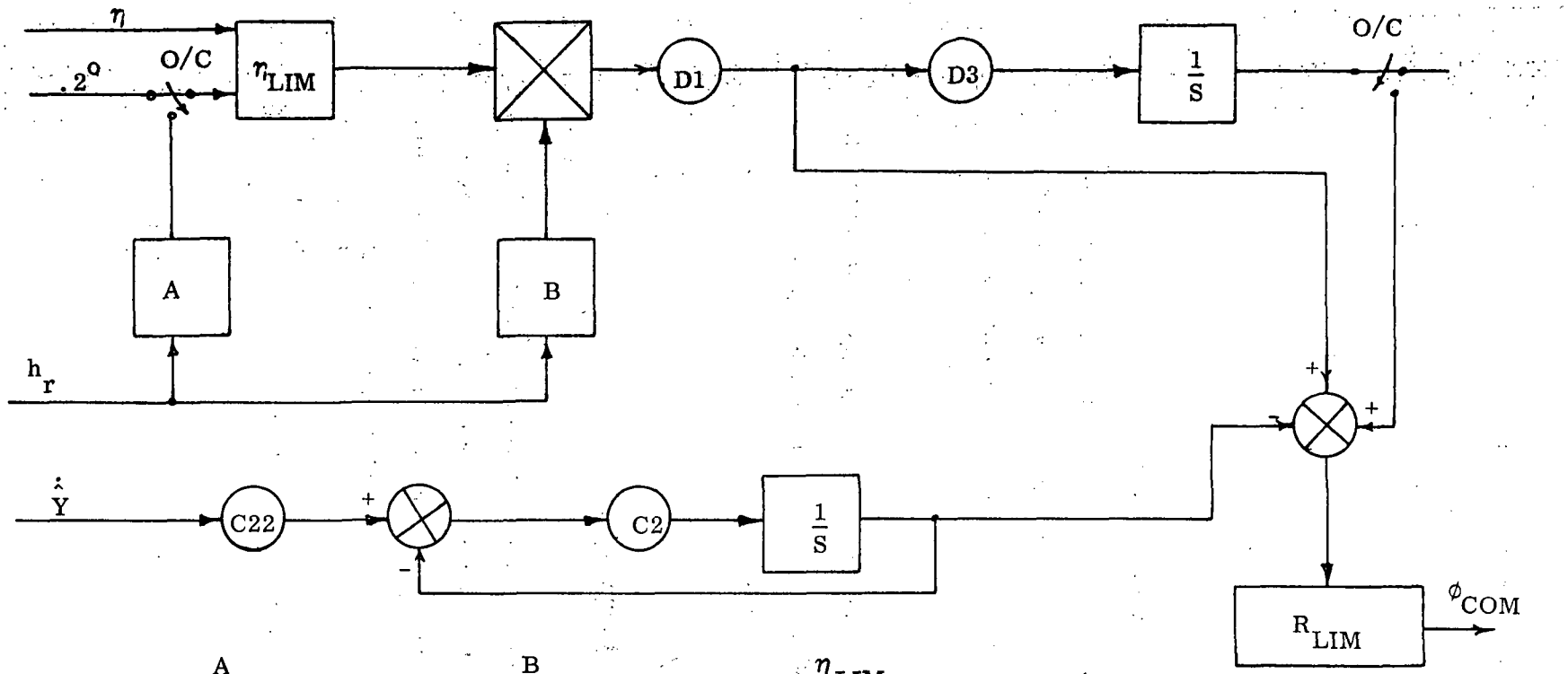

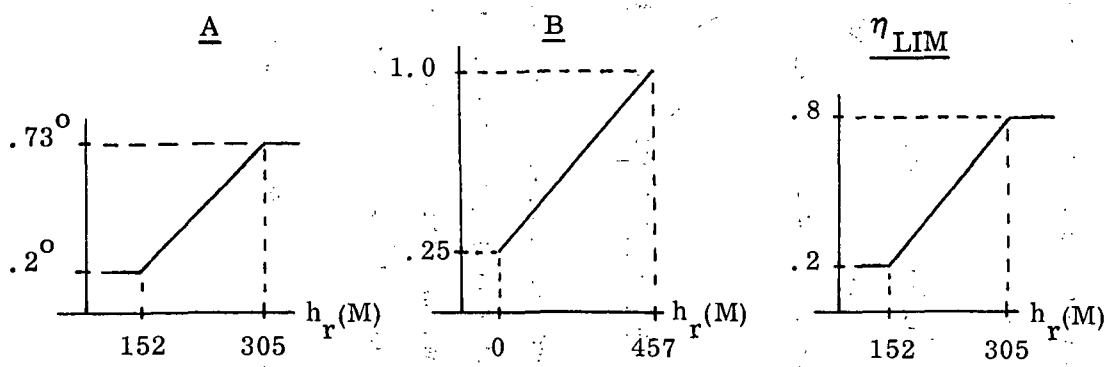

R LIM

L. E. = 25.
O/C = 10.
Flare = 5.

C22

L. E. = .706
O/C = .988

C2 = 2.5

D1 = 25.
D3 = .16

Figure 12. Flight Critical Lateral Roll Command

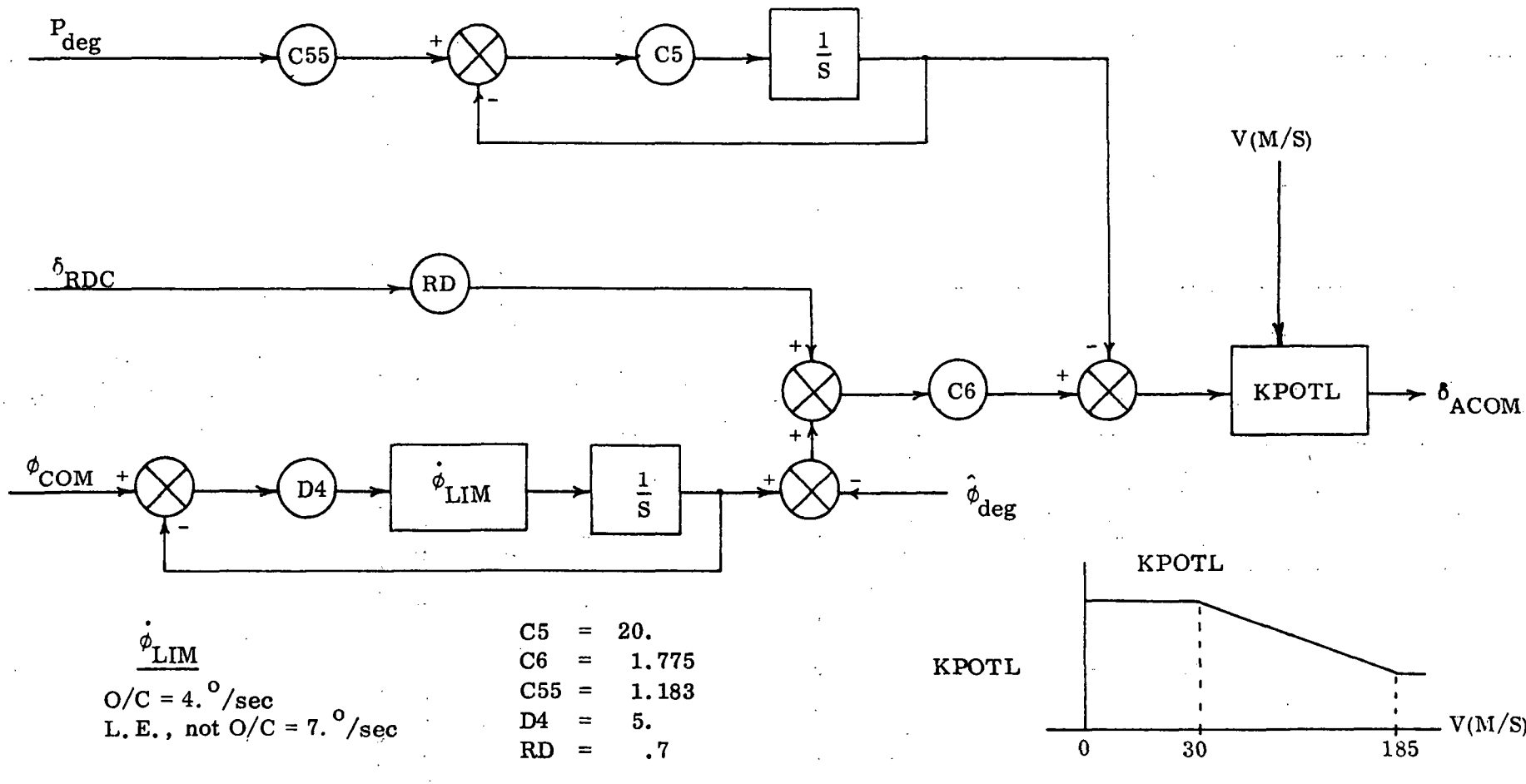

Figure 13. Flight Critical Lateral Inner Loop

$$
\begin{aligned}
\bar{\gamma} &= \text{glide slope flight path angle } (-3.^{o}) \\
\dot{h} &= -\dot{\hat{z}} \\
\ddot{h} &= -\ddot{\hat{z}} \\
RAN &= \left[(x_G - \hat{x})^2 + \hat{y}^2 + \hat{z}^2\right]^{\frac{1}{2}} \\
\beta_{GS} &= \sin^{-1}\left[\frac{(x_G - \hat{x})\sin\bar{\gamma} + \hat{z}\cos\bar{\gamma}}{RAN}\right] \\
Q_{deg} &= \hat{q}\,\frac{180}{\pi}
\end{aligned}
\tag{84}
$$

where x_G is the glide slope intercept with the runway ($x_G = 304.8$ meters)

The triggers for capture, capture plus ten seconds, and flare are given below:

C (capture) is TRUE if $|\beta_{GS}| < .108^{o}$

CP10 (capture plus 10 seconds) is TRUE ten seconds after C is actuated

F (flare) is TRUE if $.416(h_r + 15.) + 26\dot{h} \leq 0$

The block diagram for the flight critical vertical control guidance is shown in Fig. 14. The output of this control law is the elevator command.

C. Rudder Control for Landing and Decrab

The rudder control guidance contains two functions: first, to provide yaw damping during all phases of aircraft flight, including rollout and turnoff;

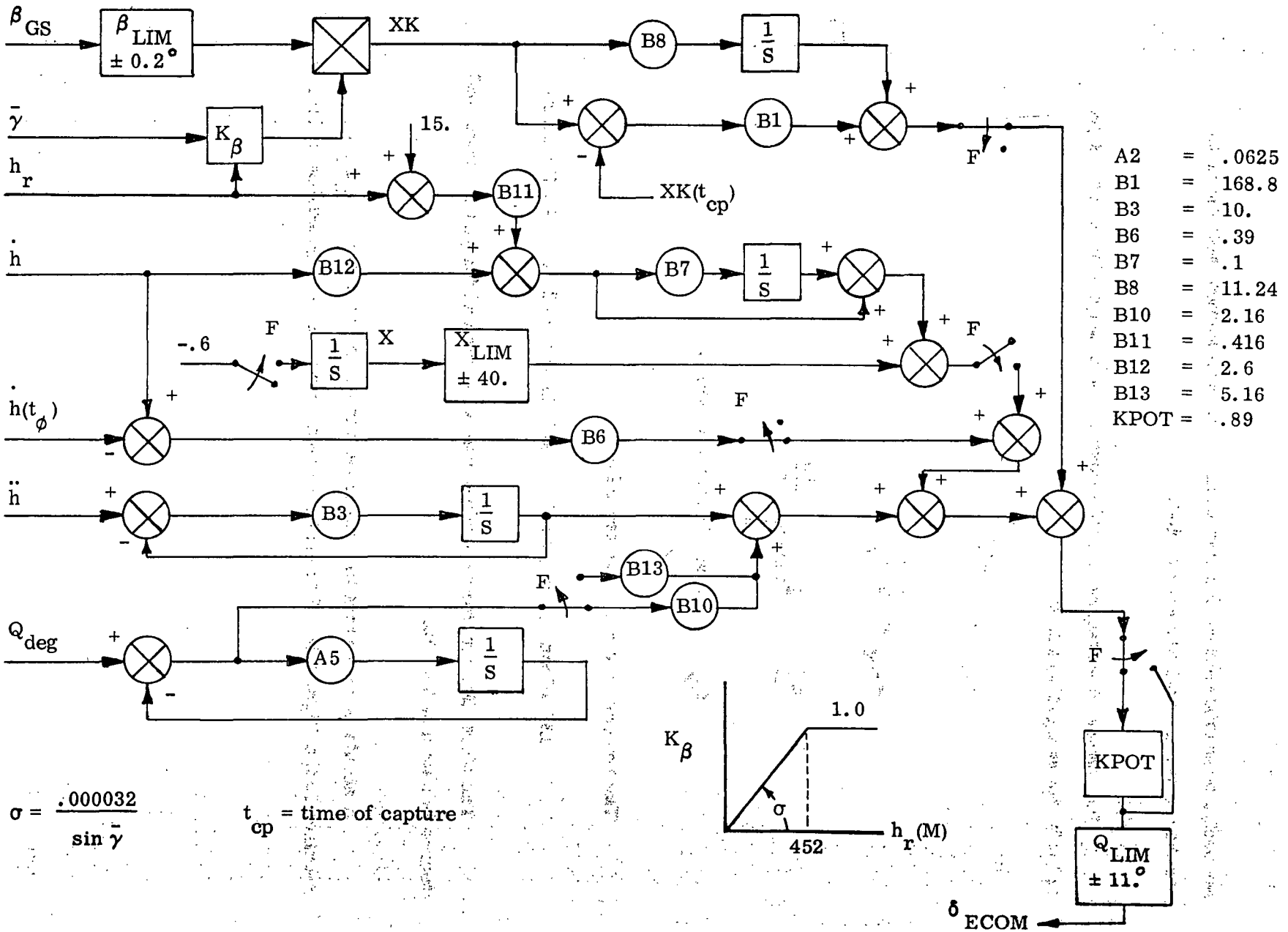

Figure 14. Flight Critical Elevator Command.

secondly, to provide the rudder command for decrab immediately prior to touchdown in the event of a cross wind.

The information required by the rudder command guidance laws is provided by the navigation filter.

$$
\begin{aligned}
R_{deg} &= \hat{r}\,\frac{180}{\pi} \\
\hat{\Psi}_{deg} &= \hat{\Psi}\,\frac{180}{\pi} \\
\Psi_R &= \Psi_{runway}\,\frac{180}{\pi} \\
t_{dc} &= \text{time of decrab initiation}
\end{aligned}
\tag{85}
$$

The trigger for decrab is given by

DC (decrab) is TRUE if O/C is true and $h_r < 45.7$ meters

The block diagram for the rudder control command for yaw damping and decrab is shown in Fig. 15.

It should be noted that the rudder decrab command signal, δ_{RDC}, required in the flight critical lateral control guidance loop is generated in Fig. 15.

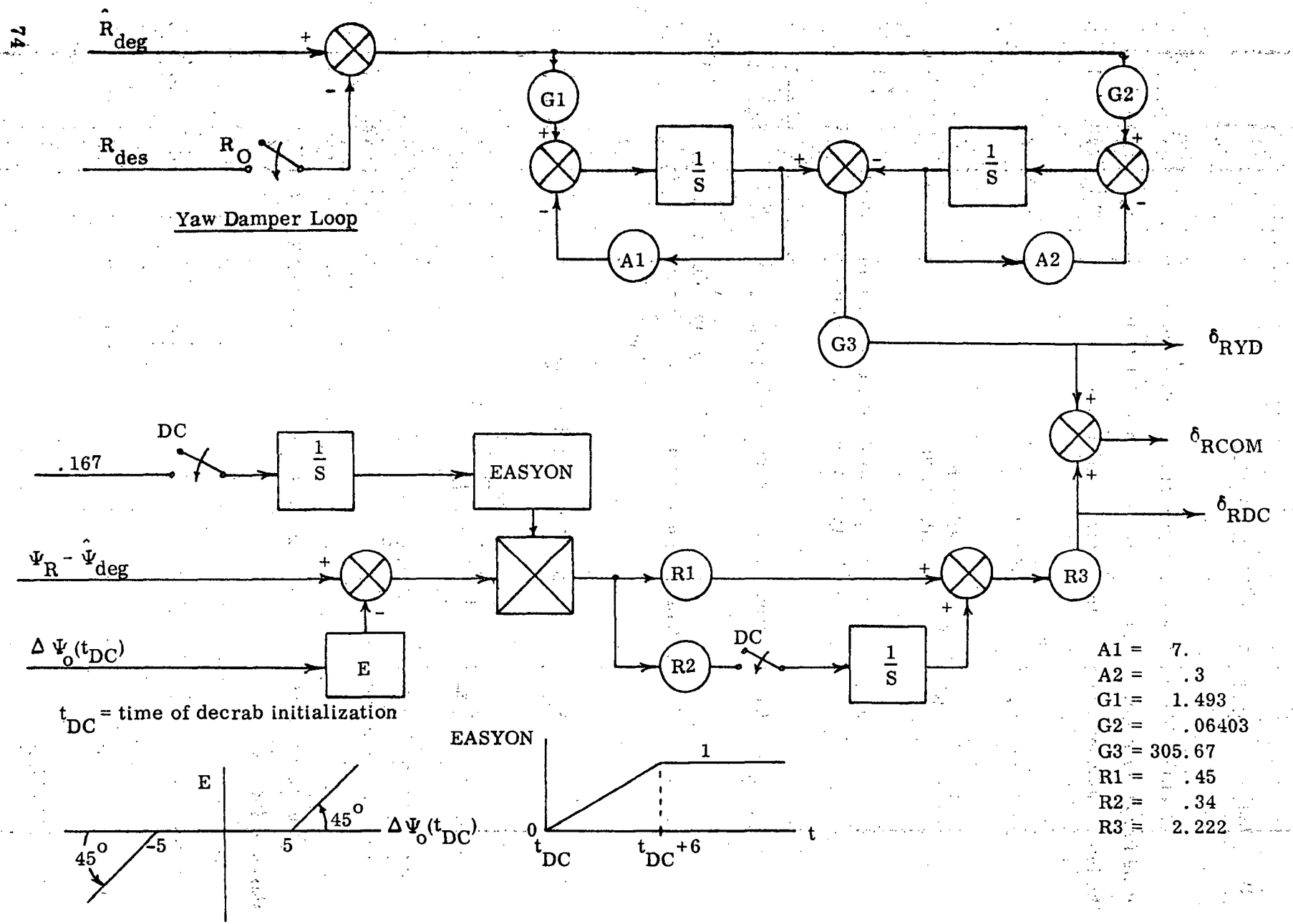

Figure 15. Rudder Yaw Damper and Decrab Command

D. Noncritical Aileron Command Guidance

Lateral guidance laws for trajectories between way points and for banked turns are governed by noncritical aileron command guidance. For banked turns, the lateral guidance requires the following information:

R_T = turn radius

SIGN = $\begin{cases} +1 & \text{left turn} \\ -1 & \text{right turn} \end{cases}$

x_w, y_w = x and y coordinates of the center of the turn circle in runway inertial coordinates

$$\text{CRTE (cross track error)} = \text{SIGN}\left[R_T - \sqrt{(\hat{x}-x_w)^2 + (\hat{y}-y_w)^2}\right] \tag{86}$$

$$\text{TANGE (track angle error)} = -\frac{(\hat{y}-y_w)\dot{\hat{y}} + (\hat{x}-x_w)\dot{\hat{x}}}{(\hat{x}-x_w)\dot{\hat{y}} - (\hat{y}-y_w)\dot{\hat{x}}} \frac{180}{\pi}$$

V_D = desired constant turn speed

$$\Phi_{des} = \left[\tan^{-1}\left(\frac{V_D^2}{G\,R_T}\right)\right]\frac{180}{\pi}$$

$$\hat{\Phi}_{deg} = \hat{\phi}\,\frac{180}{\pi}$$

The block diagram illustrating the noncritical flight aileron command is shown in Fig. 16.

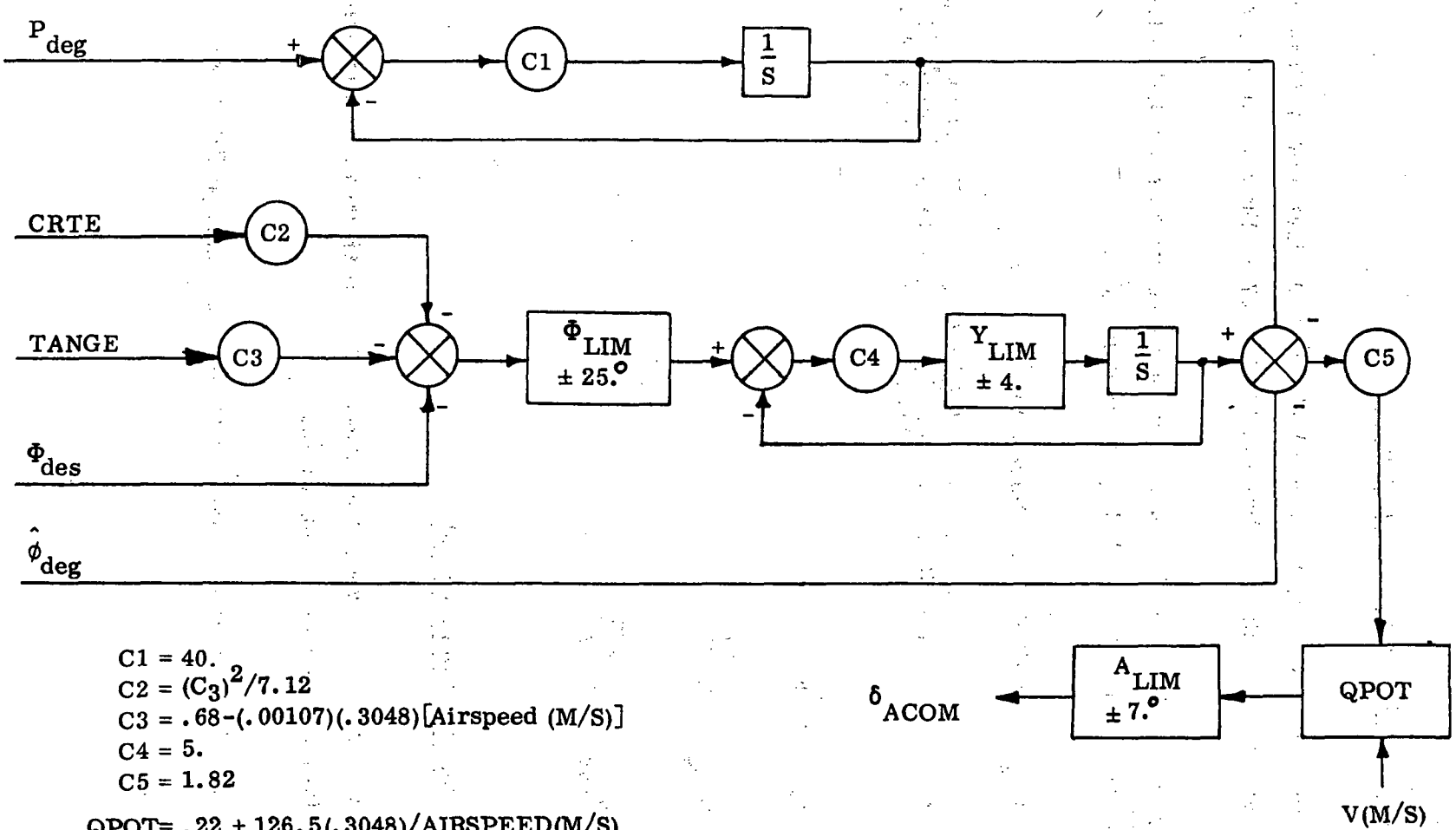

Figure 16. Noncritical Aileron Command.

E. Noncritical Elevator Control Guidance

Vertical control during the noncritical phases for trajectories between way points and in banked turns is illustrated in Fig. 17 for the elevator command.

The information needed to supply the control equations for a banked turn along a descent trajectory for a flight path angle of -3^{o} is

$$h(t_o) = \text{altitude at the start of the turn circle}$$

$$h_c = h(t_o) - \left\{ R_T \left[\left| \tan^{-1} \left(\frac{\hat{x}(t_o) - x_w}{\hat{y}(t_o) - y_w} \right) \right| - \left| \tan^{-1} \left(\frac{\hat{x} - x_w}{\hat{y} - y_w} \right) \right| \right] \sin \bar{\gamma} \right\}$$

$$\ddot{h}_c = 0 \qquad (87)$$

$$Q_{deg} = \hat{q} \frac{180}{\pi}$$

$$\Phi_{deg} = \hat{\phi} \frac{180}{\pi}$$

F. Airborne Throttle Command

Thrust control is designed to maintain a given airspeed and to compensate for the loss of lift during a banked turn.

The variables needed to operate the throttle command guidance are given below:

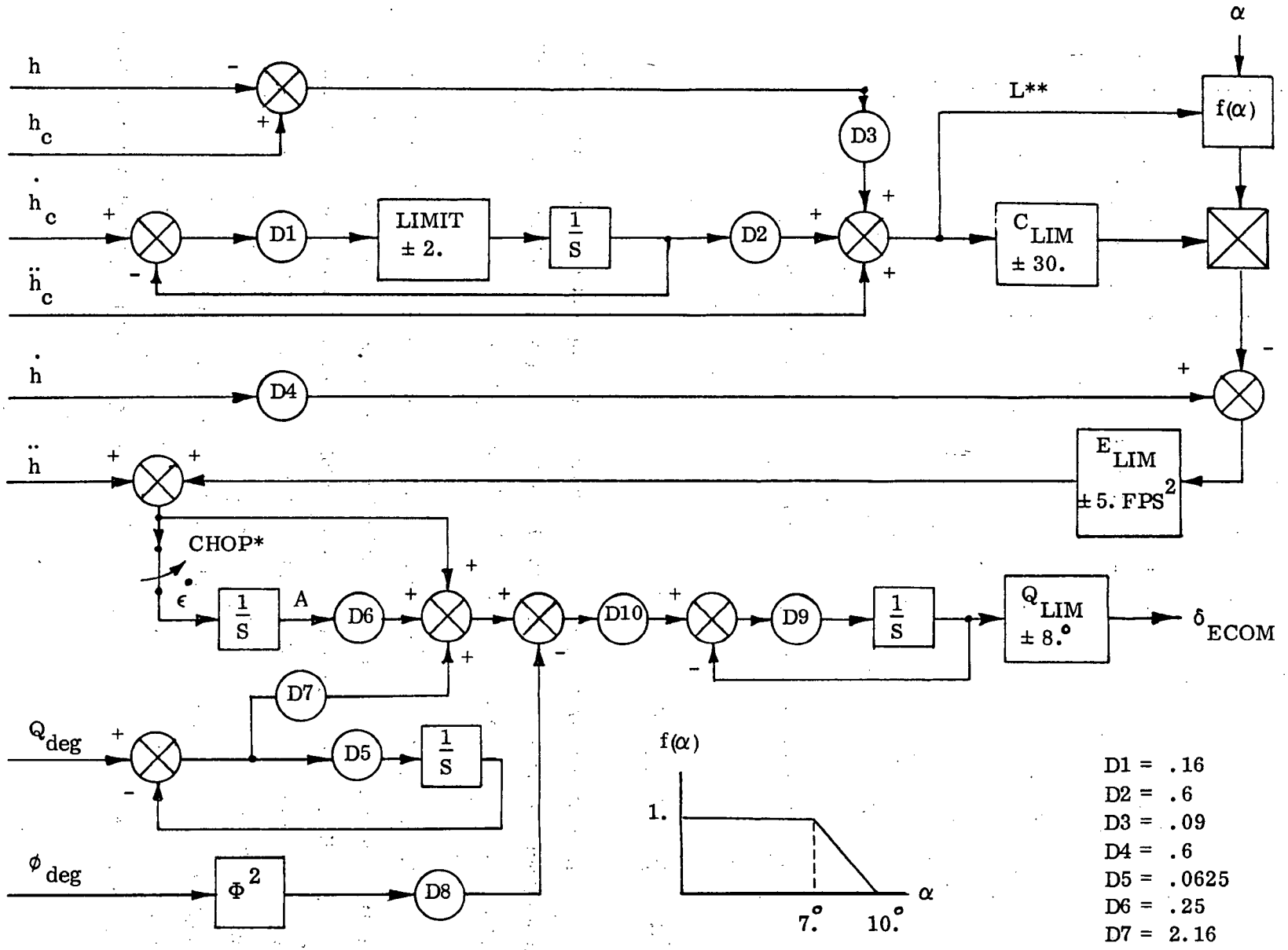

*CHOP is TRUE if trimming and (ϵ A > 0), otherwise it is false.

**If L < 0., f(α) = 1.

Figure 17. Noncritical Elevator Command.

$$f(\phi) = -\frac{1}{2}(1 - \cos\hat{\phi})$$

V(m/s) = airspeed in meters per second obtained from the airspeed indicator

$$\Delta V(m/s) = V - V_{des} \tag{88}$$

$$VG = (\dot{\hat{x}}^2 + \dot{\hat{y}}^2)^{\frac{1}{2}}$$

$$DTVG = (\ddot{\hat{x}}\,\dot{\hat{x}} + \ddot{\hat{y}}\,\dot{\hat{y}})/VG$$

The block diagram for the throttle command is shown in Fig. 18.

G. Rollout and Turnoff Guidance

Rollout and turnoff guidance encompasses rudder and/or nose wheel steering commands, thrust control commands for speed acceleration and taxiing, and finally, brake pressure commands for speed deceleration and taxiing.

Rollout guidance is activated as soon as the main gear preload is exceeded. At this instant, two commands are initiated. First, the throttle is manually set into the idle position. This action is accomplished manually in order to prevent accidental actuation of the throttle into idle detent prematurely. Secondly, a two-second (2 sec.) slow-out and slow-in is initiated to bring the inflight, pre-touchdown control surface guidance commands for the aileron, elevator, and rudder to zero and to raise the post-touchdown rudder/nosewheel steering commands to full signal strength. The mixing takes place within two seconds and is illustrated in Fig. 19.

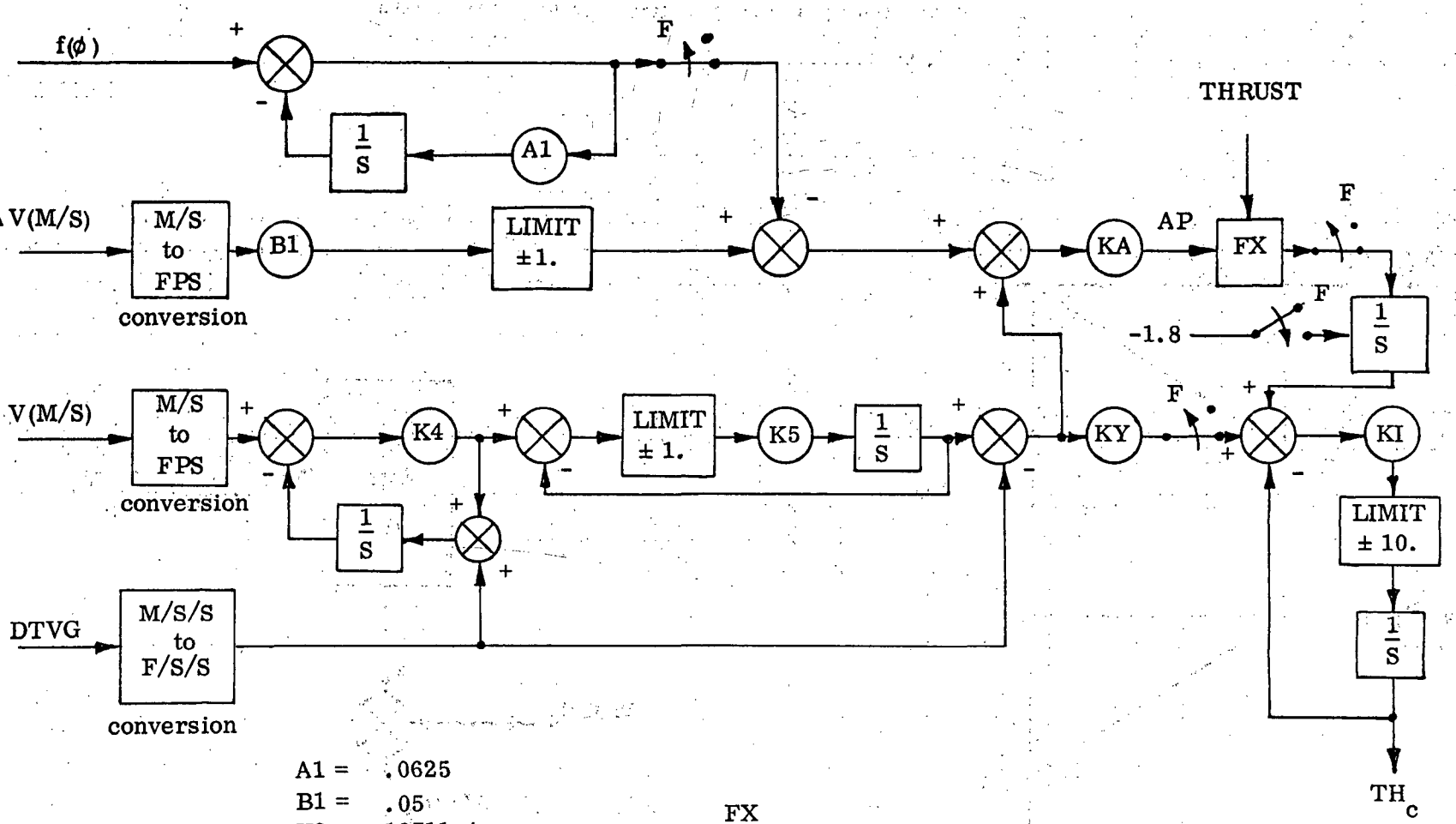

A1 = .0625
B1 = .05
K3 = 13711.4
K4 = 5.
K5 = .2
KA = 1.5
KY = 1.2
KI = 10.
KO = .9697
MX = 1.9

FX

If AP < 0., FX = AP

If AP > 0., $FX = \frac{1}{3}[MX - .1 - (\frac{1}{2}\,THRUST - KO)/K3]\,AP$

Figure 18. Throttle Control.

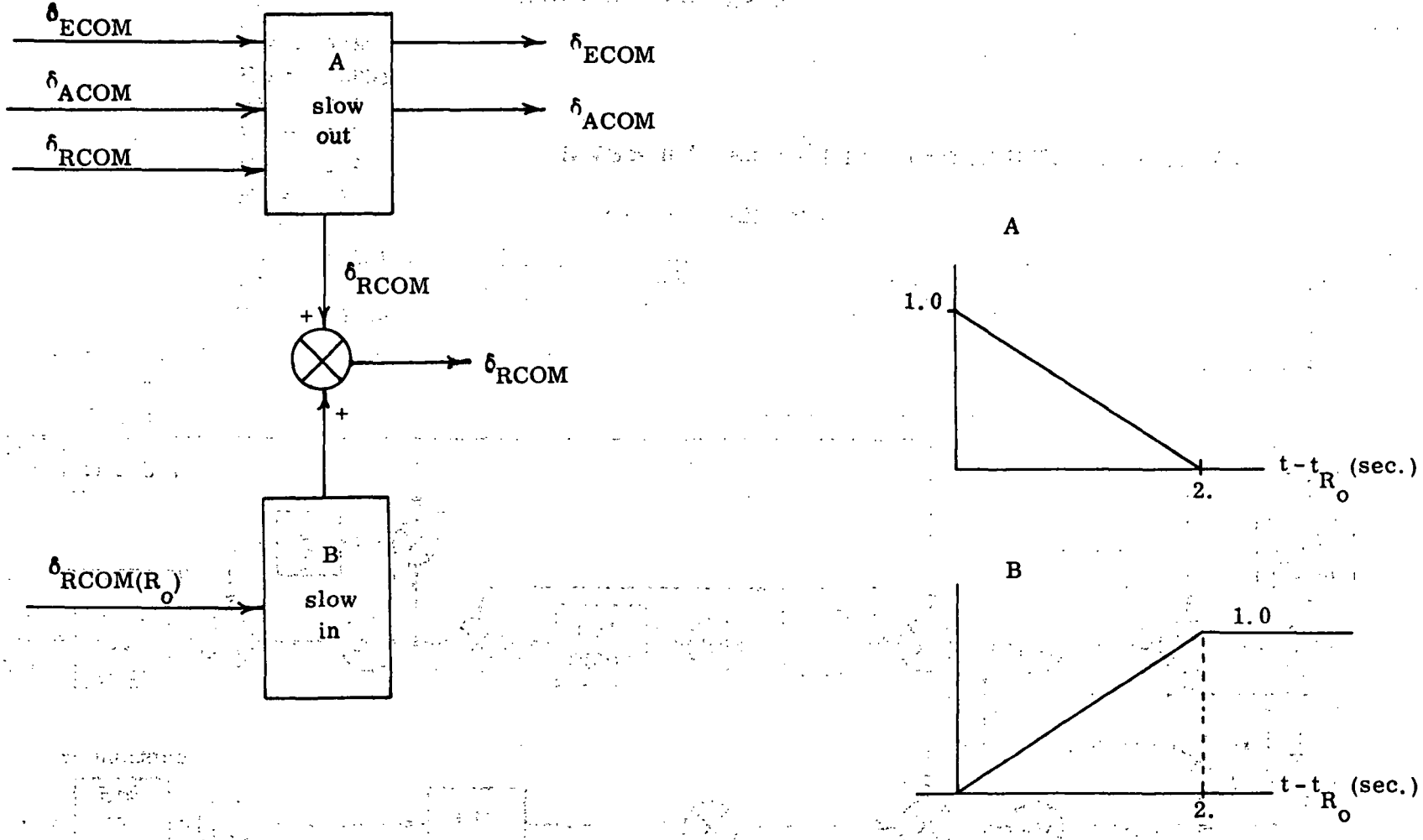

Figure 19. Rollout Control Surface Slowout Command.

The rollout and turnoff control is unified into a single guidance law by requiring the aircraft to follow a single magnetic cable. A three-coil magnetic pickup, mounted below the aircraft fuselage generates two signals; one measures the lateral deviation of the aircraft from the cable, and the other measures the yaw deviation of the aircraft from the cable. The signals necessary to provide damping stability for the lateral and yaw deviations are generated analytically, in a manner similar to the banked turn logic in the lateral noncritical flight guidance equations. By requiring that the magnetic cable consist of a sequence of piecewise straight portions, connected with circular arc segments, we are able to specify the desired ground velocity vector and the desired yaw rate for both the straight line and circular segments. By using the aircraft estimates of the ground velocity vector and yaw rate, we generate the deviations for use in guidance equations.

In order to communicate the start of each straight line or circular segment, a radio signal is given to the aircraft at the beginning of each segment. The information contains the following:

Circular Segment

1. radius of turn
2. sign of turn (+1 , right turn; -1 , left turn)
3. x_w and y_w (coordinates of turn center)
4. signal to start turn

Straight Line Segment

1. yaw angle of segment
2. x_o and y_o (coordinates of start of segment)
3. signal to start straight line guidance

The variables required to operate the rollout and turnoff guidance equations are listed below:

For Circular Turn:

$$VG = (\dot{\hat{x}}^2 + \dot{\hat{y}}^2)^{\frac{1}{2}}$$

$$R_{des} = \left(VG/R_T \frac{180}{\pi}\right)$$

$$\Delta\dot{y} = -\text{SIGN}\left[\frac{(\hat{x}-x_w)\dot{\hat{x}} + (\hat{y}-y_w)\dot{\hat{y}}}{[(\hat{x}-x_w)^2 + (\hat{y}-y_w)^2]^{\frac{1}{2}}}\right] \quad (89a)$$

$$\hat{R}_{deg} = \hat{R}\,\frac{180}{\pi}$$

For Straight Line:

$$\Delta\dot{y} = \cos\Psi_D\,\dot{\hat{y}} - \sin\Psi_D\,\dot{\hat{x}}$$

$$R_{des} = 0. \quad (89b)$$

The logic for the uniform rollout-turnoff guidance is illustrated in the block diagram shown in Fig. 20.

The logic for the brake pressure control is designed to first assist the reverse thrust in decelerating the aircraft to the coast speed (V_{coast}), and secondly, to maintain a somewhat lower taxi speed, V_{taxi}. During the first phase, 80% of maximum brake pressure is available to the brake control logic.

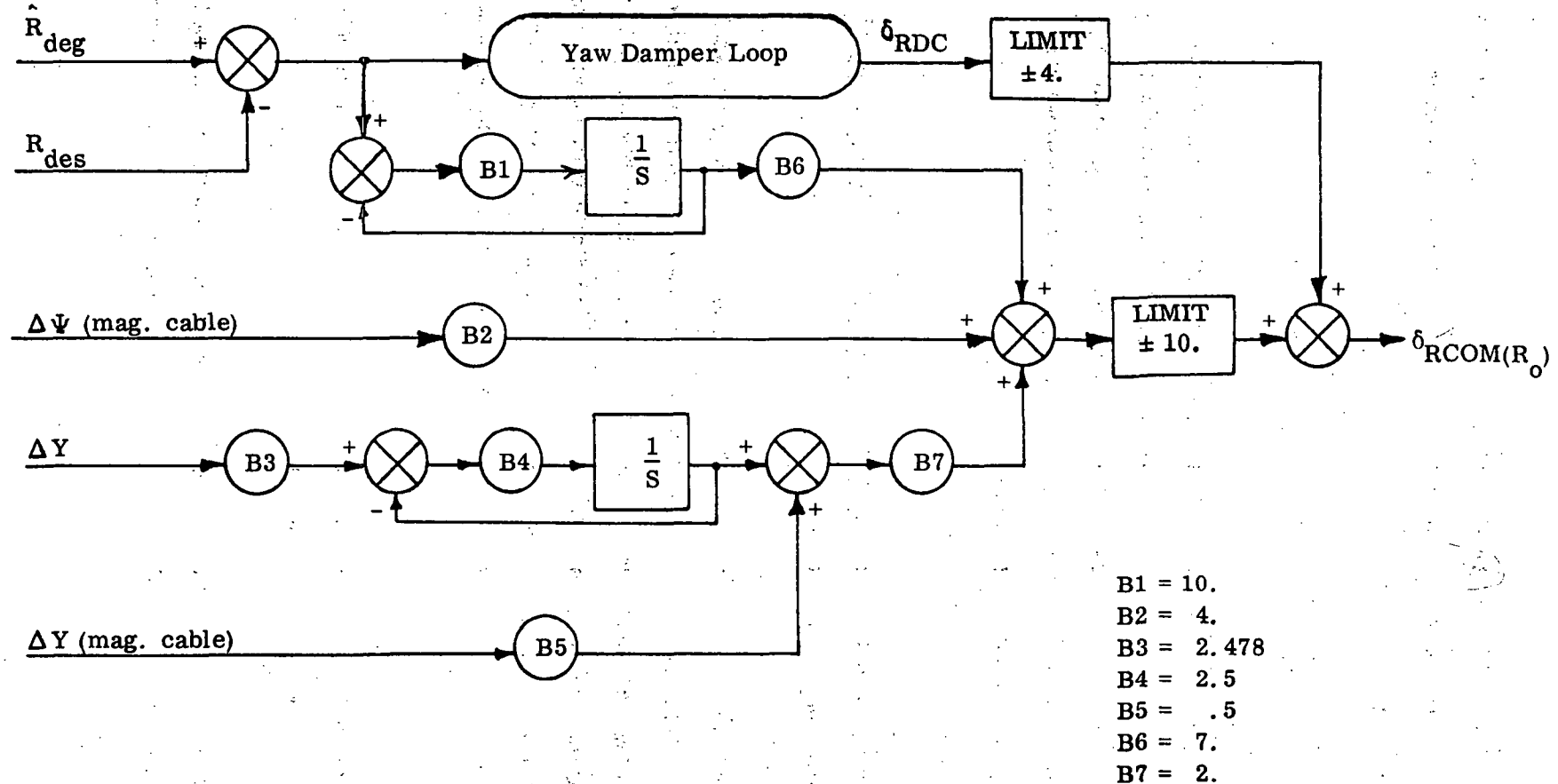

Figure 20. Rollout and Turnoff Steering Command.

During the second phase, only 40% of maximum brake pressure is available for control. An anti-skid device maintains a modulating control to prevent wheel lock and skidding.

The logic for the brake pressure is shown in Fig. 21.

The rollout thrust command is illustrated in Fig. 22. The throttle is held in the idle detent for two seconds. Following that, the thrust guidance calls for the specified reverse thrust. When the aircraft reaches a ground speed of V_{coast}, the throttle control is once again brought to the idle position and remains there throughout the taxi phase.

H. Requirements for GE Whole-Word Computer to Execute Navigation and Kalman Filtering During Rollout

This section contains estimates of the timing and storage requirements for the General Electric MCP-701 computer to execute the navigation and Kalman filtering tasks during the touchdown and rollout sequences. Since the navigation and filtering functions are programmable as separate and distinct modules, estimates of their timing and storage requirements may be made separately, and the resulting estimates may be summed to obtain total estimates for timing and storage.

Different methods were used in obtaining the estimates for the navigation function and for the Kalman filtering function.

FORTRAN code of the rollout navigation algorithm was used in making the storage and timing estimates. FORTRAN operations were translated into equivalent

MCP-701 operations in estimating both timing and the program-instructions component of storage.

A more direct approach was used for the Kalman filter. The Kalman filter is already programmed and running in single precision on the Sperry 1819A computer at the Ames Research Center. Therefore, the timing estimate is the actual 1819A running time scaled to reflect the relative performance of the MCP-701. The storage requirement for the filter is essentially identical to that of the 1819A.

Kalman Filter Requirements

To give the estimates of the filter storage and timing requirements some meaning, a brief description of the Kalman filter is in order. It is a three-axis Kalman filter with segregated horizontal and vertical channels, as depicted in Fig. 23 (for the Sperry 1819A computer). For the application under consideration, the MODILS measurements would be replaced by the equivalent MLS measurements, and the TACAN and MLS measurements would probably not be used simultaneously.

Attitude and heading data and three body-mounted accelerometers are used to give the acceleration in runway reference. Existing 1819A software performs these calculations at a 20 Hz frequency. Biases in the accelerations (estimated by the x-y and z filters) are added to the accelerations and then integrated in double precision to give the three-axis velocity vector, which is in turn integrated in double precision to give the three-axis position vector. This is the only double-precision logic and is performed in the block Navigation Equations in Fig. 23. The estimated state vector coming from this block includes the following:

3-component position vector with respect to runway
3-component velocity vector with respect to runway
3-component acceleration bias vector

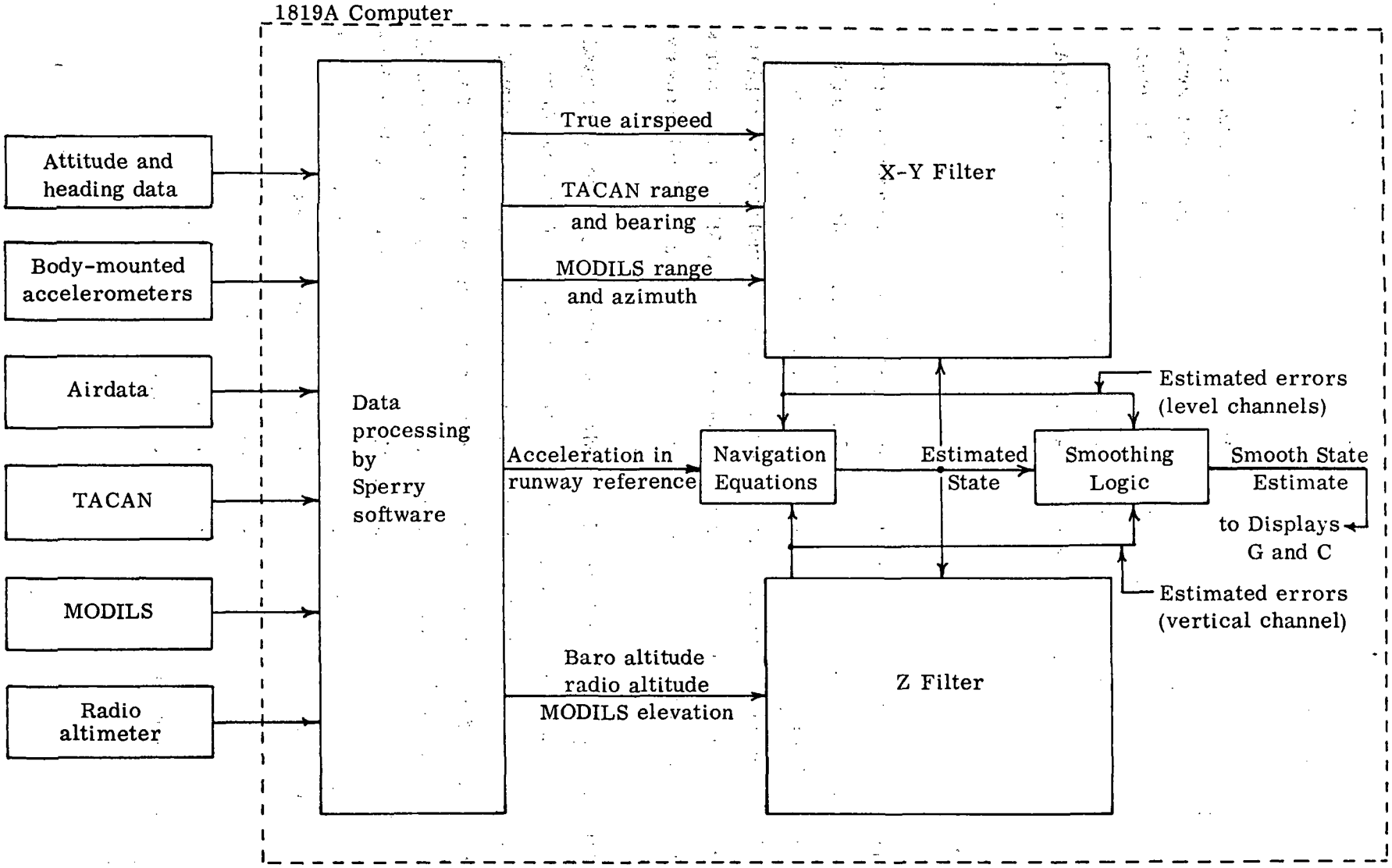

Figure 23. Block Diagram of Overall Filter Mechanization

2-component estimate of winds (x and y)

1-component estimate of TACAN range bias

1-component estimate of TACAN bearing bias

1-component estimate of baro-altimeter bias

The position and velocity components of the estimated state are updated from the acceleration data at the 20 Hz frequency. All components of the state are updated from the x-y and z filters at .667 Hz. This low-frequency update causes discrete changes in the estimated state, which are likely to be objectionable if this estimated state were used for guidance display and control purposes. The block labeled Smoothing Logic in Fig. 23 filters the discrete changes from the estimated state so that the smooth state estimate output will be free of objectionable jumps.

The x-y filter accepts the true airspeed, TACAN range and bearing, and MODILS range and azimuth measurements. This filter has 10 states, as follows:

x - position along the runway

y - position normal to the runway

$\dot{x}$ - velocity along the runway

$\dot{y}$ - velocity normal to the runway

a_x - along runway component of acceleration bias

a_y - normal to runway component of acceleration bias

b_r - bias in TACAN range measurement

b_Ψ - bias in TACAN bearing measurement

w_x - wind along the runway

w_y - wind normal to the runway

The z filter accepts altitude measurements from the barometric altimeter and radio altimeter and altitude measurements calculated from the MODULS elevation data. This filter has four states:

z - vertical component of position

$\dot{z}$ - vertical component of velocity

a_z - vertical component of acceleration bias

b_h - bias in the barometric altitude

All raw measurements are accepted at a 10 Hz frequency. Preprocessing algorithms perform residual and partial-derivative calculations as well as validity checks, and the resultant good data is accumulated for a period of one-and-one-half seconds. The accumulated information is then transferred to locations for processing by the square-root Kalman filter algorithm. Once the filter has estimated the error state for this information, the logic updates the estimated state and performs the smoothing. This concludes the brief description of the Kalman filter.

The total storage (instructions and common variables) of the filter, which is mostly in single precision, is 2,825 words on the Sperry 1819A computer. If the filter were entirely in double precision, it would require 3,053 words. These storage requirements are essentially valid for any mini-computer, since the assembly-language instructions for various mini-computers are very similar.

The filter consumes 18.3% of 1819A running time. The MCP-701 is felt to be at least twice as fast as the 1819A. In particular, double-precision additions are approximately twice as fast and single-precision multiplications are about four times as fast. Therefore, it is estimated that the filter will consume about 10% or less of MCP-701 running time if implemented mostly in single precision. A consideration of the operations necessary to implement a double-precision multiply function on the MCP-701 has yielded the conclusion that a worst-case factor of 4 would result if the filter were programmed entirely in double precision. It is estimated, therefore, that the filter would consume about 40% or less of MCP-701 running time if implemented entirely in double precision.

Navigation Requirements

A detailed investigation of each phase of the rollout navigation algorithm was performed to determine the timing and storage requirements. FORTRAN operations were translated into equivalent MCP-701 operations (or sets of operations). Timing estimates for each phase of the rollout were then estimated by directly counting the required equivalent MCP-701 operations and making use of the information in Table 6.

The rollout sequence and timing estimates are presented in Fig. 24. The times are given in microseconds and include a 50% "safety factor" over the values actually computed (i.e., a multiplicative factor of 1.5). Timing estimates are given for the assumptions of all-single-precision and all-double-precision coding, and percentages of real-time consumed are given in parentheses assuming a 20 Hz frequency. Two situations may occur during rollout:

a) braking is completed before the turn begins

b) braking continues into the turn

The latter case results in the largest percentage time load of the rollout navigation algorithm on the computer (2.5% in single precision and 8.6% in double precision).

The rollout navigation algorithm is estimated to require 702 MCP-701 instructions. The size of COMMON (where variables and constants are stored) is estimated to be 146 words if single-precision coding is sufficient, and 277 words if double precision is required. These values include a 50% "safety factor" over the values actually computed. The total storage estimate for rollout navigation is obtained by summing the instructions and COMMON values. In the single-precision mode, a total of 848 words are required, and in double precision 979 words are required.

Memory Addressable Instruction

MEMORY ADDRESSABLE INSTRUCTION FORMAT

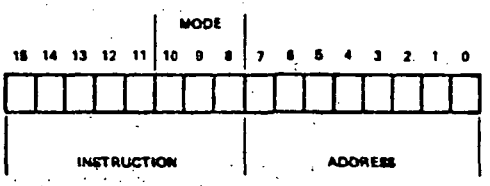

MODE VARIATION

The mode variations for memory addressable instructions define the method for generating the effective address location of data within memory.

MODE			EFFECTIVE ADDRESS GENERATION	ΔTIME (μ sec)
10	9	8		
0	0	0	Current Page	0
0	0	1	Zero Page	0
0	1	0	Indirect	1
0	1	1	Zero Page/Indirect	1
1	0	0	Index	0.2
1	0	1	Zero Page/Index	0.2
1	1	0	Indirect/Index	1
1	1	1	Zero Page/Indirect/Index	1

LOAD INSTRUCTIONS — ASSEMBLER FORMAT 1

MNE	CODE	INSTRUCTION NAME	TIME (μ sec)
LDU	08	Load Upper Register	2.2
LDL	10	Load Lower Register	2.2
LDX	18	Load Index Register	2.2
LDD	20	Load Double	3.2
LPK	28	Load Packed	2.2

STORE INSTRUCTIONS

STU	30	Store Upper Register	2.2
STL	38	Store Lower Register	2.2
STX	40	Store Index Register	2.2
STD	48	Store Double	3.2
SPK	50	Store Packed	2.4

ARITHMETIC INSTRUCTIONS

ADU	58	Add to Upper Register	2.2
ADM	60	Add to Memory	3.2
ADD	68	Add Double	3.2
SBU	70	Subtract from Upper Register	2.2
SBD	78	Subtract Double	3.2
MPY	80	Multiply	5.4
DIV	88	Divide	5.8

LOGIC INSTRUCTIONS

ANU	90	And to Upper Register	2.2
ORU	98	Or to Upper Register	2.2
EXU	A0	Exclusive Or to Upper Register	2.2
CPU	A8	Compare to Upper Register	2.2

BRANCH INSTRUCTIONS

JMP	B0	Jump Unconditionally	1.4
JMS	B8	Jump to Subroutine	2.2
MDS	C0	Memory Decrement and Skip	3.2

Non-Memory Addressable Instruction

NON-MEMORY ADDRESSABLE INSTRUCTION FORMAT

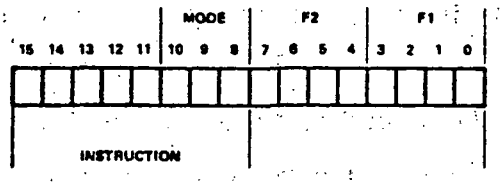

REGISTER CODES

MNE	CODE	REGISTER
UR	1	Upper Register
LR	2	Lower Register
XR	3	Index Register
SR	4	Status Register
UL	C	Upper and Lower Register

INDICATOR CODES

MNE	CODE	INDICATOR
SA	0	Sign of Adder
ZA	1	Zero Adder
AF	2	Arithmetic Fault
CF	3	Computer Fault Disable
DR	4	Device Ready
IO	5	Input/Output Disable
LA	6	Logic Indicator A
LB	7	Logic Indicator B

BRANCH INSTRUCTIONS

MNE	CODE	INSTRUCTION NAME	F2	F1	TIME (μ sec)
RASN	C8	Register Add & Skip on Neg	Register	Constant	1.6
RSSN	CA	Register Subtract & Skip on Neg	Register	Constant	1.6
RASP	CC	Register Add & Skip on Pos	Register	Constant	1.6
RSSP	CE	Register Subtract & Skip on Pos	Register	Constant	1.6
SFI	D0	Skip Forward on Ind	Indicator	Constant	1.4
SBI	D1	Skip Backward on Ind	Indicator	Constant	1.4
SFIR	D2	Skip Forward on Ind & Reset	Indicator	Constant	1.4
SBIR	D3	Skip Backward on Ind & Reset	Indicator	Constant	1.4
SFN	D4	Skip Forward on No Ind	Indicator	Constant	1.4
SBN	D5	Skip Backward on No Ind	Indicator	Constant	1.4

SET/CLEAR INSTRUCTIONS

SET	D8	Set Indicator	Indicator	Not Used	1.4
CLR	D9	Clear Indicator	Indicator	Not Used	1.4

REGISTER INSTRUCTIONS

RTF	E0	Register Transfer	From Register	To Register	1.4
ZRO	E1	Zero Register	Not Used	To Register	1.4
CPL	E2	Complement Register	From Register	To Register	1.8
INV	E3	Invert Register	From Register	To Register	1.4
ABS	E4	Absolute Value of Register	From Register	To Register	1.8

INPUT/OUTPUT INSTRUCTIONS

ENBL	E8	Enable Interrupts	Not Used		1.8
INHB	E9	Inhibit Interrupt from Device	Not Used		1.8
RST	EA	Reset Selected Device	Not Used		1.8
TAKE	EC	Take Data to Upper Register	Not Used		1.8
SNS	ED	Sense Device	Not Used		1.8
PUT	EE	Put Data from Upper Register	Not Used		1.8
SEL	EF	Select Device	Device Code		1.8

SHIFT INSTRUCTIONS

SRZ	F0	Shift Right, Enter Zeroes	Shift Count	Register	1.2 + 0.2n
SLZ	F1	Shift Left, Enter Zeroes	Shift Count	Register	1.2 + 0.2n
SRS	F2	Shift Right, Repeat Sign	Shift Count	Register	1.2 + 0.2n
SRC	F3	Shift Right Circular	Shift Count	Register	1.2 + 0.2n
NRM	F8	Normalize	Not Used	Not Used	2.6 + 0.2 (n-1)
SRX	FA	Shift Right by Index	Not Used	Not Used	1.6 + 0.2n

CONTROL INSTRUCTIONS

HALT	00	Halt	Not Used	Not Used	1.2
NOP	E0	No Operation	4	4	

Table 6. GE MCP-701 Computer Instruction Execution Times.

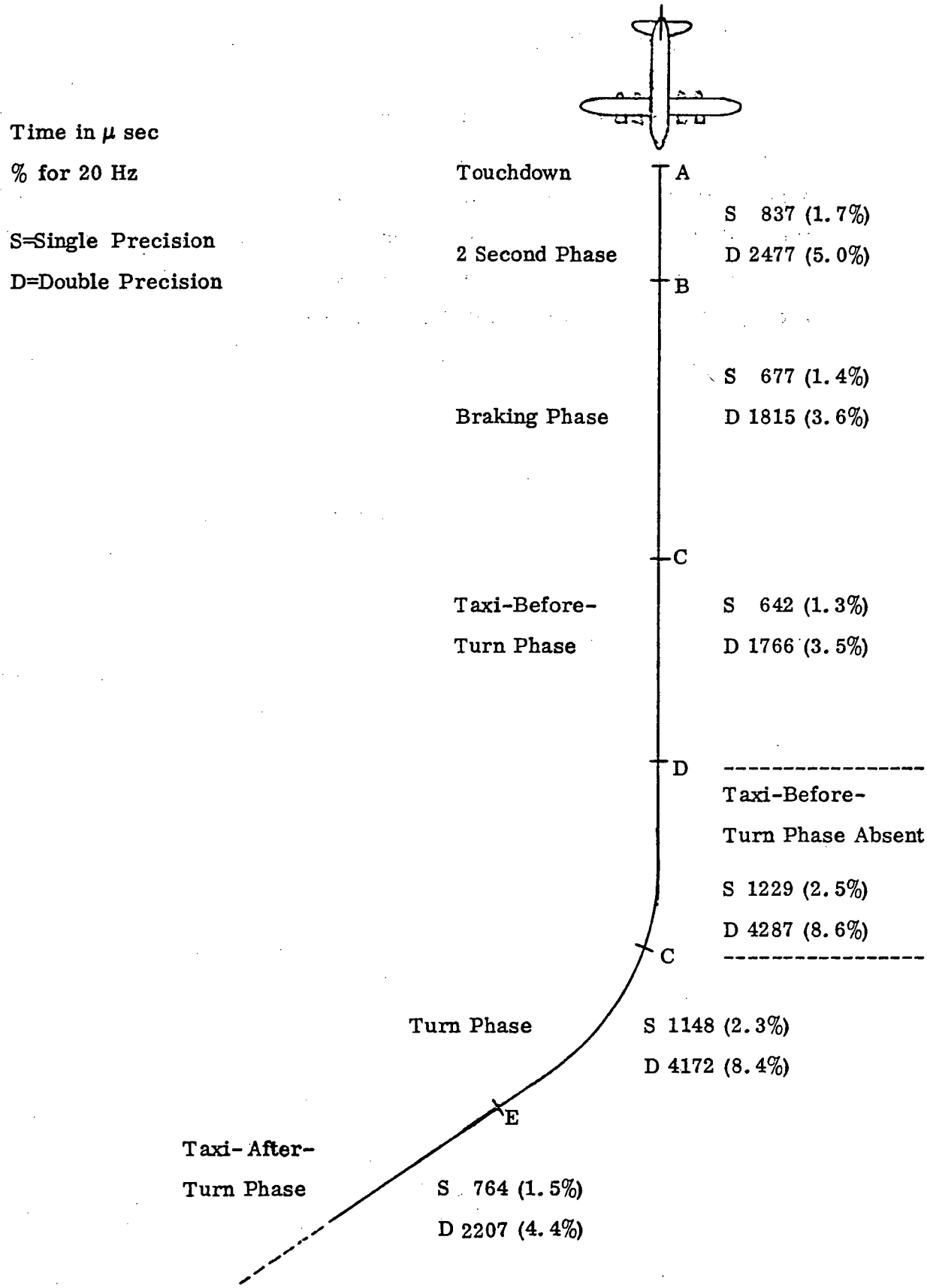

Figure 24. Rollout Navigation Timing Estimates for the MCP-701 Computer

Total Requirements

The total Kalman filter and rollout navigation requirements (with a 50% safety factor included in the navigation component) are obtained by summing the separate requirements discussed above, assuming the worst case for the rollout timing estimate. In single precision, the total requirements are 3,673 words of storage and 12.5% of real time; in double precision, the total requirements are 4,032 words of storage and 48.6% of real time.

APPENDIX A

B-737

Aerodynamic Force and Moment Coefficients

and

Dynamic Response

I. AERODYNAMIC COEFFICIENTS

The aerodynamic coefficients are functions of the velocity of the aircraft relative to the airstream, control surface deflections, altitude and altitude rates of the aircraft.

We define the following quantities:

$\bar{c}$	=	mean aerodynamic chord
$\bar{b}$	=	wing span
S	=	wing reference area
ρ	=	air density
δ_E	=	elevator deflection
δ_a	=	aileron deflection
δ_{STAB}	=	stabilizer deflection
δ_R	=	rudder deflection
δ_{SP}	=	aileron spoiler deflection
δ_{SPSUM}	=	symmetric spoiler deflection
α_o	=	fuselage offset angle

The velocity vector of the aircraft relative to the airstream in the runway coordinate system is given by

$$V = \dot{R} - \{ W + G + S \} \tag{A-1}$$

The relative velocity vector in the body system is given by

$$\begin{Bmatrix} v_{1B} \\ v_{2B} \\ v_{3B} \end{Bmatrix} = L_{BI} \{ V \} \tag{A-2}$$

The airspeed is the magnitude of the vector V.

$$v = |V| \tag{A-3}$$

The dynamic pressure is given by

$$\bar{q} = \tfrac{1}{2} \rho v^2 \tag{A-4}$$

The angle of attack is given by

$$\alpha = \sin^{-1} \frac{v_{3B}}{\sqrt{v_{1B}^2 + v_{3B}^2}}$$

or

$$\alpha = \tan^{-1} \frac{v_{3B}}{v_{1B}} \tag{A-5}$$

The aerodynamic coefficients are functions of the angle of attack relative to the mean chord line

$$\bar{\alpha} = \alpha + \alpha_o \tag{A-6}$$

The side force angle of attack is given by

$$\beta = \frac{v_{2B}}{v} \tag{A-7}$$

The effective drag coefficient is given by

$$C_D = C_{D1} + C_{D2}\bar{\alpha} + (C_{D3} + C_{D4}\bar{\alpha})\delta_{SPSUM} + C_{D6} + C_{D7}|\beta| + C_{D8}|\delta_R| + (C_{D9} + C_{D10}\bar{\alpha})\delta_{SP} + C_{D_{GEAR}} \tag{A-8}$$

The effective lift coefficient is given by

$$C_L = C_{L1} + C_{L2}\bar{\alpha} + C_{L3}\frac{\bar{c}}{2v}(\dot{\alpha} - q_{gust}) + C_{L4}\frac{\bar{c}}{2v}(\bar{q} + q_{gust})$$

$$+ C_{L5}\delta_{STAB} + C_{L6}\delta_E + (C_{L7} + C_{L8}\bar{\alpha})\delta_{SPSUM} \qquad \text{(A-9)}$$

$$+ C_{L9} + C_{L_{GEAR}}$$

The effective side force coefficient is given by

$$C_Y = C_{Y1}\beta + C_{Y2}\frac{\bar{b}}{2v}(p_{gust} + p\cos\alpha + r\sin\alpha)$$

$$+ C_{Y3}\frac{\bar{b}}{2v}(r_{gust} - p\sin\alpha + r\cos\alpha) \qquad \text{(A-10)}$$

$$+ (C_{Y4} + C_{Y5}\bar{\alpha})\delta_{SP} + C_{Y6}\delta_R$$

The aerodynamic roll moment coefficient is given by

$$L_S = \bar{q}S\bar{b}\left\{\begin{array}{l} C_{S1}\beta + C_{S2}\frac{\bar{b}}{2v}(p_{gust} + p\cos\alpha + r\sin\alpha) \\ + C_{S3}\frac{\bar{b}}{2v}(r_{gust} - p\sin\alpha + r\cos\alpha) + (C_{S4} + C_{S5}\bar{\alpha})\delta_{SP} \\ + C_{S6}\delta_a + (C_{S7} + C_{S8}\bar{\alpha})\delta_R \end{array}\right\} \text{(A-11}$$

The pitch moment coefficient is given by

$$M_S = \bar{q}S\bar{c}\left\{\begin{array}{l} C_{M1} + C_{M2}\bar{\alpha} + C_{M3}\frac{\bar{c}}{2v}(\dot{\alpha} - q_{gust}) + C_{M4}\frac{\bar{c}}{2v}(\bar{q} + q_{gust}) \\ + C_{M6}\delta_{STAB} + C_{M7}\delta_E + C_{M10}|\beta| + C_{M11} \\ + (C_{M12} + C_{M13}\bar{\alpha})\delta_{SPSUM} + C_{M14}|\delta_R| \\ + C_{M_{GEAR}} + (g^* - .25)C_L \end{array}\right\} \quad \text{(A-12)}$$

In order to compute the yaw moment coefficient, we require the lateral acceleration in the body reference frame. We have

$$\left\{\begin{array}{c} \dot{U} \\ \dot{V} \\ \dot{W} \end{array}\right\} = L_{BI}\left\{\begin{array}{c} \ddot{R} \end{array}\right\} \quad \text{(A-13)}$$

The yaw moment coefficient is given by

$$N_S = \bar{q}S\bar{b}\left\{\begin{array}{l} C_{N1}\beta + C_{N2}\frac{\bar{b}}{2v}\frac{\dot{V}}{v} + C_{N3}\frac{\bar{b}}{2v}(p_{gust} + p\cos\alpha + r\sin\alpha) \\ + C_{N4}\frac{\bar{b}}{2v}(r_{gust} - p\sin\alpha + r\cos\alpha) + C_{N6}\delta_{SP} \\ + (C_{N7} + C_{N8}\bar{\alpha})\delta_a + C_{N9}\delta_R + \frac{\bar{c}}{\bar{b}}(g^* - .25)C_Y \end{array}\right\} \quad \text{(A-14)}$$

The numerical values of the coefficients for the 737 aircraft were furnished by NASA Langley Research Center and are listed below:

AIRCRAFT AERODYNAMIC COEFFICIENTS

Drag Coefficients

C_{D1} = .185
C_{D2} = .9225
C_{D3} = .0329
C_{D4} = -.1067
C_{D5} = 0.
C_{D6} = .0075
C_{D7} = .0573
C_{D8} = .019
C_{D9} = .043
C_{D10} = -.308

Lift Coefficients

C_{L1} = 1.36
C_{L2} = 6.9328
C_{L3} = -8.0
C_{L4} = 8.208
C_{L5} = .963
C_{L6} = .464
C_{L7} = -.4584
C_{L8} = -.0258
C_{L9} = -.058
C_{L10} = 93.
C_{L11} = .008
C_{L12} = -.625
C_{L13} = .7735

Side Force Coefficients

C_{Y1} = -1.564
C_{Y2} = .4871
C_{Y3} = .189
C_{Y4} = -.0487
C_{Y5} = -.1067
C_{Y6} = .4383

Roll Moment Coefficients

C_{S1} = -.3152
C_{S2} = -.645
C_{S3} = .395
C_{S4} = .0967
C_{S5} = .0817
C_{S6} = .0816
C_{S7} = .06
C_{S8} = -.1899

Pitch Moment Coefficients

$C_{M1} = -.155$

$C_{M2} = -1.4719$

$C_{M3} = -2.375$

$C_{M4} = -24.29$

$C_{M5} = -.0064$

$C_{M6} = -3.437$

$C_{M7} = -1.6545$

$C_{M8} = .1089$

$C_{M9} = .4842$

$C_{M10} = -.34$

$C_{M11} = .003$

$C_{M12} = -.02$

$C_{M13} = -.859$

$C_{M14} = .115$

Yaw Moment Coefficients

$C_{N1} = .268$

$C_{N2} = -.0332$

$C_{N3} = -.2265$

$C_{N4} = -.2856$

$C_{N5} = 0.$

$C_{N6} = .0215$

$C_{N7} = .011$

$C_{N8} = .0343$

$C_{N9} = -.1862$

The geometric parameters for the 737 aircraft are listed below:

$\bar{c}$	=	3.41376 meters	(11.2 ft.)
$\bar{b}$	=	28.3464 meters	(93 ft.)
S	=	91.045 meters^2	(980 ft.^{2})
a_T	=	1.524 meters	(5 ft.)
Mass	=	36287.5 kg	(80,000. lb.)
I_{XX}	=	142572 newton meters^2	(345,000. lb. ft.^{2})
I_{YY}	=	328148 newton meters^2	(794,062.5 lb. ft.^{2})
I_{ZZ}	=	490738 newton meters^2	(1,187,500. lb. ft.^{2})
I_{XZ}	=	21351 newton meters^2	(51,667. lb. ft.^{2})

II. DYNAMIC STABILITY COMPARISON

In order to check the accuracy of the dynamic model of the aircraft, the response of the plane to an elevator impulse and a rudder impulse was tested. The response curves are shown in Figs. A1 and A2. These runs were made with the automatic control equations inoperative in order to obtain the period, damping, and the decay time to one-half amplitude of the plane for the short period, phugoid, and dutch roll motions, at an airspeed of 66.88 m/sec. (130. knots) and an altitude of 426.7 meters (1400 ft.)

A comparison of these results was made with 737 aircraft characteristics supplied by Langley Research Center. The results, shown in Table 7, are in good agreement.

Dynamic Response to Elevator Impulse

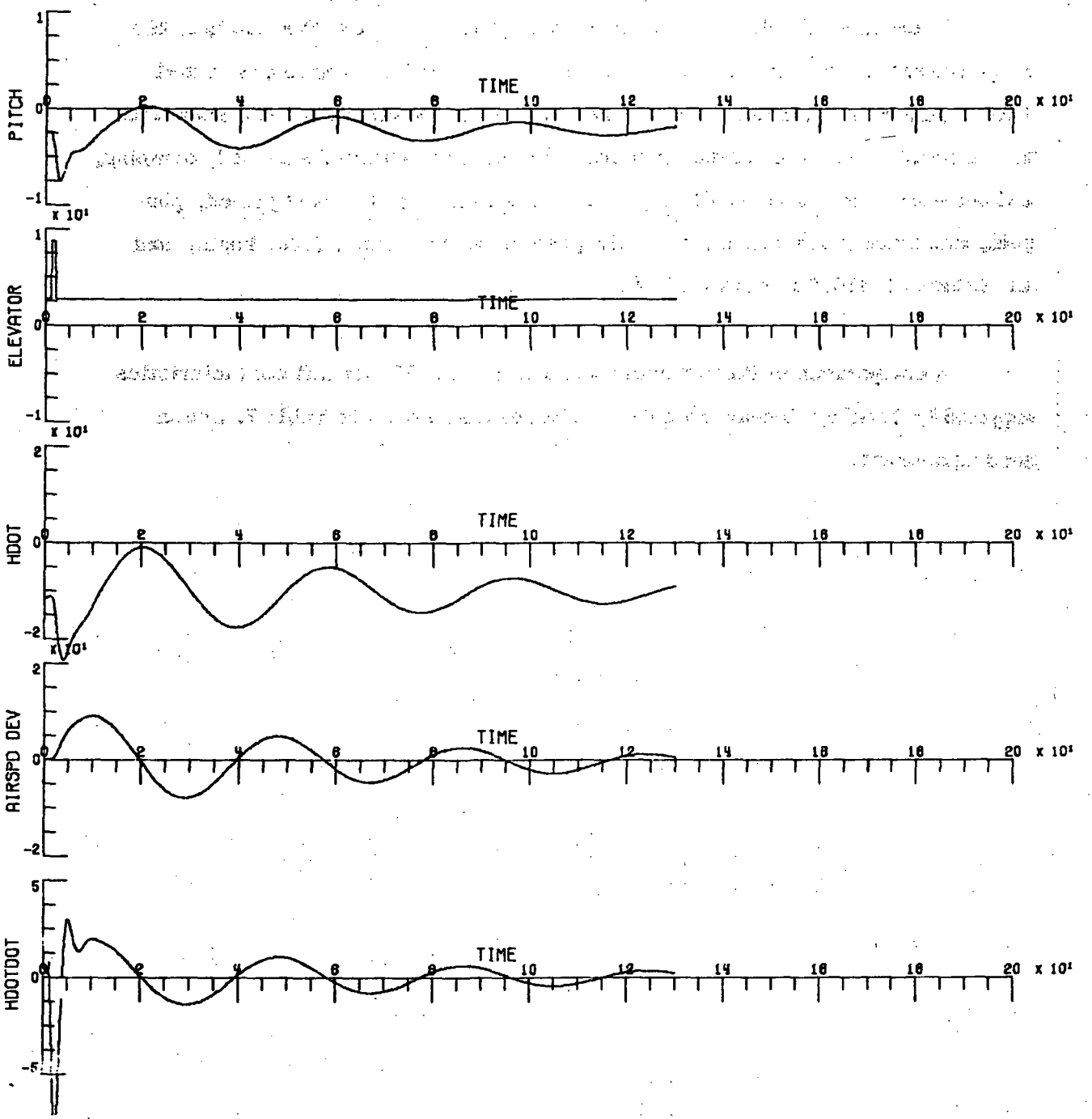

Figure A1. Phugoid and Short Period Modes

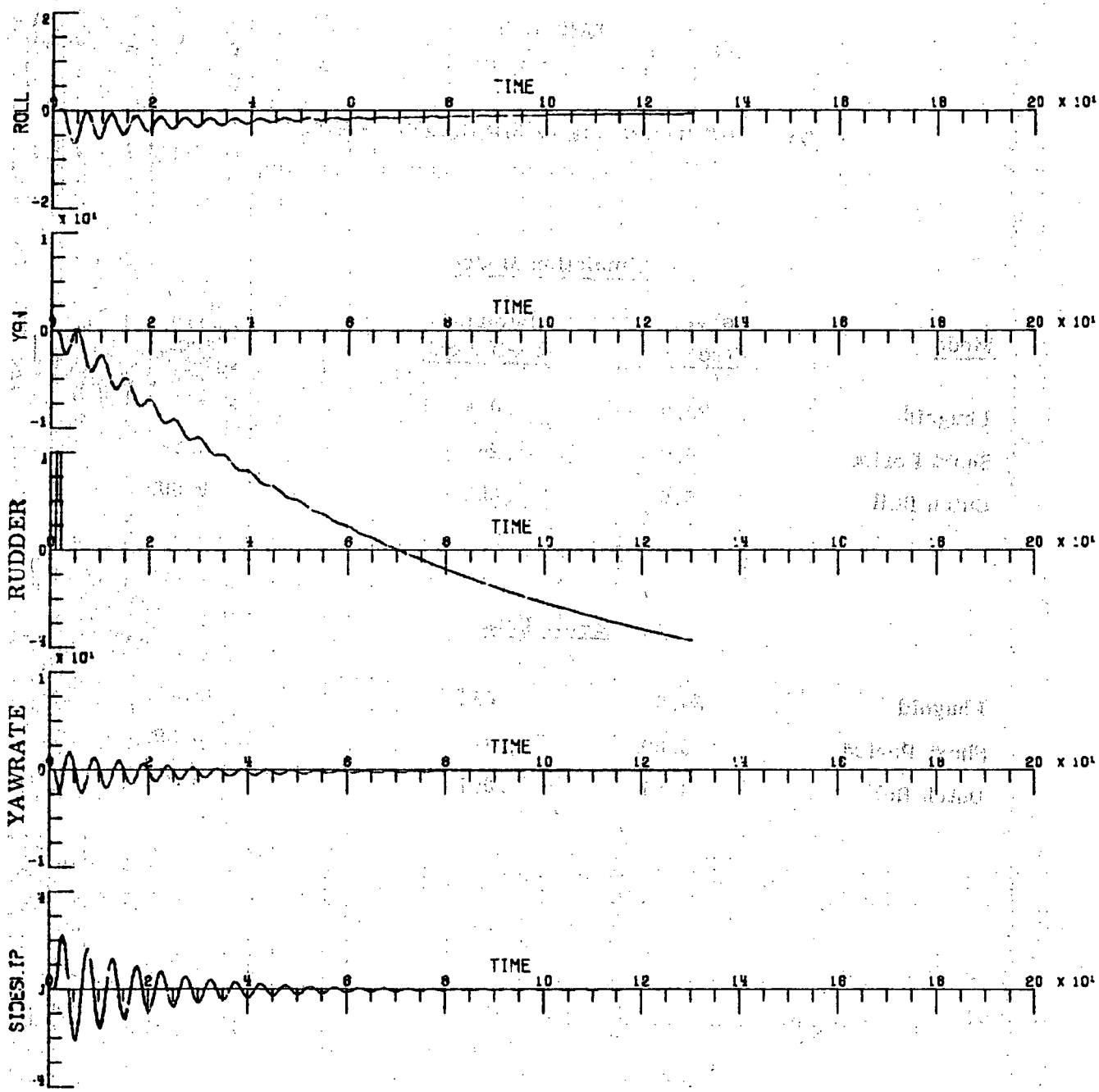

Figure A2. Dutch Roll Mode

TABLE 7

DYNAMIC RESPONSE COMPARISON — B-737

Simulation Model

Mode	Period (sec.)	Damping Coefficient	$T_{1/2}$ (sec.)
Phugoid	39.0	.098	43.7
Short Period	5.0	.25	4.84
Dutch Roll	5.0	.055	9.99

B-737 Data

Phugoid	34.0	.084	43.7
Short Period	5.39	.41	5.39
Dutch Roll	4.81	.057	9.31

APPENDIX B

Computer Simulation Results for

Rollout and Turnoff

I. DESCRIPTION OF TEST DATA

This section contains the results of computer runs of the ALERT program in the form of plots. Although the B-737 aircraft simulation program is capable of executing automated banked turns and landing approaches including capture, oncourse, flare, and decrab, the main purpose of this study was to develop and test a guidance law for rollout and turnoff. The computer plots contained in this section illustrate the terminal portion of each landing from touchdown to the end of turnoff. Turnoff, in the context of this study, is defined to be completed when the aircraft is at a fixed desired taxi speed, at a fixed constant heading (30^{o} yaw relative to the landing runway centerline), and at a distance of 91.44 meters (300 ft.) from the runway centerline.

In order to reduce the computer run time to complete the study for a range of wind conditions, runway conditions, and taxi speeds, the entire airborne program was run for different wind conditions. The aircraft variables at touchdown were stored, and a set of rollout and turnoff runs were made at different taxi speeds and runway conditions (dry and wet) for each fixed landing condition.

A description of the plot variables and units is given. Each landing case contains eleven plots. The horizontal variable is always time from touchdown in seconds. The first plot is the aircraft thrust in newtons. (One pound of force is equal to 4.4482216 newtons.) The specified reverse thrust for this aircraft is 62275. newtons (14,000.#) The steady state idle thrust is 6672. newtons (1500.#) The thrust is manually set at idle and, after a two-second slowout, the thrust logic calls for maximum retro thrust which continues until the aircraft reaches the required V_{coast} speed, at which time the thrust logic calls for idle thrust throughout the taxi period.

The second plot is the automatic braking pressure plotted in percent of maximum allowed pressure. 100% of maximum allowed braking pressure corresponds to a friction coefficient, μ, of .4. Thus, the automatic braking logic is not designed to command the full capabilities of the tire on a good dry runway. Zero brake pressure corresponds to the condition where only rolling friction is operative. Maximum brake pressure is available during deceleration to V_{coast}. Following that, only medium brake pressure ($\mu = .2$) is available to the automatic braking logic. During landings on wet runways, the anti-skid device moderates the pressure to that allowable to forestall wheel lock.

The third plot is the forward acceleration in the body system, $\dot{u}$. The units are in meters/sec.^{2}. 1.0g is 9.817 m/sec.^{2}. For rapid turnoffs, a maximum deceleration of 5 m/sec.^{2} is considered within the limits of passenger comfort.

The fourth and sixth plots are the x and y components of the winds plus shear and gust. These are measured in meters/sec.

The fifth plot is the aircraft ground speed. This is measured in meters/sec. The flat portion after the linear deceleration illustrates how well the aircraft keeps the desired V_{taxi} speed.

The seventh plot is the first plot on the second page of each case. The variable CRTE is the cross track error, or the lateral deviation from the buried magnetic cable. It is measured in meters.

The eighth plot is the lateral acceleration in body system. It is measured in meters/sec. Passenger comfort requires that this variable not exceed an absolute value of .15g's or 1.472 m/sec.^{2} (4.83 ft./sec.^{2}). This limits the maximum taxi speed if fast turnoff times are required.

The ninth plot is the aircraft yaw angle.

The tenth plot is the nose wheel steering angle.

The final plot is the difference between the magnetic cable yaw angle and the aircraft yaw angle.

For the purposes of this simulation, the magnetic cable is laid out in three segments: first, a straight segment along the runway centerline to the turnoff position; secondly, a turn with a fixed input radius making a change in yaw of 30^{o} heading; finally, a straight line segment at a fixed yaw heading of 30^{o}.

Following the plot of the eleventh variable is a short data set giving the wind condition, the V_{coast} and V_{taxi} inputs, and the runway condition.

II. SIMULATION RESULTS AND DISCUSSION

Figures B1, B2, B3, and B4 are acceptable fast turnoffs on good dry runways. Figure B5 is a repeat of Run B3 for a wet runway. For this case, because of the inability to apply braking at high speeds, the desirable taxi speed of 50 knots was not achieved and high lateral acceleration resulted. In order to produce acceptable turns at high speeds on wet runways, it was found necessary to lower the V_{coast} speed (the speed at which the retro thrust is switched to idle) to exceed the desired V_{taxi} speed by 5 knots. With this change, acceptable fast turns are achieved on wet runways. Figure B6 is an illustration of a good 6.0 knot turn on a wet runway.

Figures B7 through B14 are all acceptable high-speed turns on wet runways for different wind conditions.

Figure B15 is an illustration of high-speed turnoff on a good dry runway, replacing the Kalman filter with the complementary filter in the navigation loop. Examination of the cross track error in Fig. B15 shows that the complementary filter does a good job until the turn is completed, at which time it ends up with an error in lateral deviation of 5 meters as compared with the Kalman filter deviation of only 2 meters.

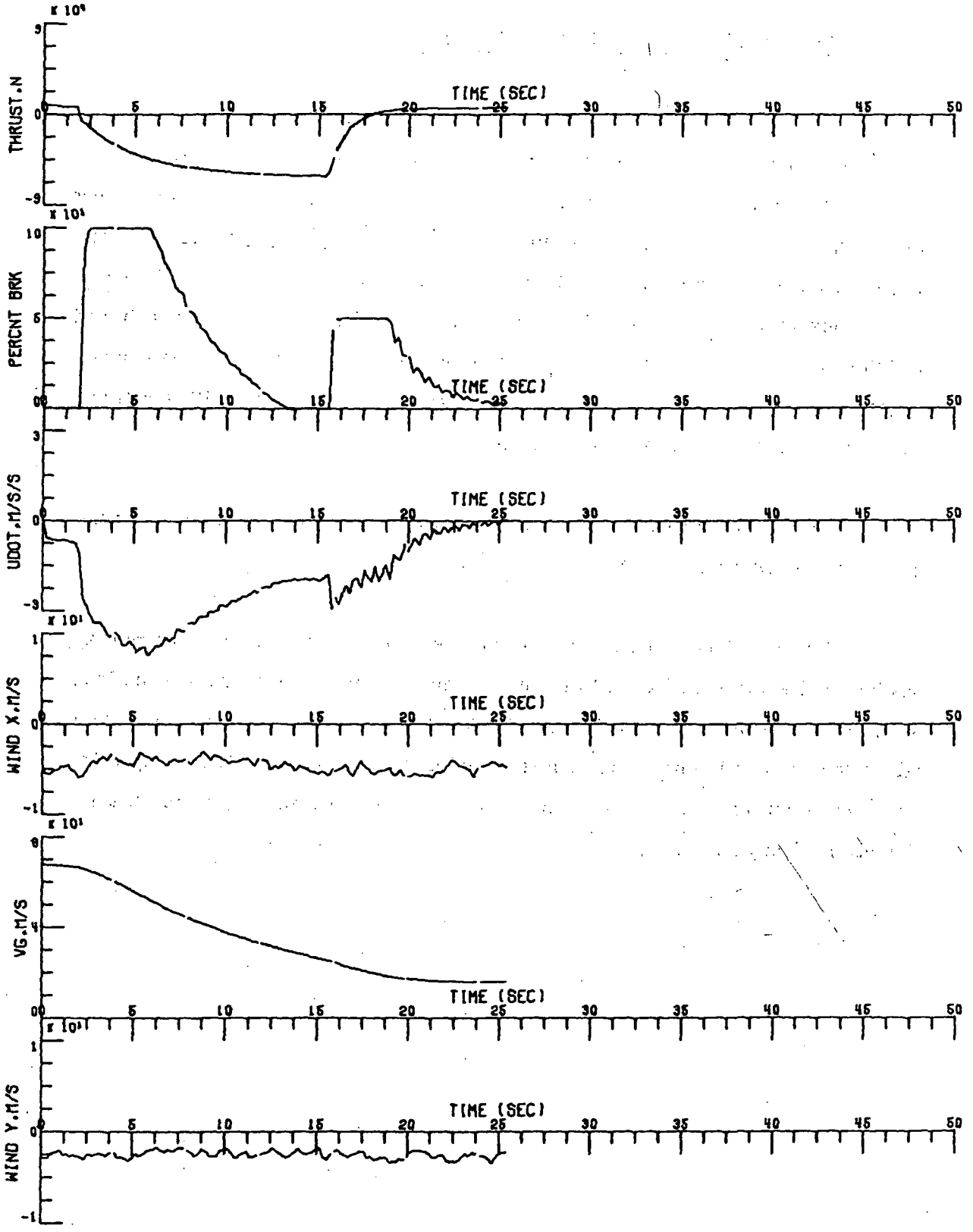

Figure B1a. High-Speed Turnoff on Dry Runway

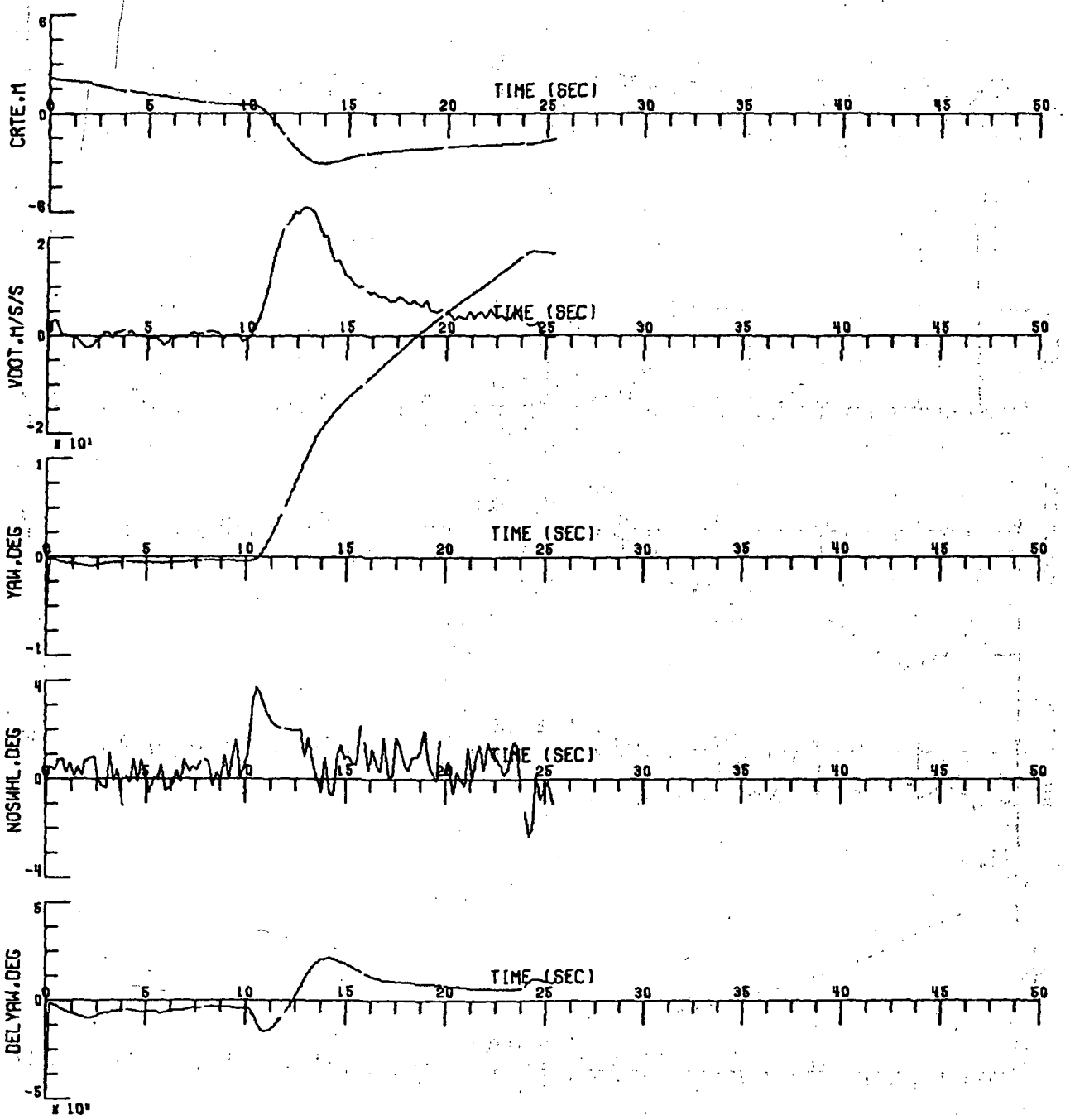

Figure B1b. High-Speed Turnoff on Dry Runway

30^{o} Tail Wind, 5.144m/sec (10 knots)
V_{coast} = 25.72 m/sec (50 knots)
V_{taxi} = 15.43 m/sec (30 knots)
R_T = 609.6 meters (2000 ft.)

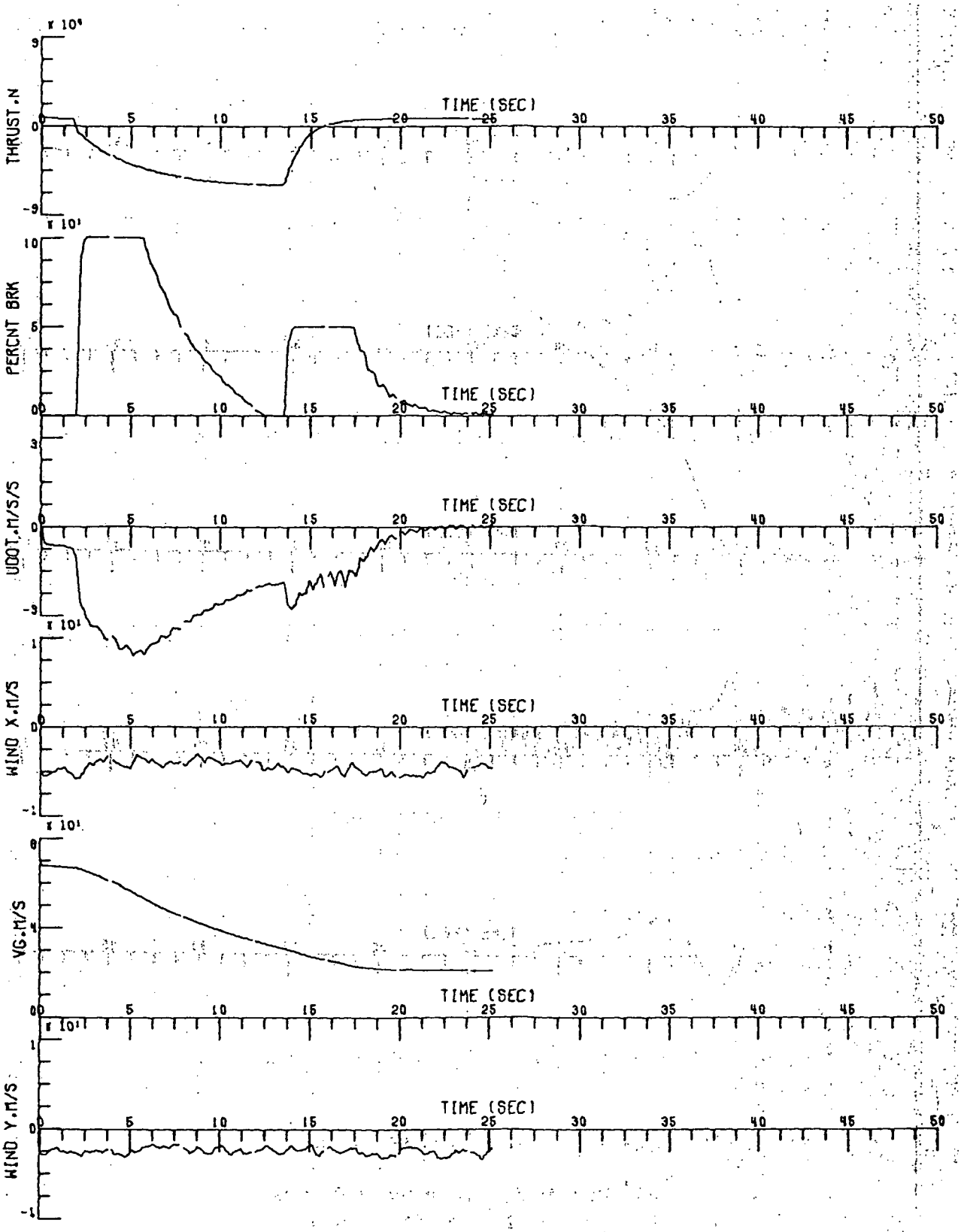

Figure B2a. High-Speed Turnoff on Dry Runway

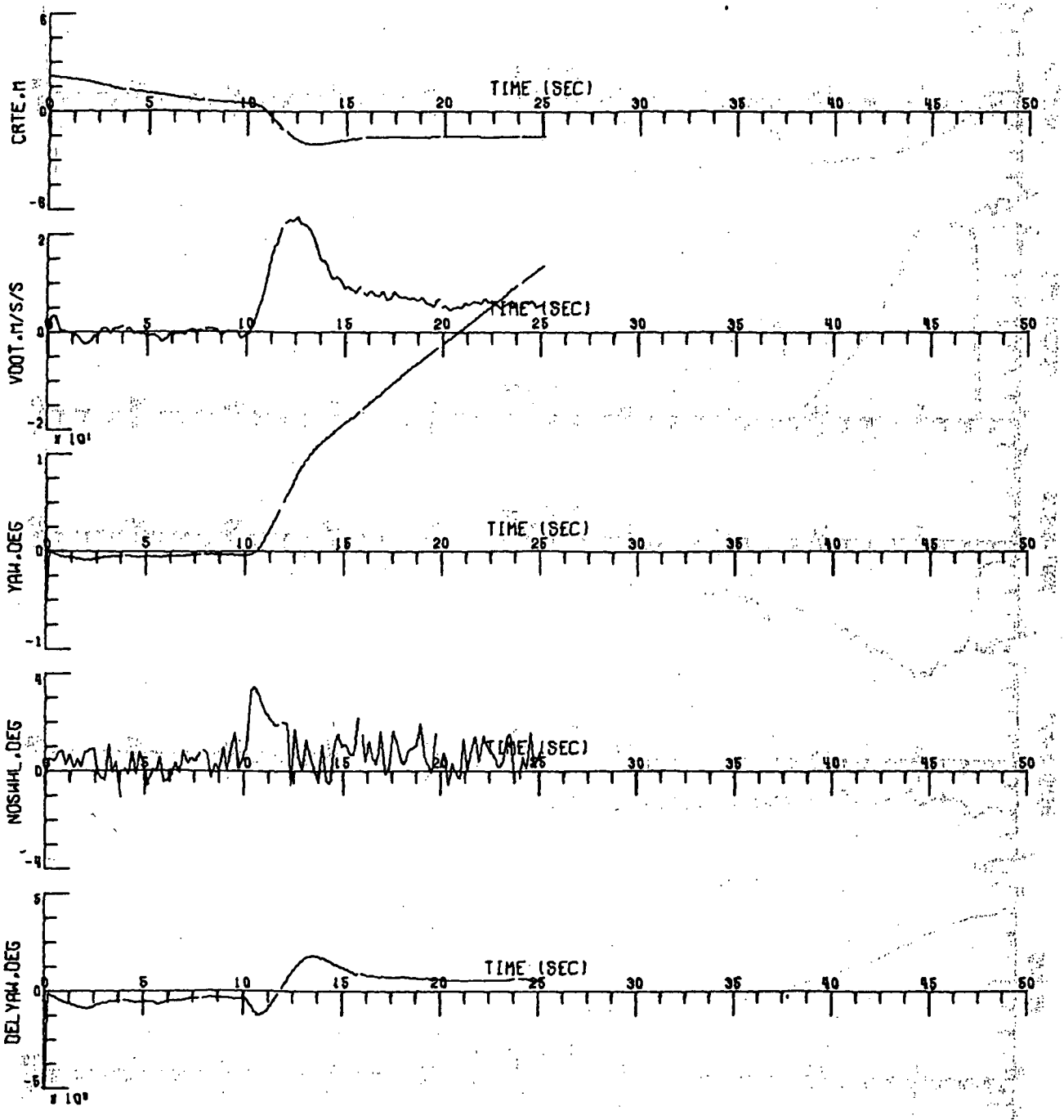

Figure B2b. High-Speed Turnoff on Dry Runway

30^{o} Tail Wind, 5.144 m/sec (10 knots)

V_{coast} = 30.86 m/sec (60 knots)

V_{taxi} = 20.57 m/sec (40 knots)

R_T = (2500 feet)

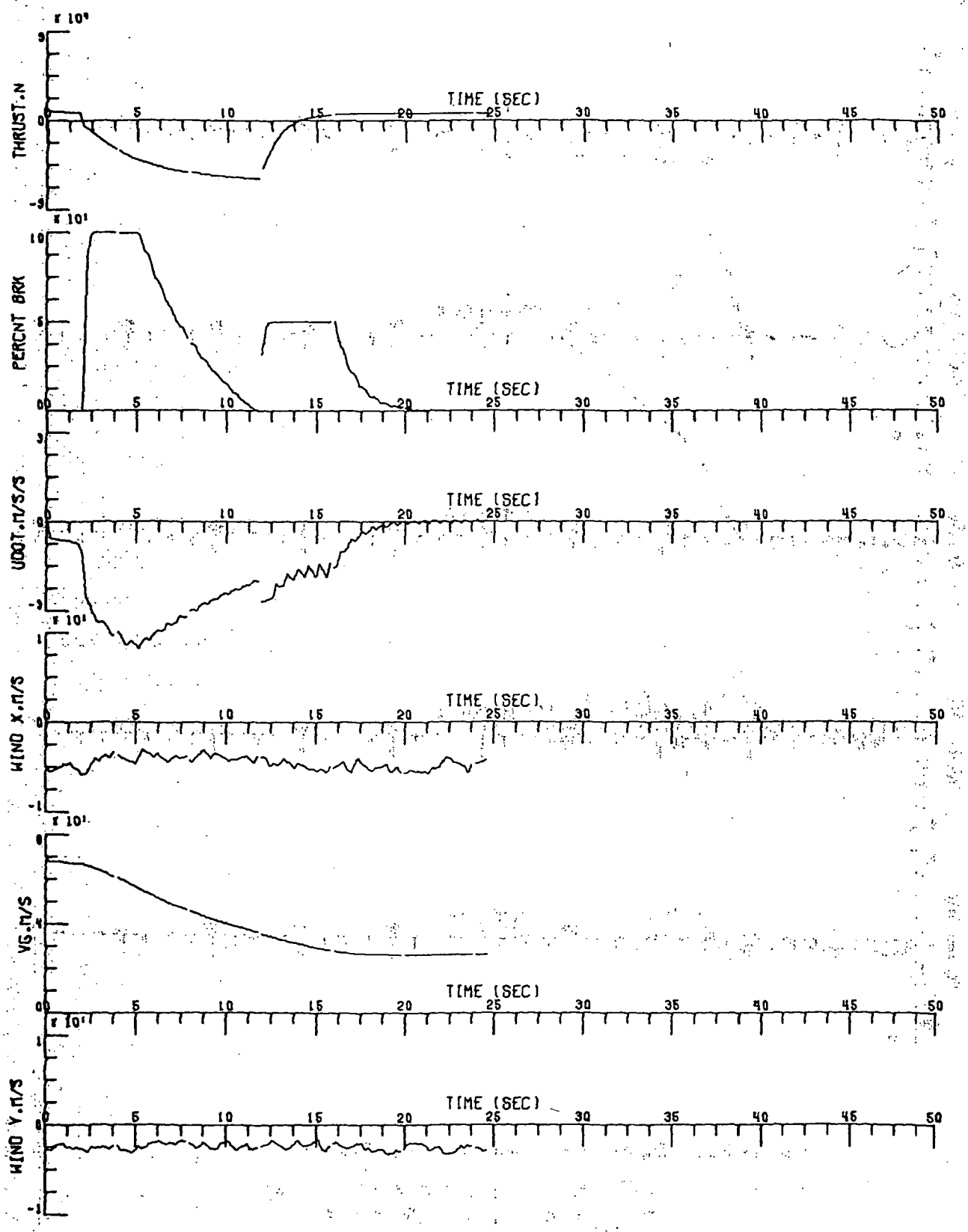

Figure B3a. High-Speed Turnoff on Dry Runway

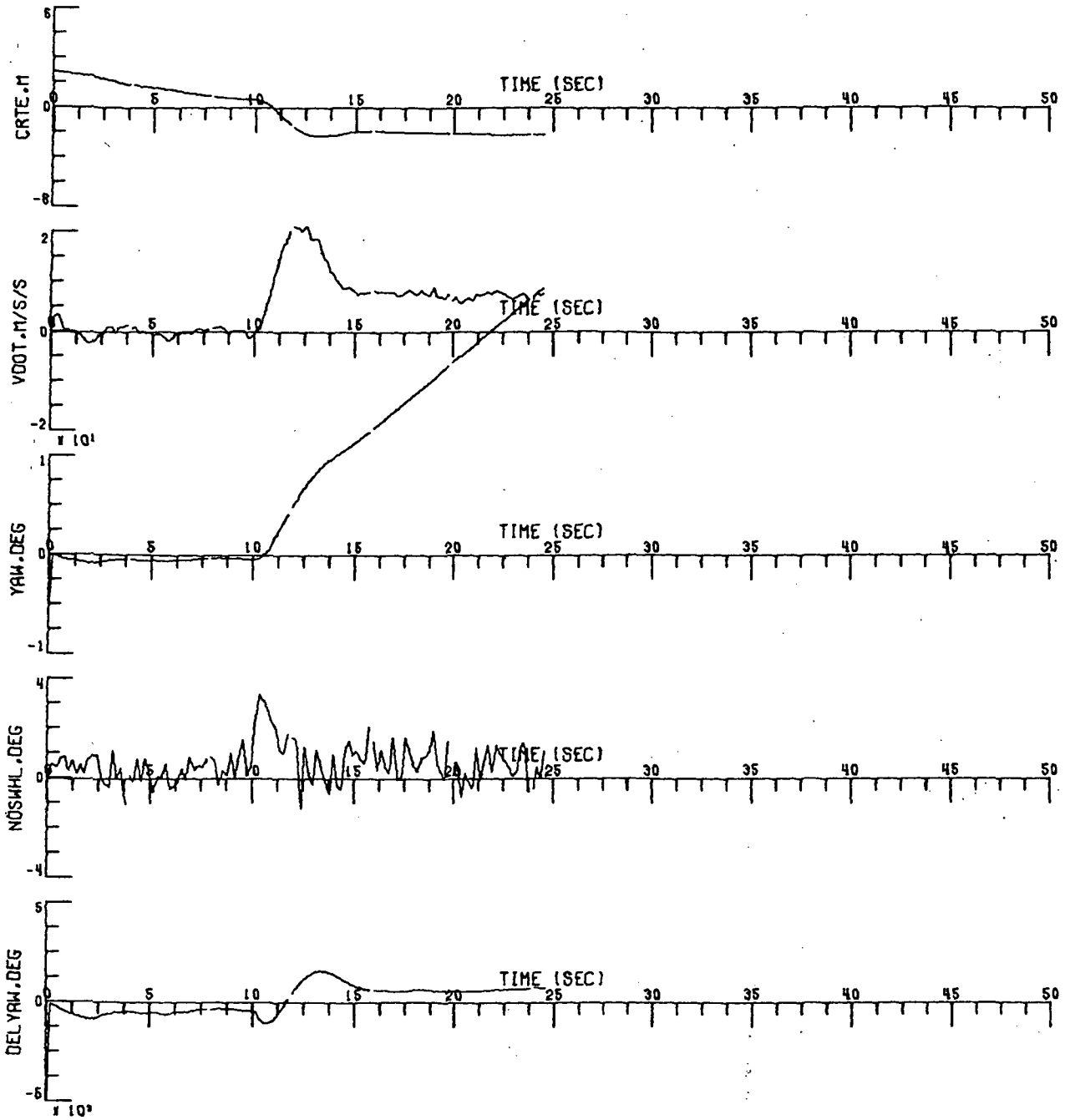

Figure B3b. High-Speed Turnoff on Dry Runway

30^{o} Tail Wind, 5.144 m/sec (10 knots)
V_{coast} = 36.01 m/sec (70 knots)
V_{taxi} = 25.72 m/sec (50 knots)
R_T = (3500 feet)

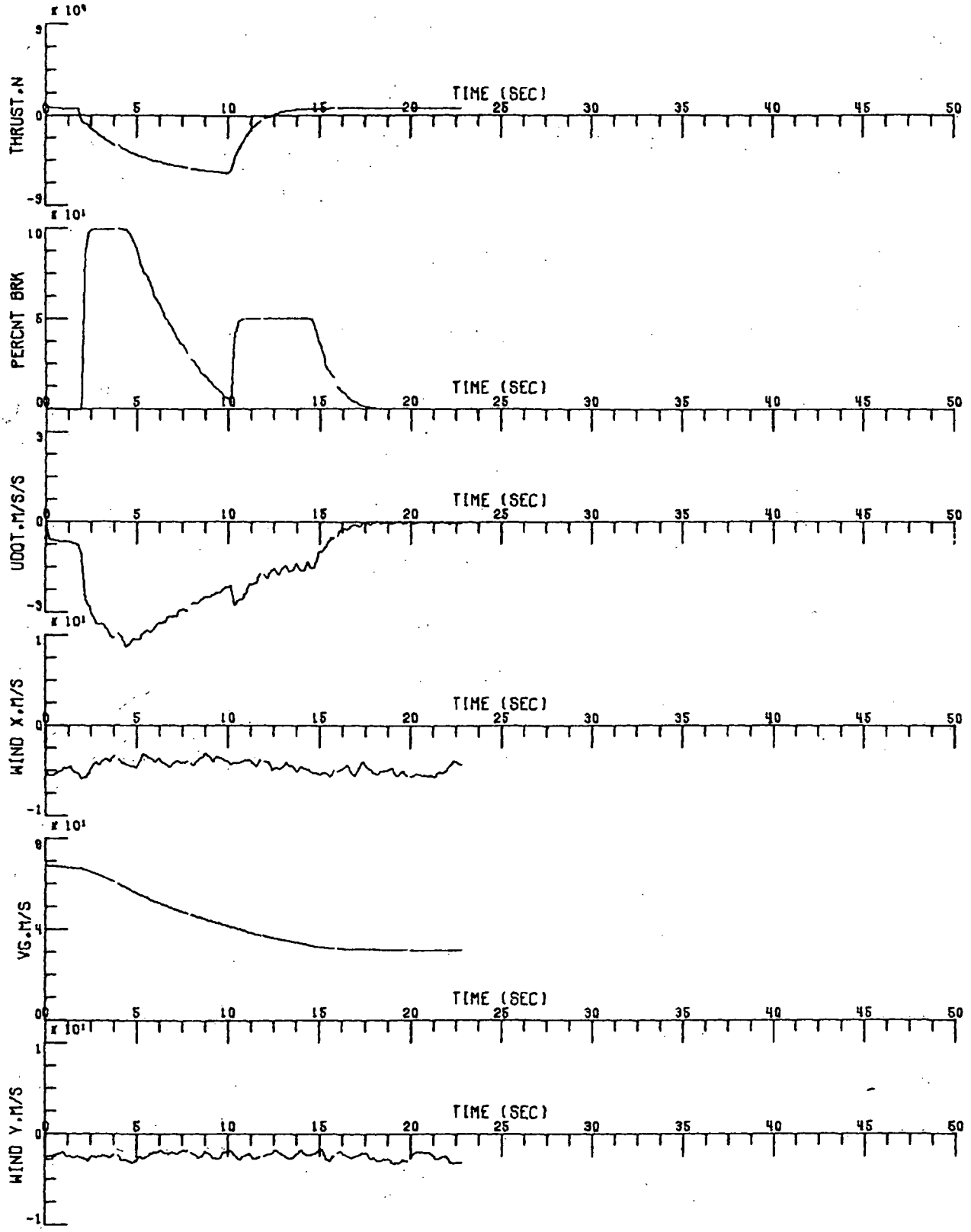

Figure B4a. High-Speed Turnoff of Dry Runway

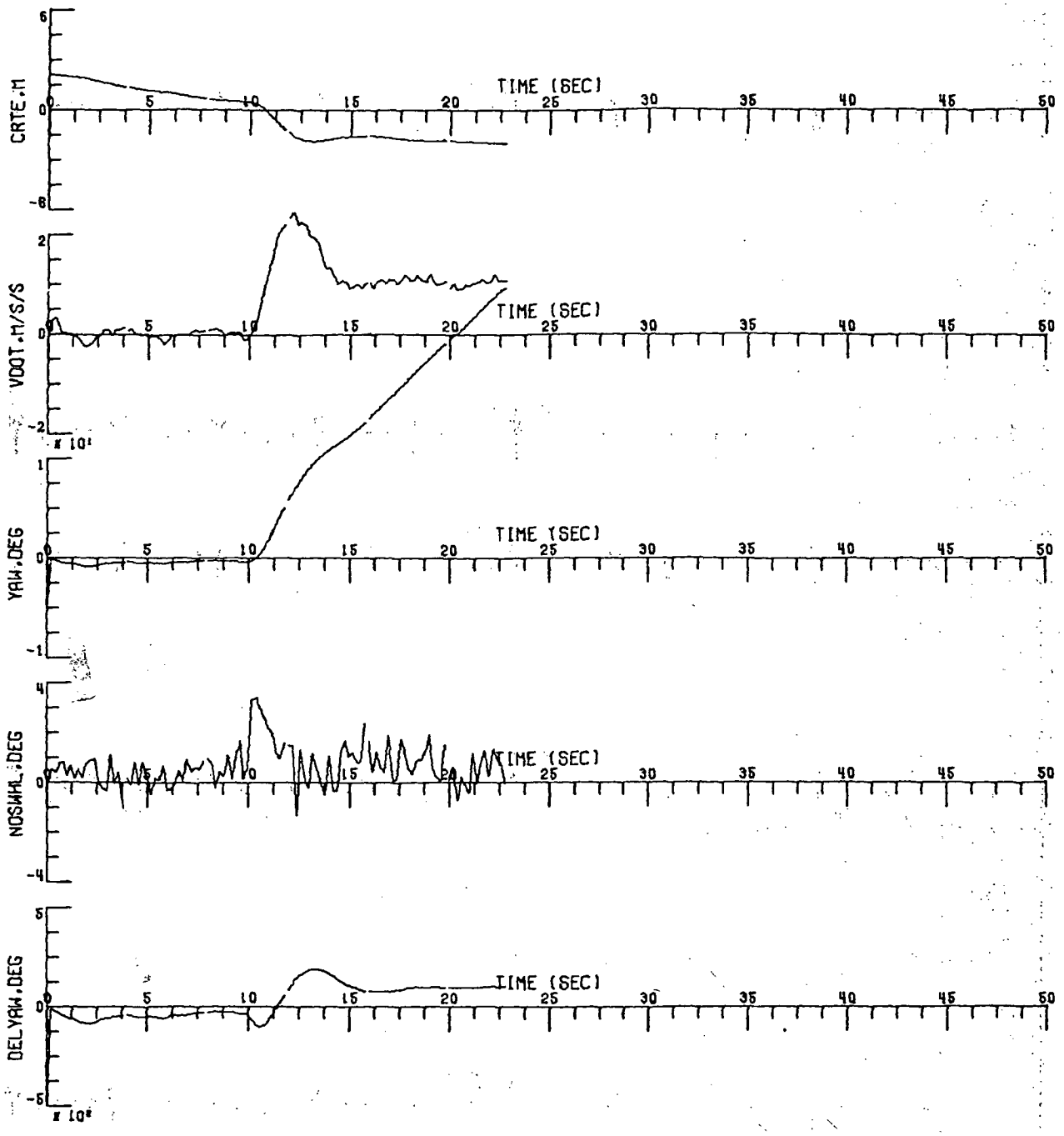

Figure B4b. High-Speed Turnoff on Dry Runway

30^{o} Tail Wind, 5.144 m/sec (10 knots)
V_{coast} = 41.16 m/sec (80 knots)
V_{taxi} = 30.87 m/sec (60 knots)
R_T =(3500 feet)

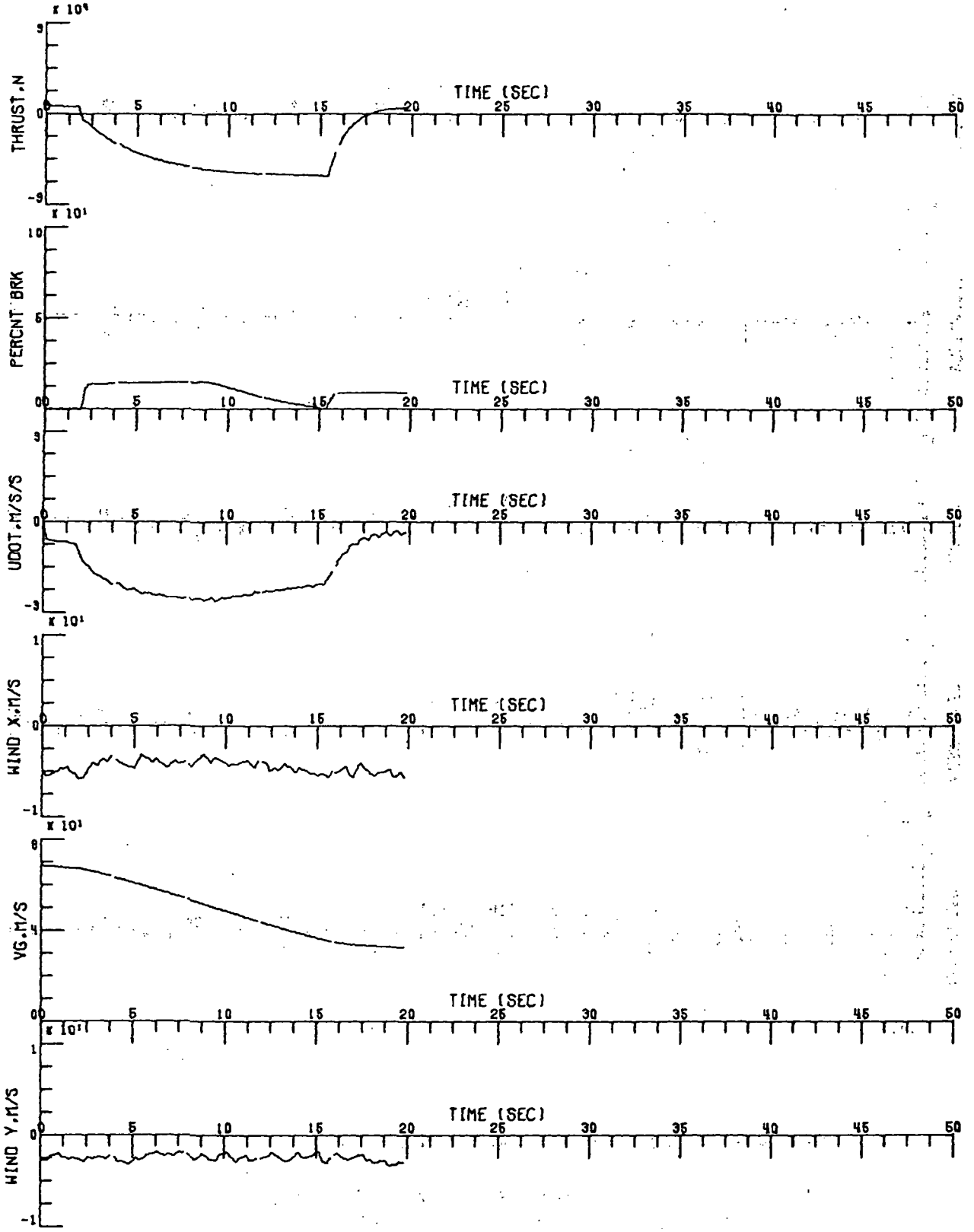

Figure B5a. High-Speed Turnoff on Wet Runway

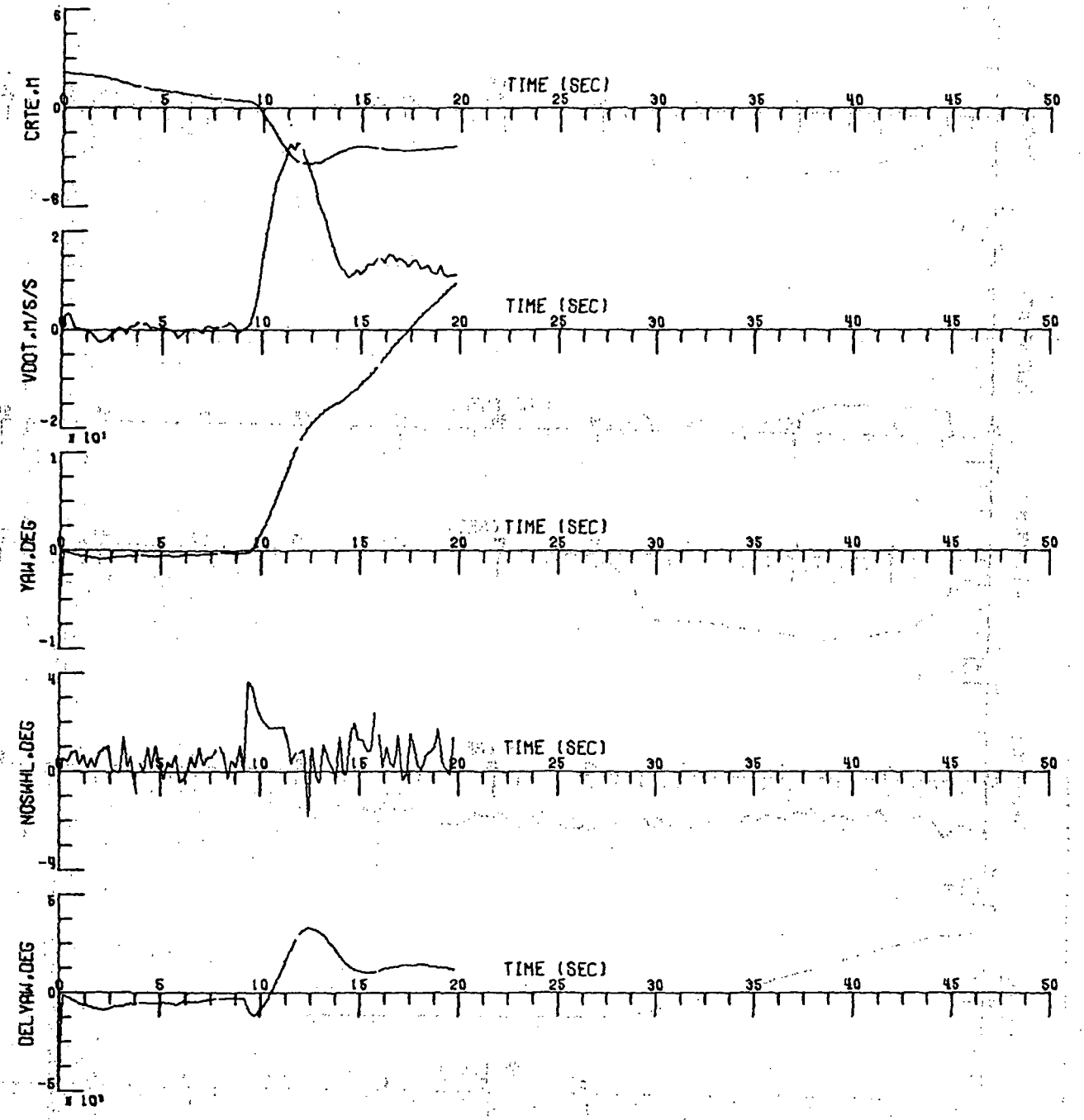

Figure B5b. High-Speed Turnoff on Wet Runway

30^{o} Tail Wind, 5.144 m/sec

V_{coast} = 36.01 m/sec (70 knots)

V_{taxi} = 25.72 m/sec (50 knots)

R_T = (3000 feet)

Runway turnoff distance = (3500 feet)

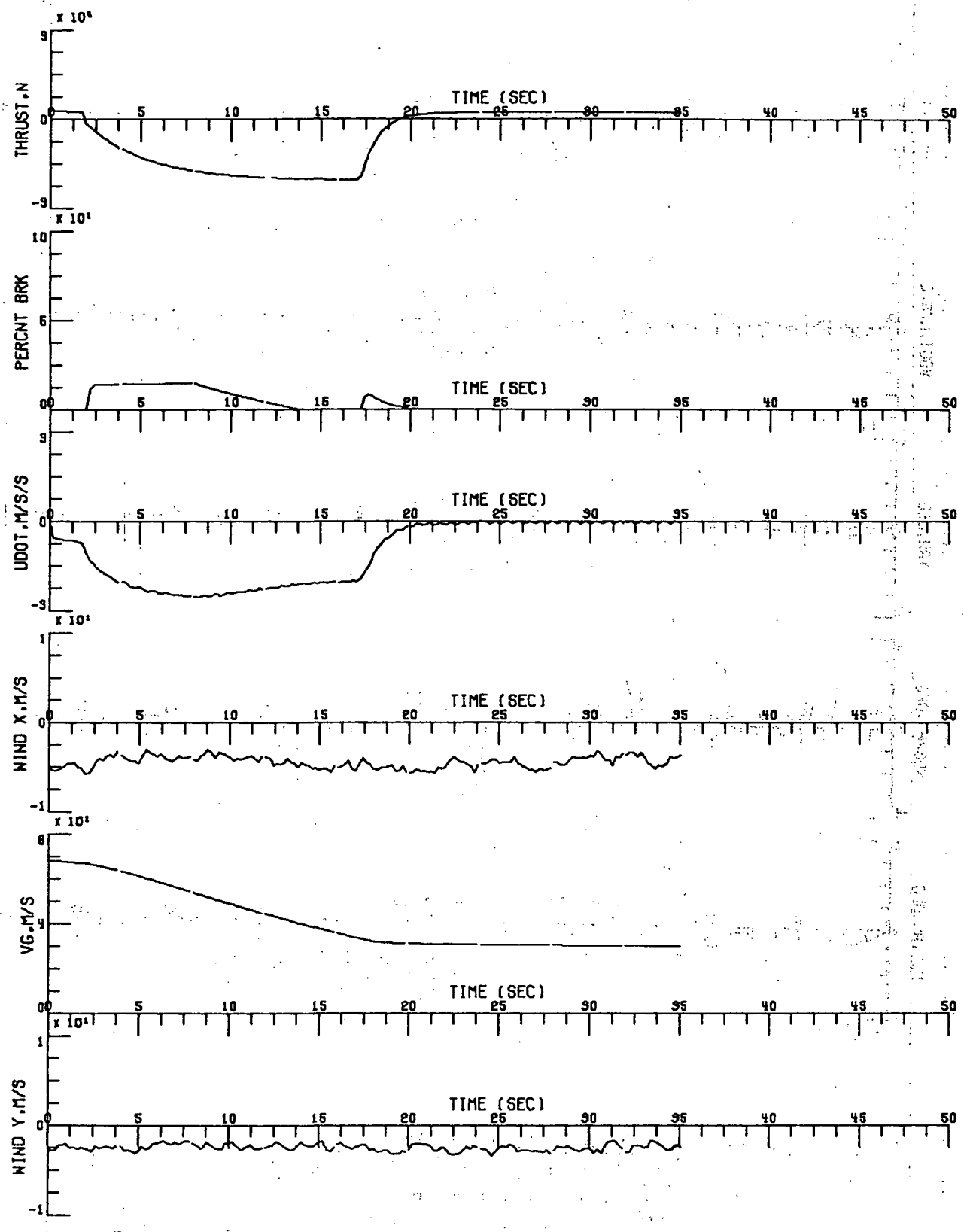

Figure B6a. High-Speed Turnoff on Wet Runway

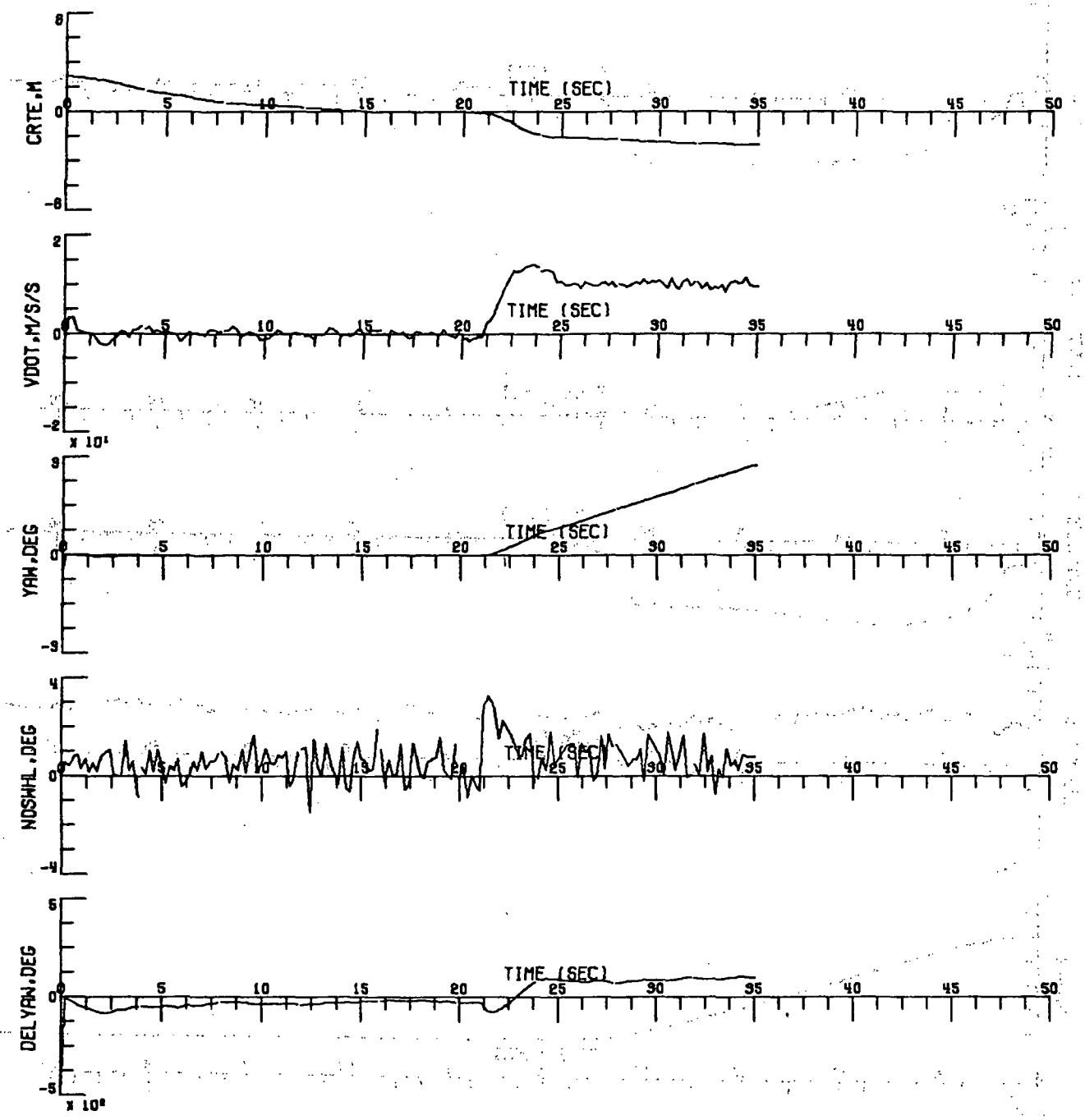

Figure B6b. High-Speed Turnoff on Wet Runway

30^{o} Tail Wind, 5.144 m/sec (10 knots)
V_{coast} = 33.44 m/sec (65 knots)
V_{taxi} = 30.87 m/sec (60 knots)
R_T = (3000 feet)
Runway turnoff distance = (5000 feet)

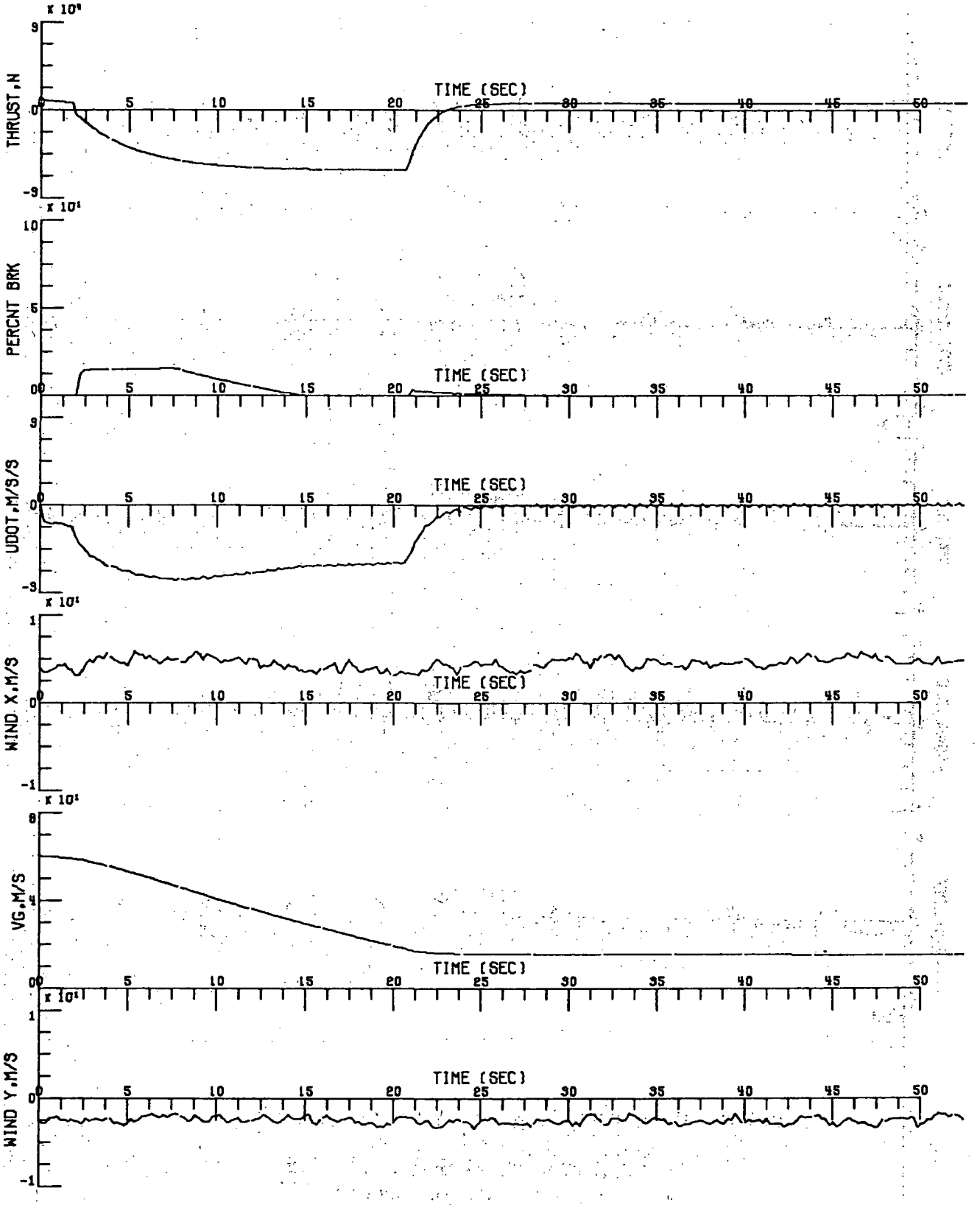

Figure B7a. High-Speed Turnoff on Wet Runway

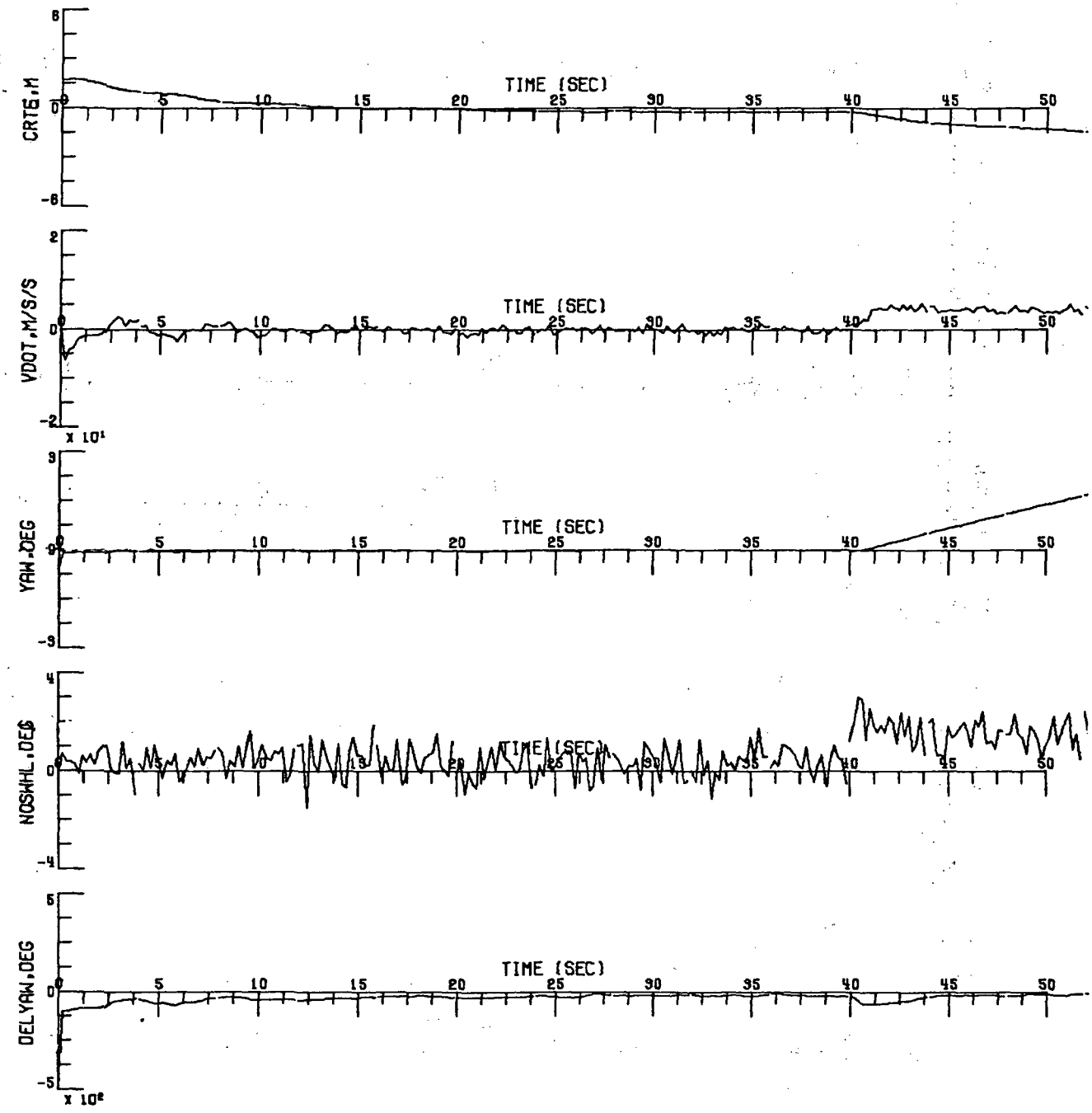

Figure B7b. High-Speed Turnoff on Wet Runway

150^{o} Head Wind, 5.144 m/sec (10 knots)
V_{coast} = 18.00 m/sec (35 knots)
V_{taxi} = 15.43 m/sec (30 knots)
R_T = (2000 feet)
Runway turnoff distance = (5000 feet)

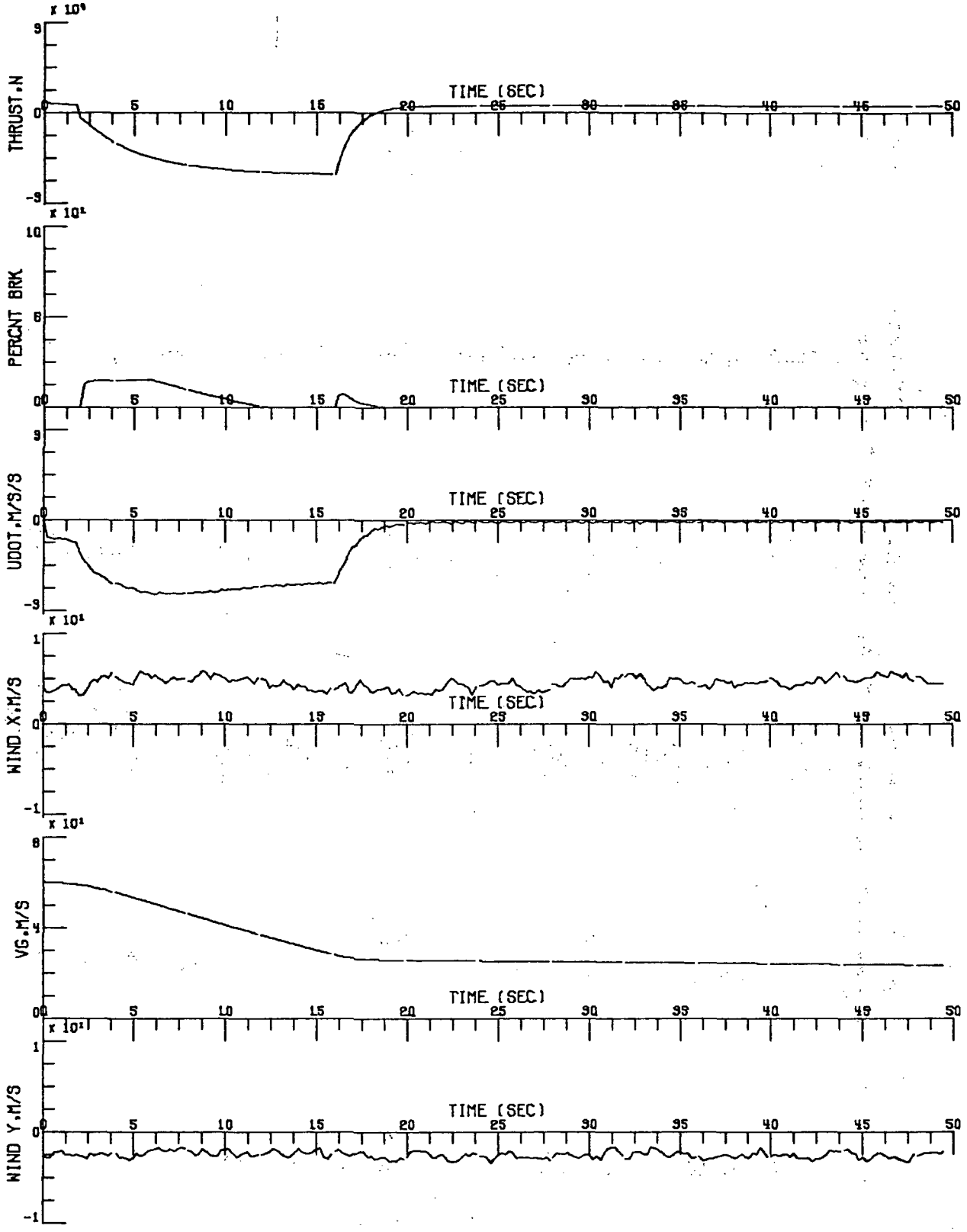

Figure B8a. High-Speed Turnoff on Wet Runway

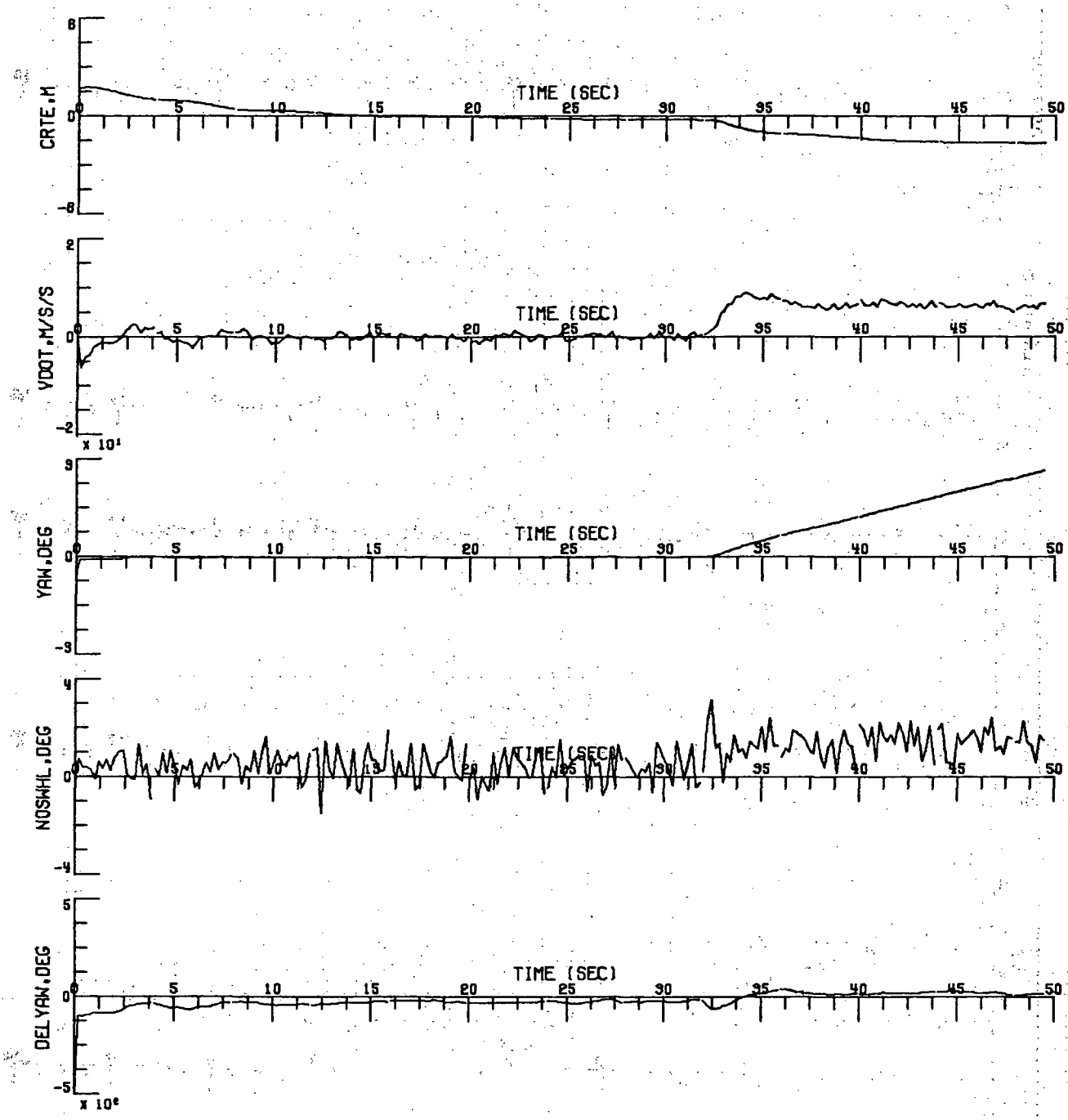

Figure B8b. High-Speed Turnoff on Wet Runway

150^{o} Head Wind, 5.144 m/sec (10 knots)
V_{coast} = 28.29 m/sec (55 knots)
V_{taxi} = 25.72 m/sec (50 knots)
R_T = (3000 feet)

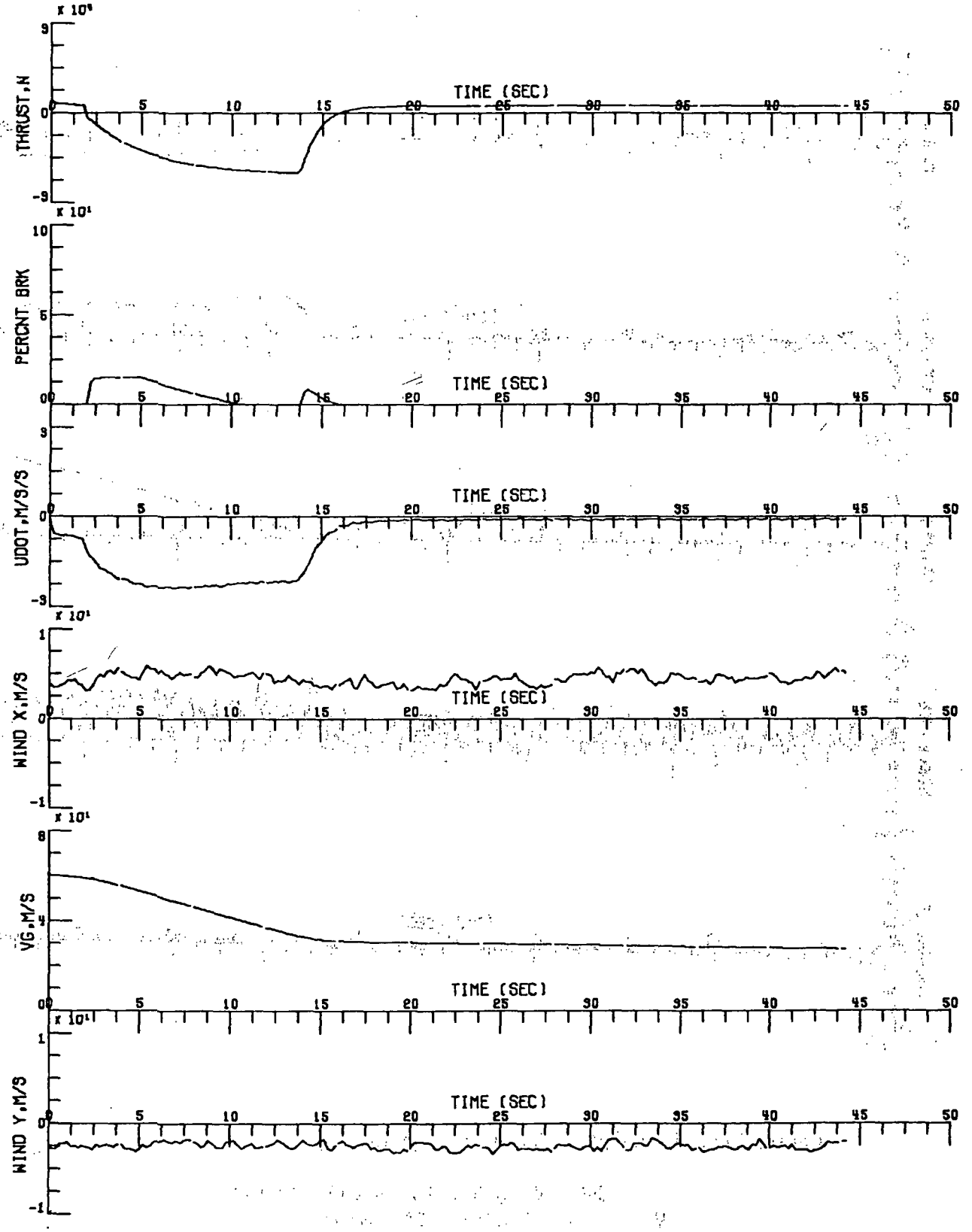

Figure B9a. High-Speed Turnoff on Wet Runway

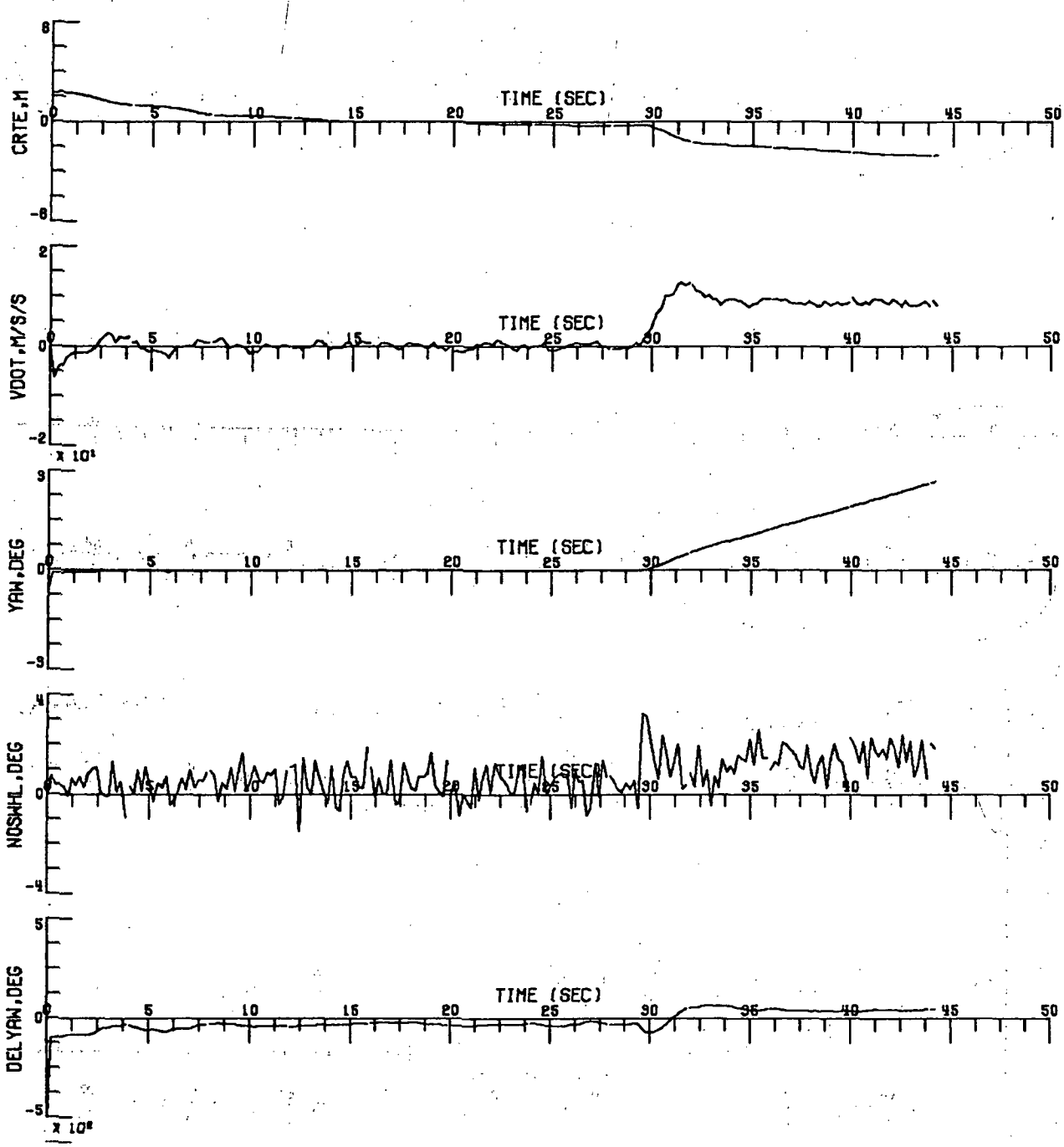

Figure B9b. High-Speed Turnoff on Wet Runway

150^{o} Head Wind, 5.144 m/sec (10 knots)
V_{coast} = 33.44 m/sec (65 knots)
V_{taxi} = 30.87 m/sec (60 knots)
R_T = (3000 feet)

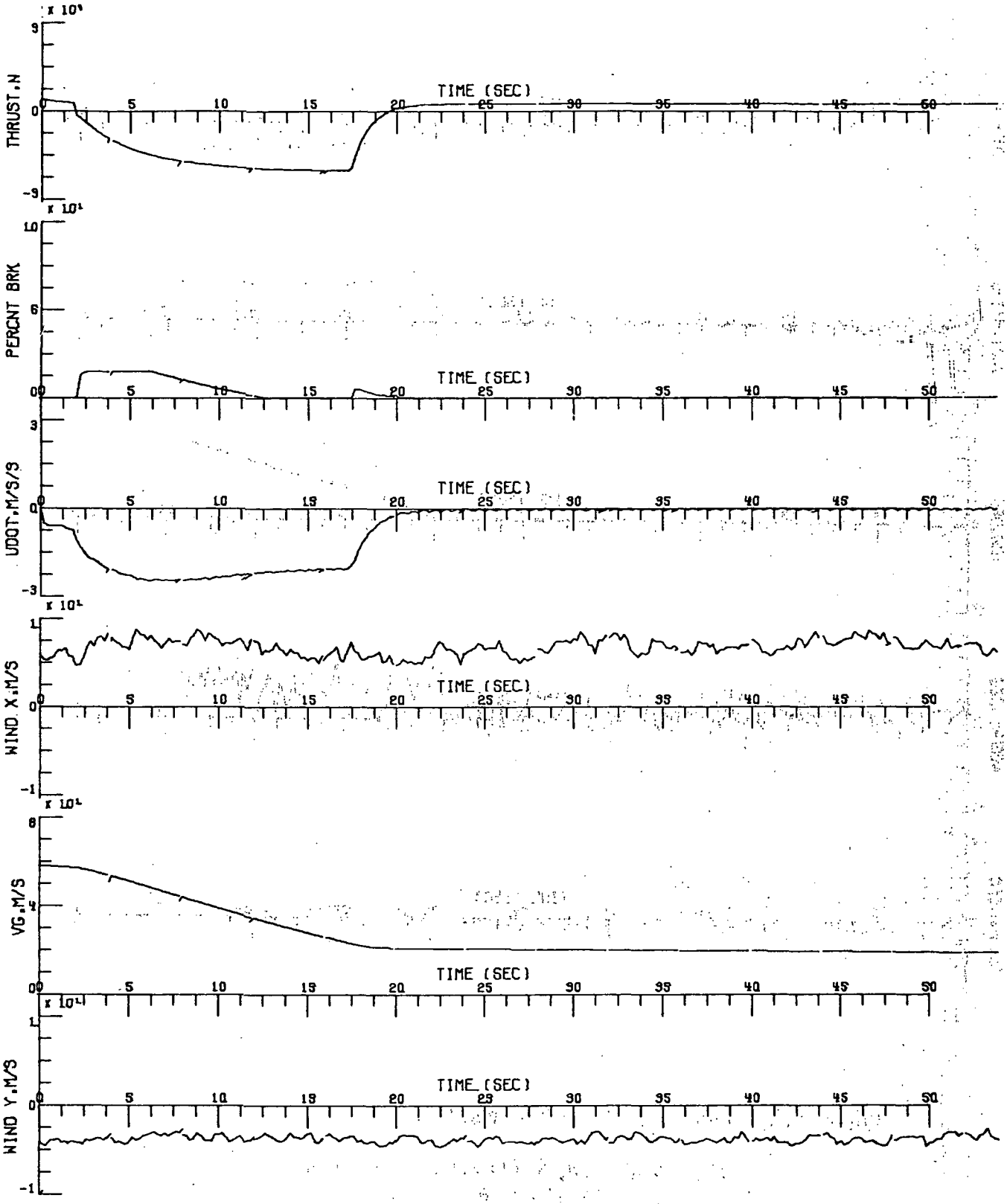

Figure B10a. High-Speed Turnoff on Wet Runway

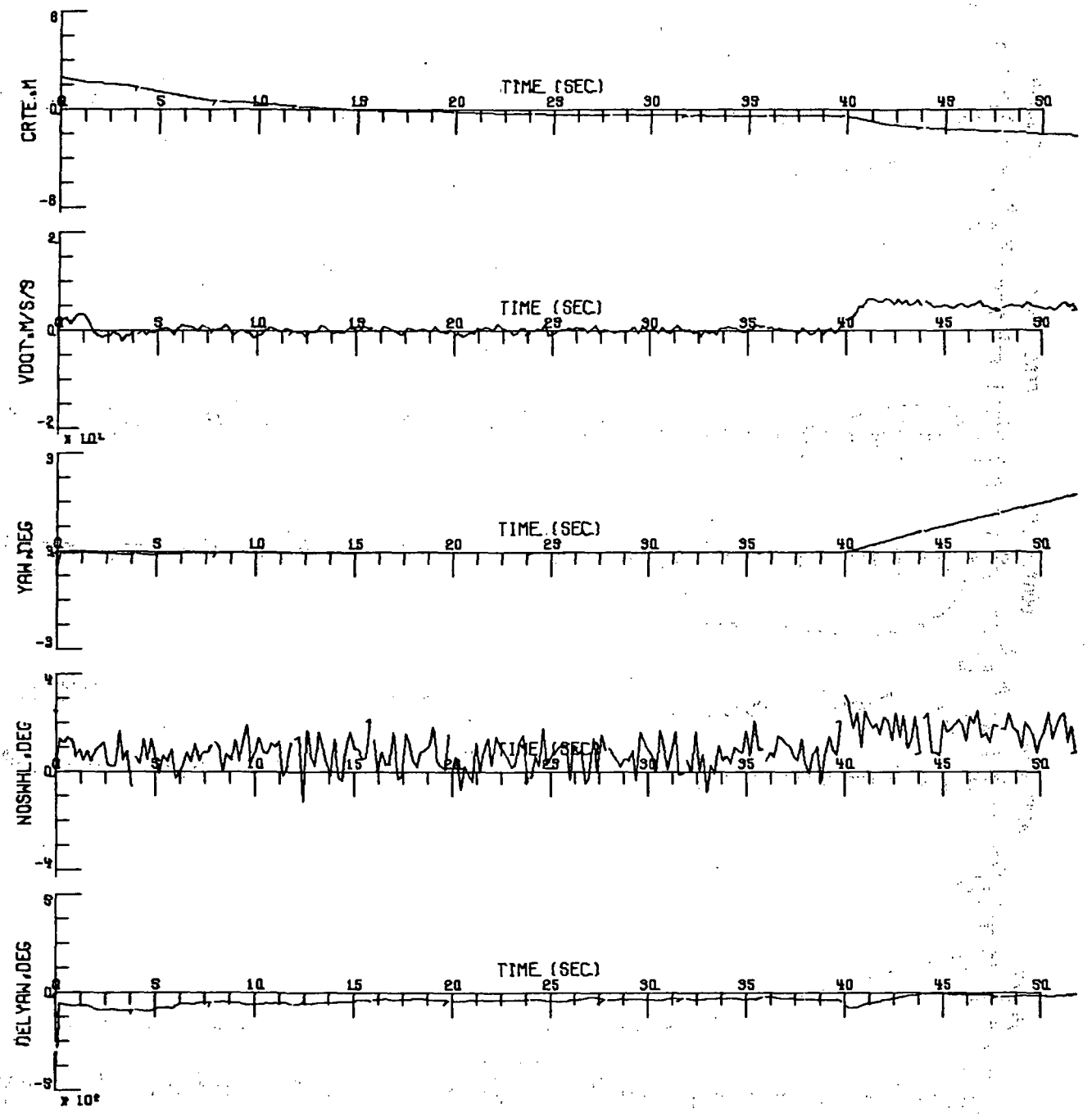

Figure B10b. High-Speed Turnoff on Wet Runway

150^{o} Head Wind, 7.716 m/sec
V_{coast} = 23.15 m/sec (45 knots)
V_{taxi} = 20.58 m/sec (40 knots)
R_T = (2500 feet)
Runway turnoff distance = (5000 feet)

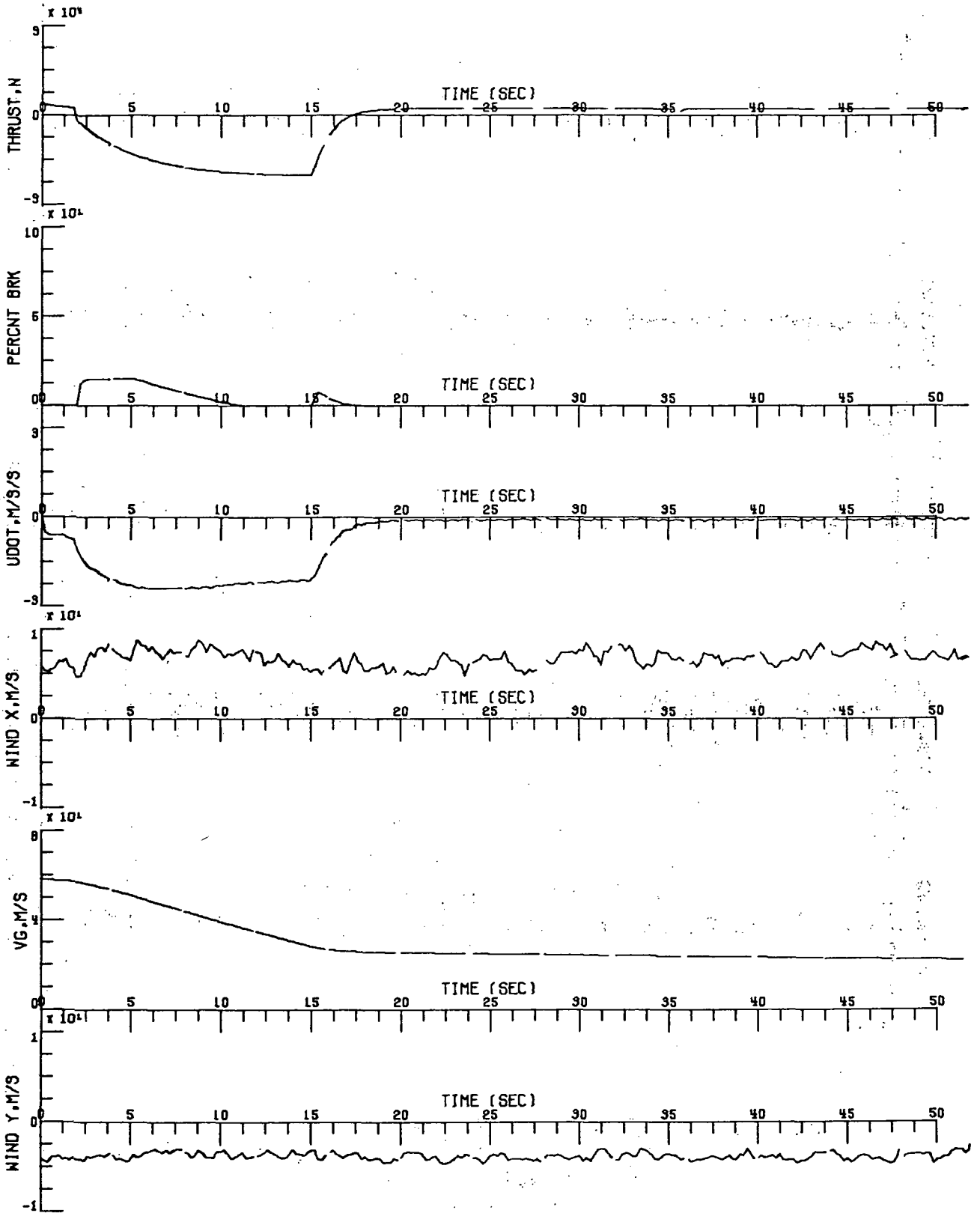

Figure B11a. High-Speed Turnoff on Wet Runway

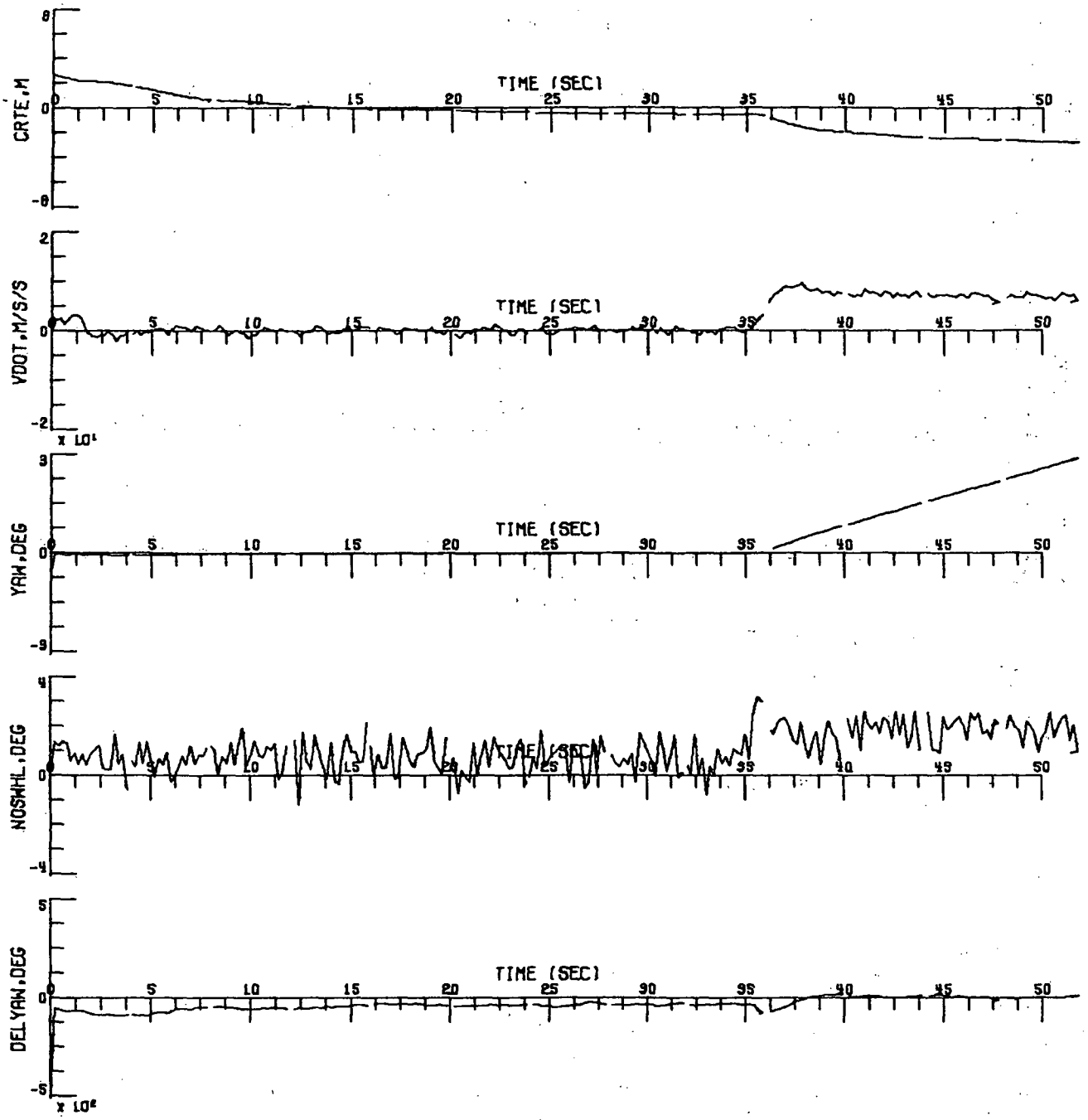

Figure B11b. High-Speed Turnoff on Wet Runway

150^{o} Head Wind, 7.716 m/sec (15 knots)
V_{coast} = 28.29 m/sec (55 knots)
V_{taxi} = 25.72 m/sec (50 knots)

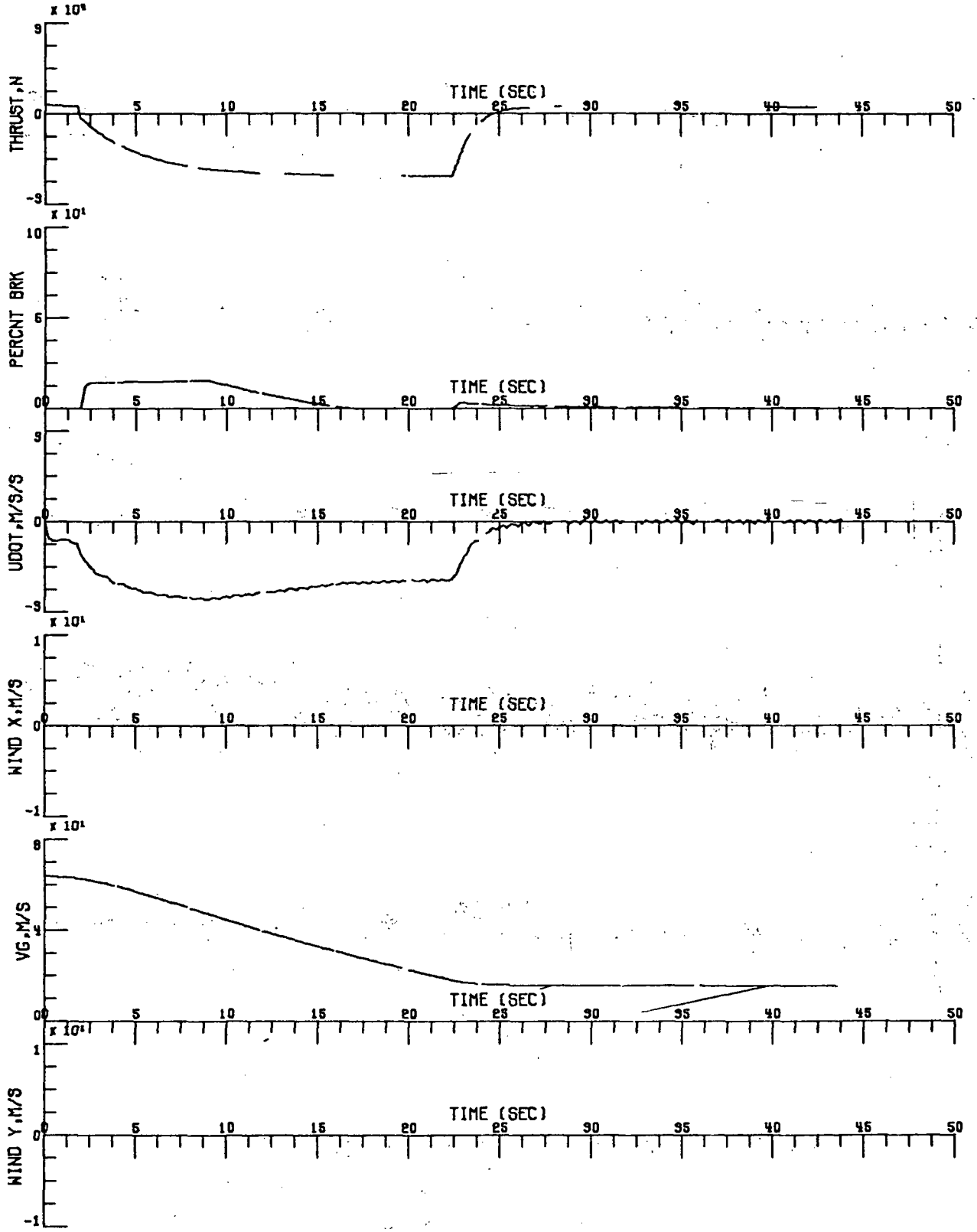

Figure B12a. High-Speed Turnoff on Wet Runway

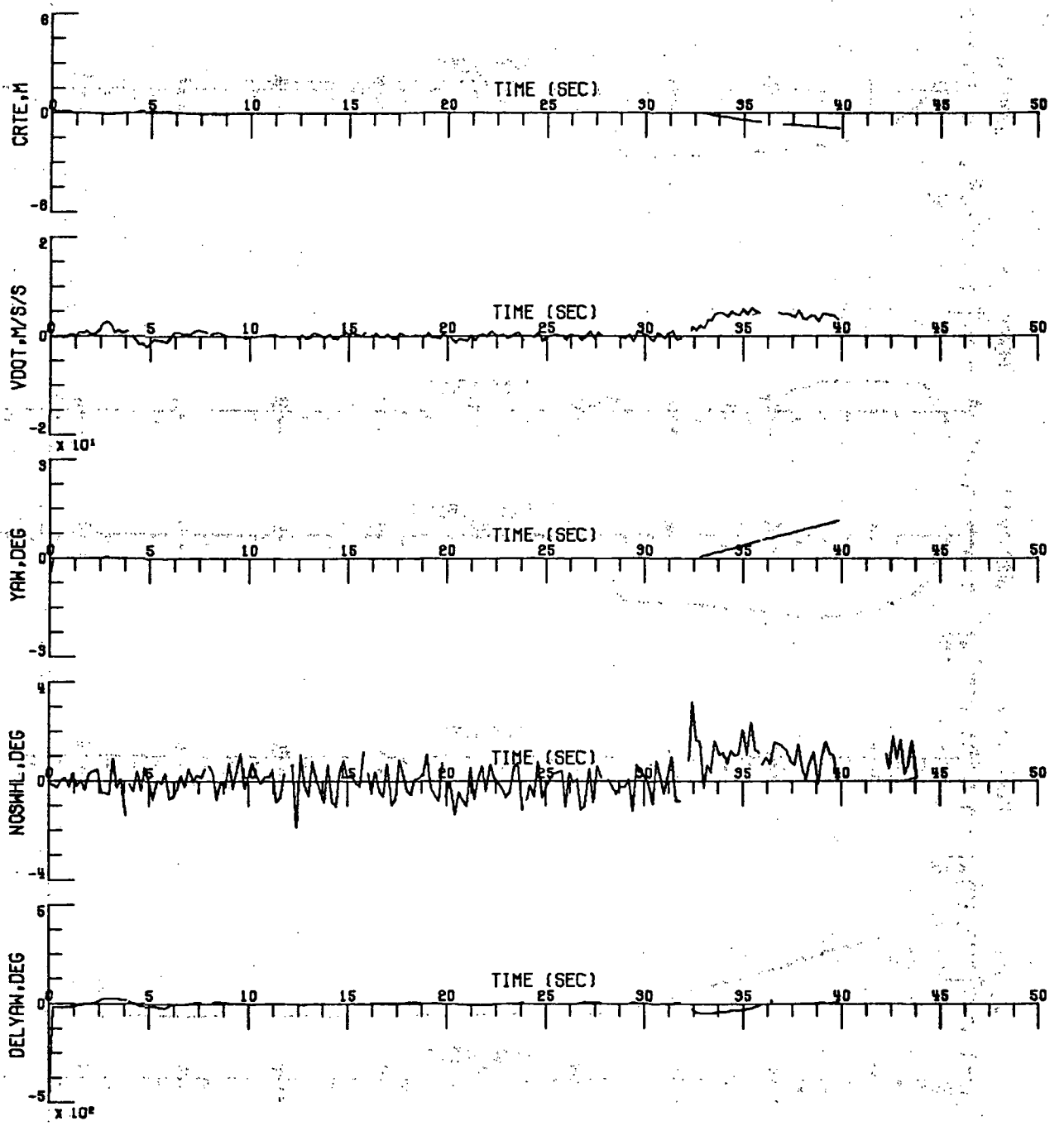

Figure B12b. High-Speed Turnoff on Wet Runway

No Winds
V_{coast} = 18.00 m/sec (35 knots)
V_{taxi} = 15.43 m/sec (30 knots)
R_T = (2000 feet)
Runway turnoff distance = (5000 feet)

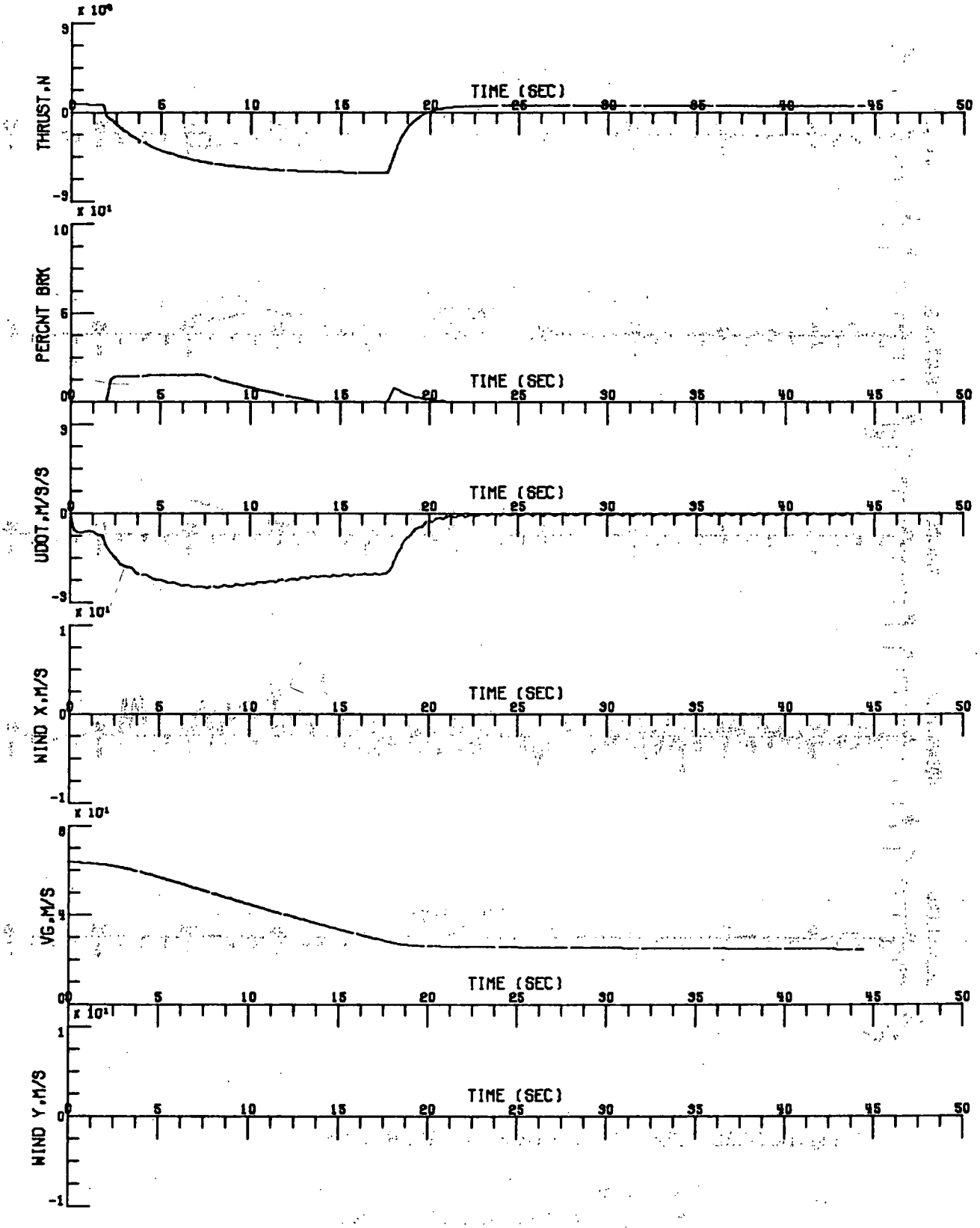

Figure B13a. High-Speed Turnoff on Wet Runway

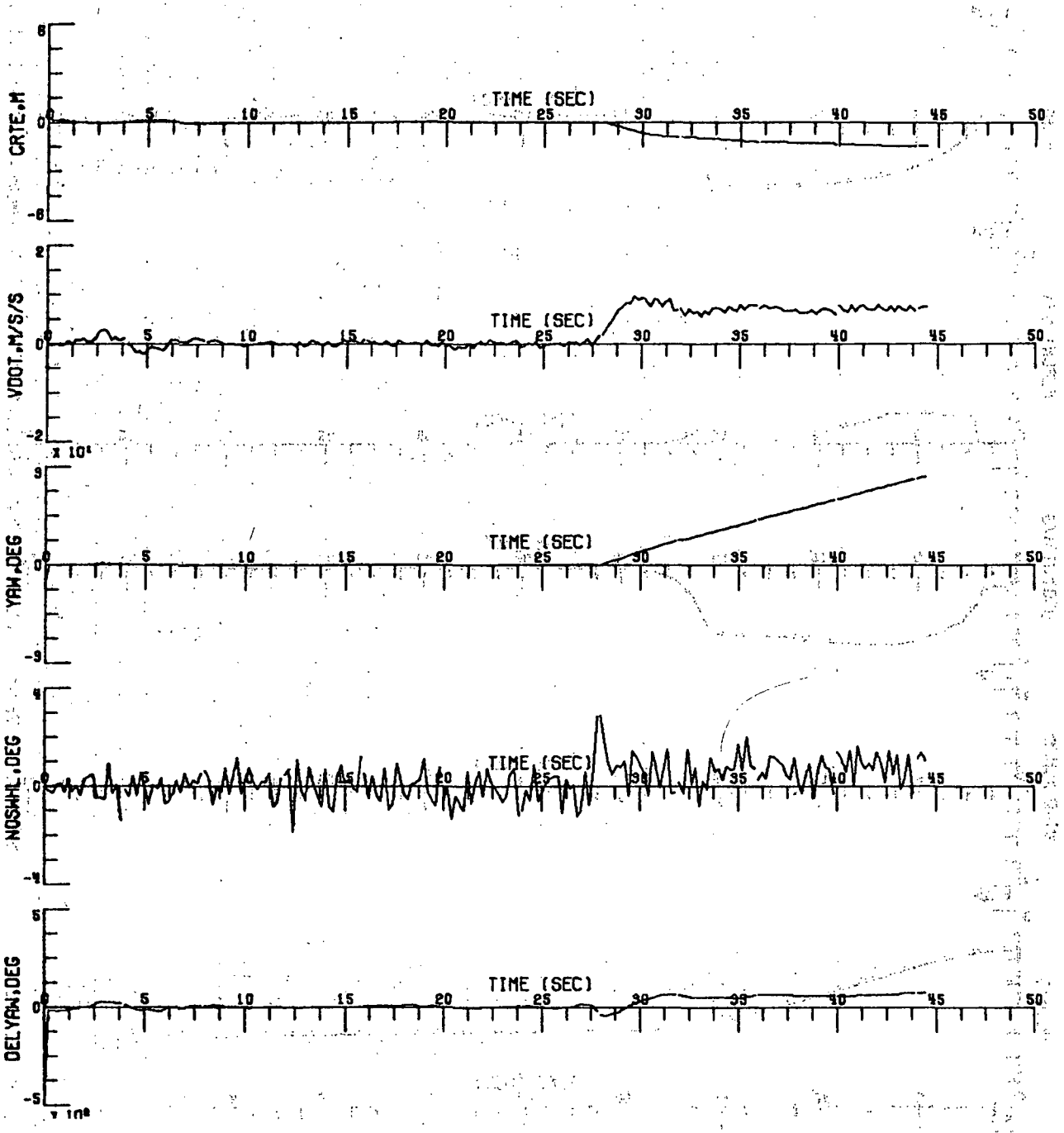

Figure B13b. High-Speed Turnoff on Wet Runway

No Winds

V_{coast} = 28.29 m/sec (55 knots)

V_{taxi} = 25.72 m/sec (50 knots)

R_T =(3000 feet)

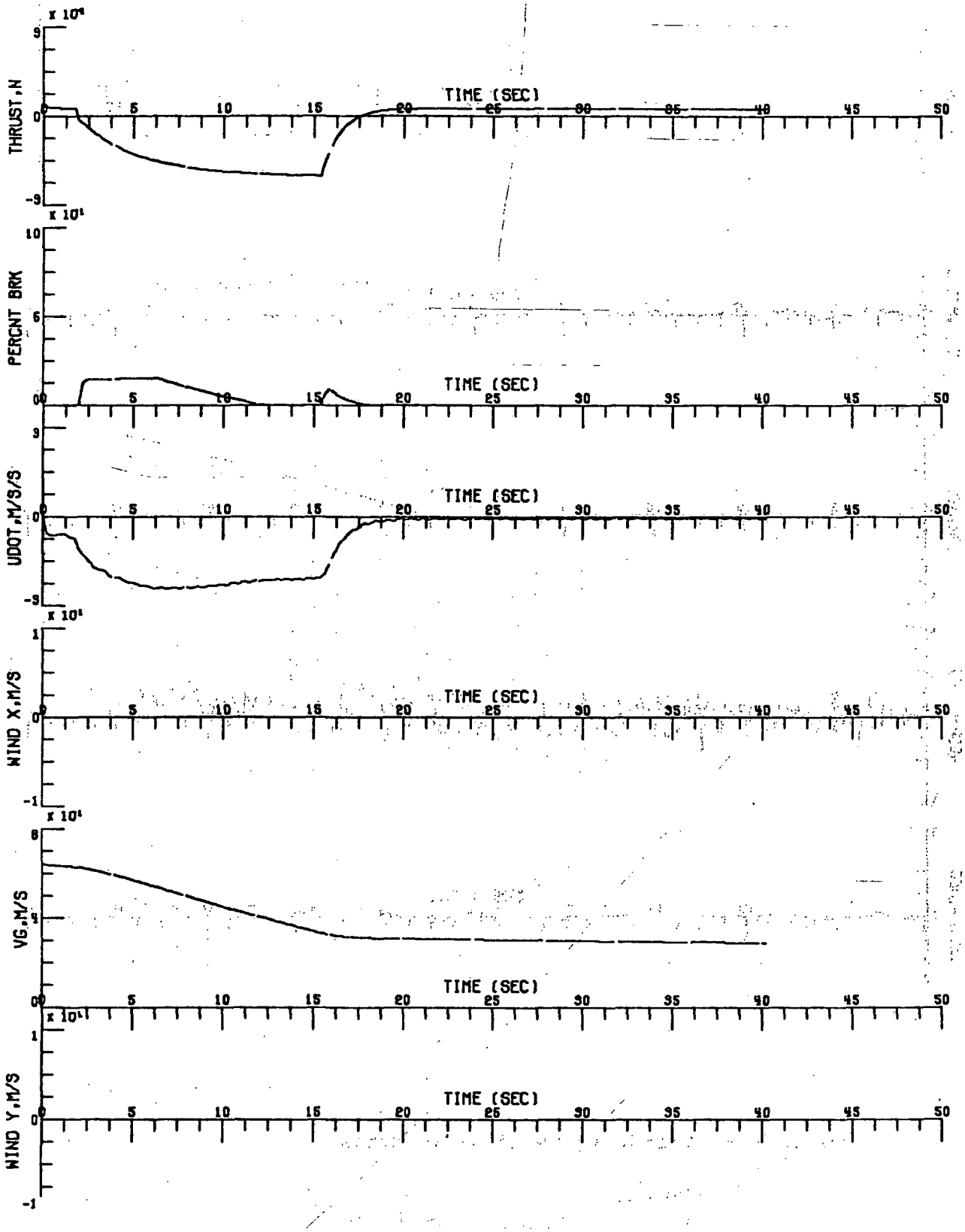

Figure B14a. High-Speed Turnoff on Wet Runway

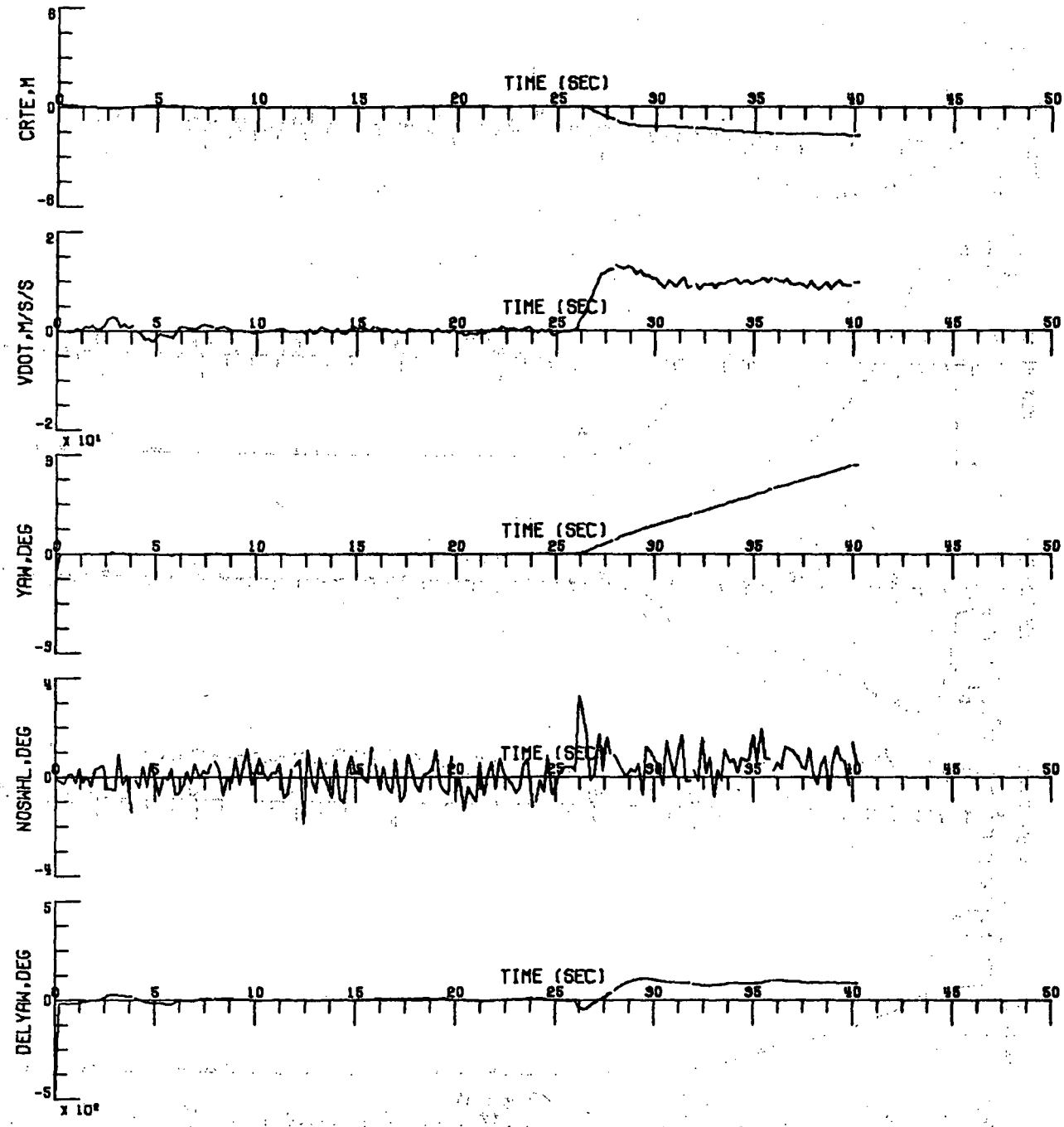

Figure B14b. High-Speed Turnoff on Wet Runway

No Winds

V_{coast} = 33.44 m/sec (65 knots)

V_{taxi} = 30.87 m/sec (60 knots)

R_T = (3000 feet)

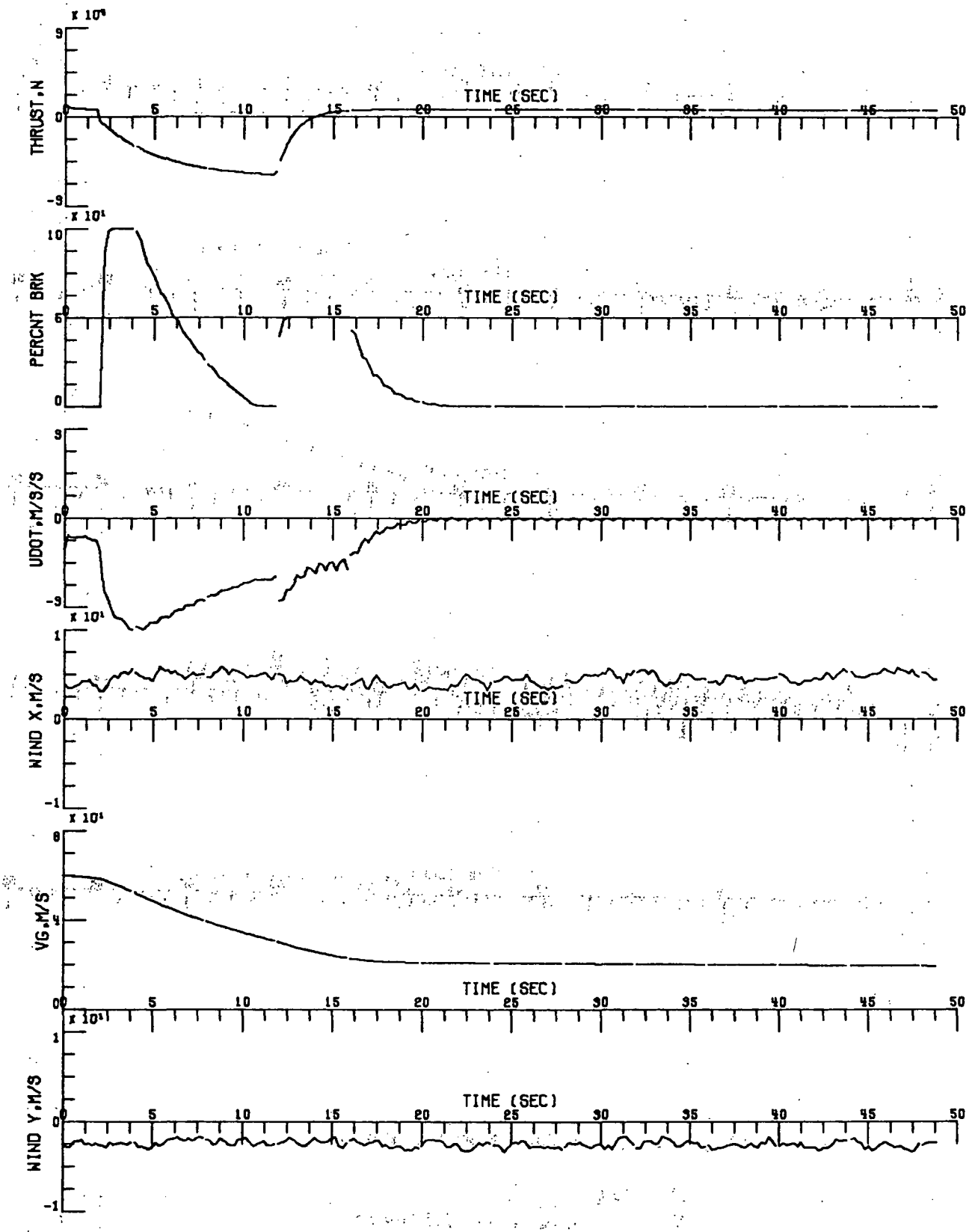

Figure B15a. High-Speed Turnoff on Dry Runway

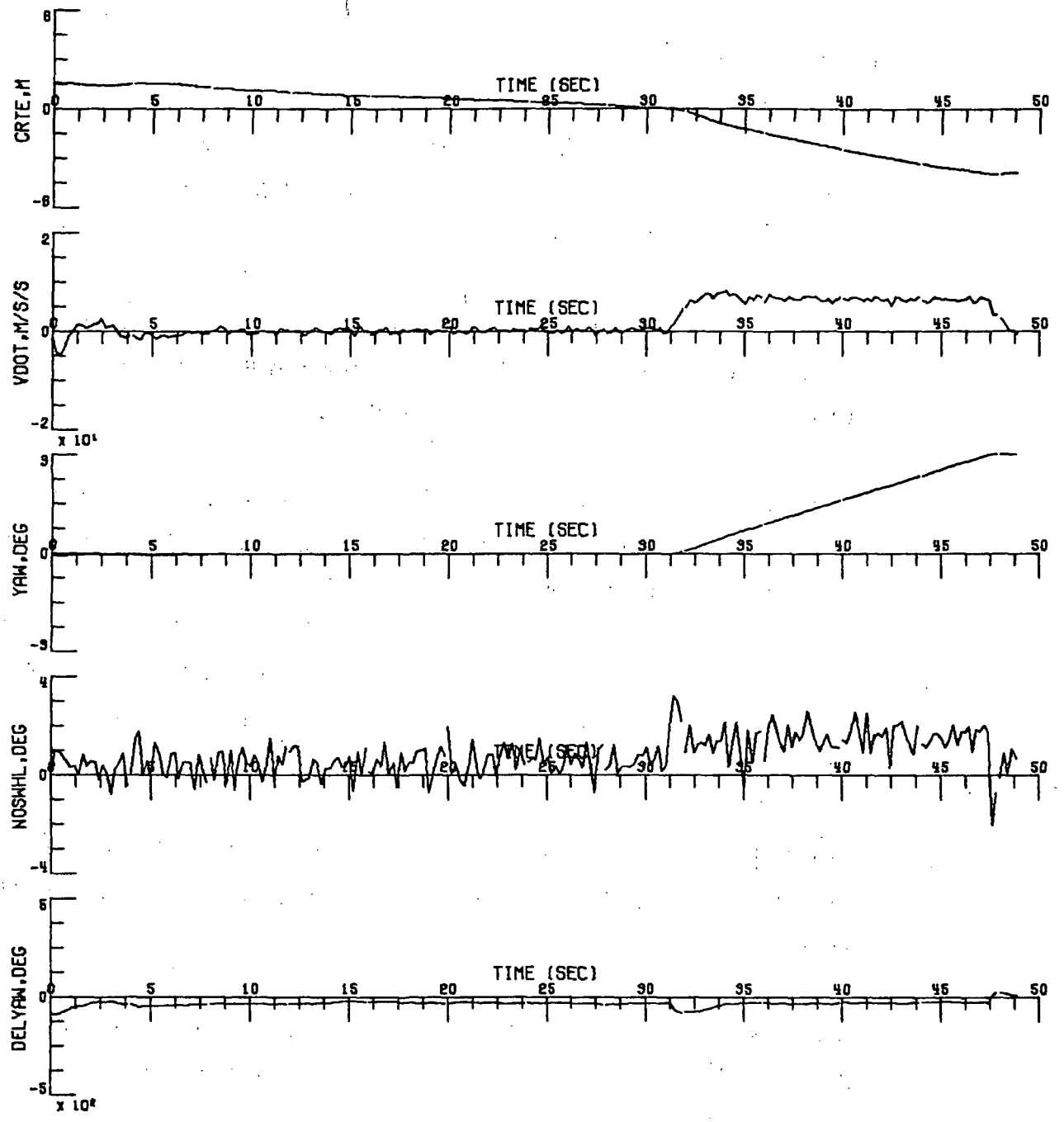

Figure B15b. High-Speed Turnoff on Dry Runway

150^{o} Head Wind, 5.144 m/sec (10 knots)
V_{coast} = 30.87 m/sec (60 knots)
V_{taxi} = 20.58 m/sec (40 knots)
R_T = (2000 feet)
Complementary filter used

REFERENCES

1. Attri, N.S. and Dunn, R.; "NASA Request for Data in Landing Gear, Tires, Antiskid, Thrust, Nose Wheel Dynamics, and Rudder Aerodynamics," Boeing Document B-8190-75-5, March 25, 1975.

2. Horne, W.B. and Leland, T.J.W.; "Influence of Tire Tread Pattern and Runway Surface Conditions on Braking Friction and Rolling Resistance of a Modern Aircraft Tire," NASA TN D-1376, 1962.

3. Kaminski, P.G., Bryson, A.E., Jr. and Schmidt, S.F.; "Discrete Square Root Filtering. A Survey of Current Techniques," IEEE Transactions on Automatic Control, December 1971.

4. Duff, William G., Guarino, Charles R.; "Refinement and Validation of two Digital Microwave Landing System (MLS) Theoretical Models", NASA CR-132713, August 15, 1975.

5. Morgan, H.C. and England, P.; "A Taxi Guidance System for Aircraft Using a Single Magnetic Leader Cable," R.A.E. Technical Report #66065, February 1966.

6. Olson, K.W., Fenton, R.E. and Melocik, G.C.; "Studies in Vehicle Automatic Lateral Control - Theory and Experiment," Ohio State University Report EE 1-276A-16, September 1974.

*U.S. GOVERNMENT PRINTING OFFICE: 1977 - 735-004/41

National Aeronautics and Space Administration

Washington, D.C.
20546

Official Business
Penalty for Private Use, $300

THIRD-CLASS BULK RATE

Postage and Fees Paid
National Aeronautics and
Space Administration
NASA-451

NASA

POSTMASTER: If Undeliverable (Section 158 Postal Manual) Do Not Return